THE DETECTION OF OIL IN WATER BY NEAR INFRARED PULSED PHOTOACOUSTIC SPECTROSCOPY

Peter Hodgson

Thesis Submitted for the Degree of Doctor of Philosophy

Department of Physics,
Heriot-Watt University,
Edinburgh,
March 1994

Table of Contents

List of Figures

Acknowledgements

The first thanks must go undoubtedly to Dr. Hugh MacKenzie, for our countless discussions and his guidance, advice and never-ending flow of suggestions. I am also indebted to him for a thorough critical review of this thesis. To the other members of the environmental monitoring and medical diagnostics group in the Department, I also owe a great deal. To Dr. Graham Christison for his pioneering work and for the comfort of having someone who went before me, to Dr. Ke Ming Quan for bringing his acoustic expertise to bear on the project at just the right time, and most recently to Scott Freeborn, my worthy successor, for helping with the characterisation of the photoacoustic instrumentation. I would also like to thank Andy Jamieson of Shell Expro, for his continued financial support, but more so for his encouragement and great enthusiasm for the project.

Many other people have helped me to complete this thesis. Thanks to Gordon Robertson and Malcolm Dunn for their time and assistance when exploring the use of OPOs. I am indebted to Steve Ganley of the Institute of Offshore Engineering for his help in characterising oil in water emulsions, and to Peter Heron and Mark Stewart of the workshop for turning ideas and sketches into tangible hardware. Thanks to Frank Greig for his electronics prowess and down to earth approach, and to Eion Johnston and David Binnie. Latterly the contributions made by Duncan Hand and Tommy Carolan in providing the interferometer expertise should not go unmentioned.

The role of my peers is more difficult to qualify. Thanks in particular to Susie, Raul, Chris, Tommy and Ben - it's good to know that when things get tough, it's the same for everybody else! I would like to express my gratitude to Susie, Mum and Dad, Lynne, Pam, and Mike for keeping me connected to the real world. Also thanks to my Gran, to whom this thesis is dedicated. The final word goes to those who have been through this before : it really was how you said it would be.

Abstract

An experimentally based study to investigate near infrared laser photoacoustic spectroscopy as a technique to measure oil pollution is described. Photoacoustic spectroscopy is shown to be well suited to the application of monitoring oil in water in a pipeline. The role of the physical parameters important to photoacoustic generation is shown to lead to an effective amplification of differences in the optical absorption coefficients for many hydrocarbons and alcohols in water. This amplification is typically an order of magnitude and persists at low concentrations of analyte, such that a Nd:YAG source (2 mJ pulses) yields a 7.2 % increase in the photoacoustic signal magnitude for a 500 mg/l oil in water sample compared to distilled water, corresponding to a detection limit of 4 mg/l. Using a 904 nm diode laser as a source for photoacoustic generation, a detection limit of 400 mg/l of oil is demonstrated. In addition there is found to be no discernible effect on the magnitude of the photoacoustic signal caused by the presence of optically scattering particles. The design and development of a photoacoustic instrument to measure oil in water is described, and the performance of such an instrument is compared to that of the competing technology.

CHAPTER 1

Introduction

1.1. Overview

Issues of pollution and pollution control continue to be forced into the political thinking of all concerned parties. The Government has responded to the current increase in public awareness of environmental issues by producing a White Paper, entitled "This Common Inheritance" (1.1), in which a general strategy is outlined aimed at tackling many of the environmental problems facing Britain. The Paper calls for the best scientific data to be collected and made available to assist in making environmental policy decisions. It also outlines two approaches, those of regulation and market signals, to controlling pollution that rely on such scientific information. There is a clear requirement for new instruments and sensors that are capable of meeting the increasingly strict specifications called for by the relevant legislative regulations on pollution control. This thesis describes an experimentally based study of one physical technique, the photoacoustic effect, which could be used as the basis for the trace analysis measurement required of many types of environmental instrumentation. Photoacoustic techniques have key advantages over other monitoring methods under certain measurement conditions, and these could lead to photoacoustics finding a worldwide role in many different applications of quantitative analysis.

Much of the impetus behind this study has originated from one very specific application concerned with the monitoring of oil in water in a pipeline on oil production

platforms. Consequently the thesis concentrates on describing the photoacoustic effect as a monitoring method with reference to this oil in water problem (essentially the detection of C-H bonds in water) and in the latter stages, instrument concepts are described with this in mind.

This introduction is split into two sections. The first provides a little of the background to the oil in water monitoring problem. Although specific references to North Sea oil field statistics are used, the subject of this thesis is also relevant to worldwide oil production. Included is information on the current and likely future regulations governing the operators of offshore oil platforms, and the operating conditions under which a monitoring system would have to work. Some of the alternative techniques that are also possibilities for making the necessary measurement are introduced. The second section of the Introduction gives an outline of the structure of the thesis, through a brief overview of each of the six other chapters that together constitute this thesis.

1.2. The Offshore Oil Industry

Much of today's worldwide oil reserves are to be found underneath the sea. The recovery of these resources has many associated problems, not least of which is the pollution of the sea as a result of exploration for and production of oil.

1.2.1. The North Sea Oil Industry

In the U.K. sector of the North Sea there were 48 oil fields, producing 92 million tonnes of oil in 1990 (1.2), representing 50% of the total North Sea oil production. The platforms used to retrieve this oil have several functions, the key ones of interest to this thesis being :

1) drilling and recovery of the oil

2) separation of oil, gas and water in production separators

3) cleaning of the water discharged back into the sea.

1.2.2. Produced Water

When oil is recovered from a reservoir underneath the seabed, water from two sources is frequently mixed in with the fluid that emerges at the platform. Formation water originated within the rocks of the oil reservoir, and is released along with the oil by the drilling operation. Water injected into the reservoir at high pressure to help force the oil up to the production platform often returns to the platform with the oil. Production separators are used to separate the water component from the hydrocarbons. The resulting water is known as produced water and typically contains > 1% dispersed oil, as well as dissolved oil, sand, other solids and well-head chemicals. Before this water can be discharged into the sea, the concentration of oil must be reduced to the levels demanded by the current legislation. Fig. 1.1 is a schematic following the path of produced water on an oil production platform. The position of an oil in water monitor in the water pipeline relative to other key installations, but before the water is discharged overboard, is clearly shown.

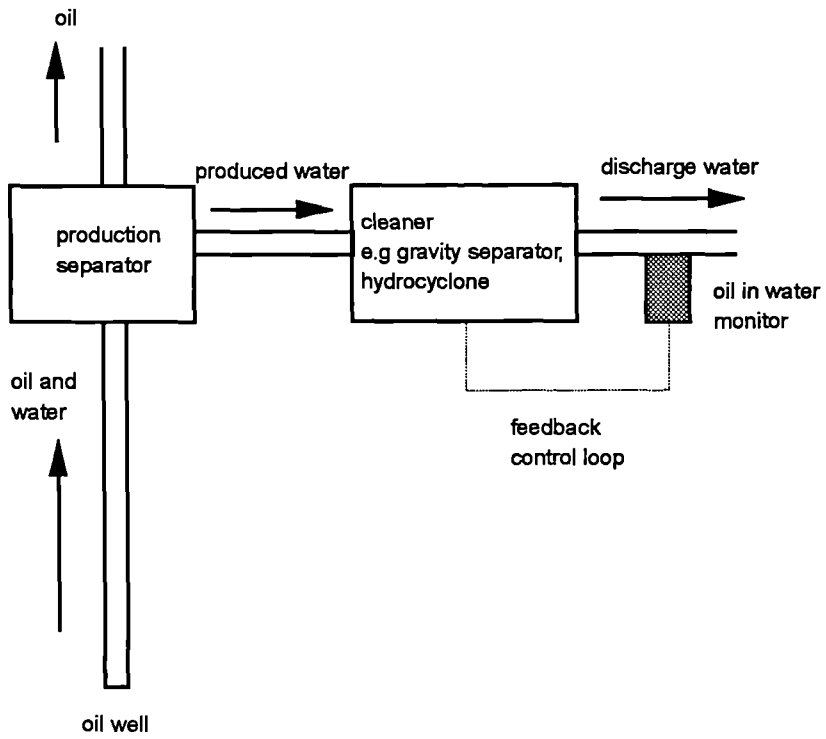

Fig. 1.1 Produced Water on an Oil Production Platform

Since 1987, the production of water by U.K. offshore oil platforms has exceeded the production of oil. In 1990 water production was 120 million tonnes and this level is likely to continue increasing as the existing reservoirs become more oil depleted. Contained within the 120 million tonnes of water discharged into the sea, there was 4400 tonnes of oil. This formed approximately 25% of the total oil input into the North Sea from all sources in the North Sea oil and gas industry. With this high and increasing contribution to the oil pollution of the North Sea, the quality of the cleaned produced water is under scrutiny, with pressure to improve the levels of oil in water increasingly likely.

1.2.3. Oil Pollution Regulations

An Act of Parliament forms the current regulations governing the discharge of oils into the waters around the United Kingdom. This Act, the Prevention of Oil Pollution Act (1971), prohibits the discharge of crude oil in any quantity into the sea as the result of the exploration of the sea-bed or exploitation of the natural resources therein. The Act provides a legislative framework, to which may be added more detailed information as the current circumstances dictate. The Secretary of State allows exemptions to the law that no oil shall be discharged into the sea. In the case of oil production platforms, these are currently accepted if:

the average oil over each month < 40 mg/l (≡ 40 parts per million (ppm) by weight)
< 4% of samples exceed 100 mg/l
there is at least twice daily sampling
records of discharge rate and volume are maintained

The limits highlighted above are determined to a large extent by the capabilities of the best available cleaning and monitoring technology. Future limits are likely to become more severe as the performance of the available technology improves. Already there has been considerable discussion aimed at lowering the

average oil limit to 30 mg/l in the North Sea and on-line monitoring is increasingly likely to be stipulated. In other regions of the world, the regulations differ in the allowed limits they set and in the types of oil component to be detected. There is nevertheless a clear trend, also evident in many other fields of environmental concern such as the quality of public water supplies, of tightening legislatory standards.

1.2.4. Regulatory Compliance

The most common current method by which companies monitor their compliance with the Prevention of Oil Pollution Act is dependent upon extraction of the oil contained in a sample of the discharge water and subsequent infrared analysis of C-H bonds (see section 4.3.3). This technique depends upon the use of a solvent such as carbon tetrachloride (CCl4), or a chlorofluorocarbon (CFC), themselves harmful to the environment through the well documented ozone layer depletion. The use of such solvents is under review, and is likely to be phased out or banned in the near future. Current targets are a phasing out of CFC consumption starting in July 1997, and the elimination of production by the year 2000 (Montreal Protocol).

1.2.5. Automatic Monitoring Methods

As well as the legislative need to find a replacement for solvent based extraction techniques for oil content montoring, the oil companies are keen to pursue developments that would lead toward the continuous and on-line monitoring of operating processes, for two main reasons in addition to the previously mentioned likelihood of regulatory requirements in that vein. Firstly, there is the financially attractive prospect of operating unmanned production platforms, which becomes a feasible one with automatic monitoring techniques. The most common current method of oil in water monitoring (infrared absorption following solvent extraction) is both time consuming and labour intensive. Secondly, an on-line monitor brings the possibility of implementing rapid feedback into the process control mechanisms on an operating platform, allowing an improvement in the performance of the operating procedures. An

on-line monitor in the water discharge pipeline would provide feedback as to the performance of the oil and water separation processes (see fig. 1.1).

There is a clear need for an instrument that:

is capable of measuring oil in water at and below the level of 40 mg/l,
can measure dissolved and dispersed oil components,
is capable of on-line and automatic operation,
does not use harmful solvents,
can operate in a harsh environment,
and requires low maintenance and few consumables,

but that is unaffected by:

the presence of solids,
the presence of free gases,
the oil droplet size,
the oil type,
the presence of oilfield chemicals,
sample temperature fluctuations,
ambient temperature fluctuations,
and changes in water salinity.

Not surprisingly there are several attempts being made world-wide to develop new and existing instruments that could meet these requirements, for the potential rewards are enormous. Mostly the instruments (or proposed instruments) may be categorised by principle of operation into one of the following categories:

light scatter,

ultraviolet (UV) absorption,

UV fluorescence,

direct infrared absorption (no initial solvent based extraction), and

acoustic reflections.

The principle of operation of these instruments is discussed more fully in Section 6.5. However the relative merits of these methodologies are summarised in Table 1.1, adapted from (1.3). It is clear that no single technique meets all the requirements for an automatic, in-pipeline monitor and that there is a clear opportunity for another technique to make a significant impact in this area.

Technique	Advantages	Disadvantages
optical scatter	fast response time high sensitivity simple and robust	affected by solids
UV absorption	fast response time high sensitivity	affected by solids affected by oil drop size oil type specific not robust
UV fluorescence	fast response time high sensitivity	affected by solids affected by oil drop size oil type specific
infrared absorption	detects dissolved oil measures hydrocarbons directly	background absorption clogging problem
acoustic detection	fast response time used in-line	affected by solids affected by gas

Table 1.1 Principles of Oil in Water Detection (from ref. (1.3))

1.2.6. Discussion

The future is likely to bring a continued tightening of all kinds of legislative standards for pollution control worldwide. This will apply to all types of industry, not least that of oil production. In the North Sea, the quantification and reduction of produced water contaminants will be one of the more important environmental issues. As the technology to clean produced water is advanced, parallel improvements in the detection of contaminants will be required, and these improvements will have to be made by techniques that do not rely on the use of harmful solvents. At the same time, the economics of developing new, more difficult oil fields will place a greater emphasis on the process control implemented on production platforms, as well as providing an impetus towards unmanned operations.

There is a clear need for a new oil in water monitoring technique. This thesis describes a dominantly experimental study of the photoacoustic effect as the scientific basis of an oil in water monitor, in which some of the questions posed by the need to continuously monitor low levels of oil in water are answered.

1.3. Thesis Outline

Following this introduction, Chapter 2 gives a comprehensive description of the photoacoustic effect, a little of the history of its development as an analytical technique, and an up to date review of the applications in which the photoacoustic technique has found usage. A qualitative explanation of the generation of acoustic waves in liquids by optical excitation is described, before a more rigorous theory is presented in outline. The important conclusions about the magnitude and time dependence of the photoacoustic pressure waveform to be drawn from this theory are highlighted. In addition, the role of optical scattering on the photoacoustic waveform and the properties of acoustic waves in liquids are discussed. The principles of the detection of acoustic waves in liquids, both by piezoelectric and optical means, are included along with the considerations to be taken into account when designing a piezoelectric acoustic detector.

Chapter 3 concentrates on near infrared spectroscopy, both conventional transmission and photoacoustic, as a means of making analytical measurements, and explains the advantages and disadvantages of using the near infrared spectral region for such measurements. The two techniques are compared, through the spectroscopy of pure compounds, such as water and some of the constituents of crude oil, for example benzene and pentane. The comparison extends to a discussion of the effect that the presence of solid scattering particles has on the techniques, supplemented by experimental results.

In Chapter 4, experiments are described which tested the fundamental sensitivity of the photoacoustic technique in measuring the spectroscopic response of C-H bonds from organic analytes in water, to determine whether legislatively important detection limits for oil in water could be reached. These begin with a study of a simple system, that of methanol in water and advance to encompass oil in water measurements. Following the characterisation of the oil emulsions, the photoacoustic spectroscopy of oil emulsions is described. Studies of the acoustic frequencies generated in liquids are included, in particular the response from oil emulsions. A detailed analysis of the acoustic waveforms from such samples is presented.

The emphasis in Chapter 5 is in describing several of the optical sources suitable for a practical instrument based on the photoacoustic technique. There are several new developments in near infrared laser technology that are of particular interest for those developing spectroscopic instruments. The chapter gives an overview of the current situation, and describes the principle of operation of the most relevant new lasers. Photoacoustic experiments with two of these laser types are described, in which low concentrations of oil in water are measured. The use of diode lasers in particular as sources for photoacoustic measurements is discussed in some detail.

Chapter 6 continues the theme of practical instrumentation issues begun in Chapter 5. A significant feature of photoacoustic instrumentation could be realised with the implementation of optical detection of the generated acoustic waves, thereby removing sensitive detection electronics away from the measurement area. This would lead to the realisation of an all-optical measurement head, with the inherent advantages that would bring. The first section of Chapter 6 explores the implementation of an all optical measurement head through the description of experiments in which a fibre optic interferometer was used to detect photoacoustically generated waves in liquids. The latter stages of this chapter describe the design and construction of a pre-prototype instrument, and a demonstration system, incorporating a flow pipeline and fibre optic delivery of the optical source. A remote optical source combined with fibre optic delivery has an advantage over a local optical source in a hazardous and noisy environment such as might be encountered on an oil production platform. To conclude this chapter, a more complete description of the competing technologies for an oil in water monitor can be found. The expected performance of a photoacoustic based oil in water monitor under some of the operational conditions likely to be encountered in the field is discussed.

Chapter 7 brings together the experimental work presented in Chapters 3 through 6, and re-iterates the advantages and disadvantages of the photoacoustic technique in an oil monitor in the light of the results. The nature of the outstanding problems, with reference to the requirements of an in-line oil in water monitor, is used to form a suggested programme for future studies with which progress to a field instrument will be made. There is also a discussion of the relevance of photoacoustic techniques to the detection of other pollutants and in other monitoring applications.

1.4. References

(1.1) This Common Inheritance, HMSO, September 1990

(1.2) U.K. North Sea Oil and Gas Industry: Environmental Inputs, Impacts and Issues, doc. 92/063, Institute of Offshore Engineering, Heriot-Watt University, 1992

(1.3) Simms K., Zaidi A., 'On-line Monitoring of Oil in Water in Oilfield Brines', 2nd Intl. Conf. on Water Management Offshore, Aberdeen, U.K., 1991

CHAPTER 2

The Generation and Detection of Photoacoustic Phenomena in Liquids

2.1. Overview

This chapter outlines the major advances made in understanding and applying the photoacoustic (PA) effect, from its discovery by Bell in the 1880s to the present day. Following a brief history of significant photoacoustic developments, a structured resume of the development of the theory relevant to the generation of photoacoustic waves in liquids is presented, ending with the currently accepted model for generation by pulsed optical sources. The main conclusions to be drawn from this theory are discussed in detail. The properties of acoustic waves relevant to this thesis are described and the bearing these have on detector considerations is highlighted. Several different piezoelectric and optical methods for the detection of photoacoustic waves in liquids are discussed in some detail. Photoacoustics is widely applied in many fields of investigation at the present time, and a brief review is given here of the latest and most significant work.

2.2. Discovery and Brief History of Photoacoustics

It is Alexander Graham Bell who is generally credited with the discovery of the photoacoustic effect (2.1). Through his experiments in which he modulated sunlight illuminating an absorbing sphere, he was able to transmit and receive audible acoustic

signals. This method of communication was overtaken by other techniques, and the subject of photoacoustics remained largely forgotten for several decades. Indeed the subject was only given forceful impetus in the 1960s with the advent of the laser. The intense optical radiation provided by these new sources was ideal for the generation of acoustic waves in matter. The majority of the early laser studies were of acoustic generation in gases, but solids and liquids were soon the subject of attention too. The 1970s and 1980s were times of tremendous activity in the field of photoacoustics and it was in this period that the understanding of the physical mechanisms involved in the photoacoustic process was largely evolved. The current name of photoacoustic effect also became widely adopted during this period, replacing the term optoacoustic effect, which had been likely to cause confusion with the acousto-optic effect. The interest in the PA effect continues at a lively pace in the 1990s, in theoretical aspects, analytical experimentation and in the availability of commercial photoacoustic spectrometers.

2.3. Theories of Photoacoustic Generation in Liquids

2.3.1. Mechanisms for Acoustic Generation by Modulated Illumination

Aside from infrequent investigations during the first half of the twentieth century, the photoacoustic effect was not the subject of much activity until the demonstration of the first working laser by Maiman in 1960. Almost immediately the relevance of this new optical source to the study of the generation of acoustic waves in matter was realised. The effect of the passage of a ruby laser light beam of approximate pulse duration 1 μs through water was reported by Askar'yan *et al* (2.2). The formation of bubbles, caused by localised heating, boiling and consequent vaporisation was observed. This was true to the extent that explosive ejection of the water contained in the cell occurred when a dye was used to increase the optical absorption coefficient at the ruby laser wavelength.

However this is just one manner in which the illumination of a sample by a light beam can cause the generation of acoustic energy. Figure 2.1 shows some of the

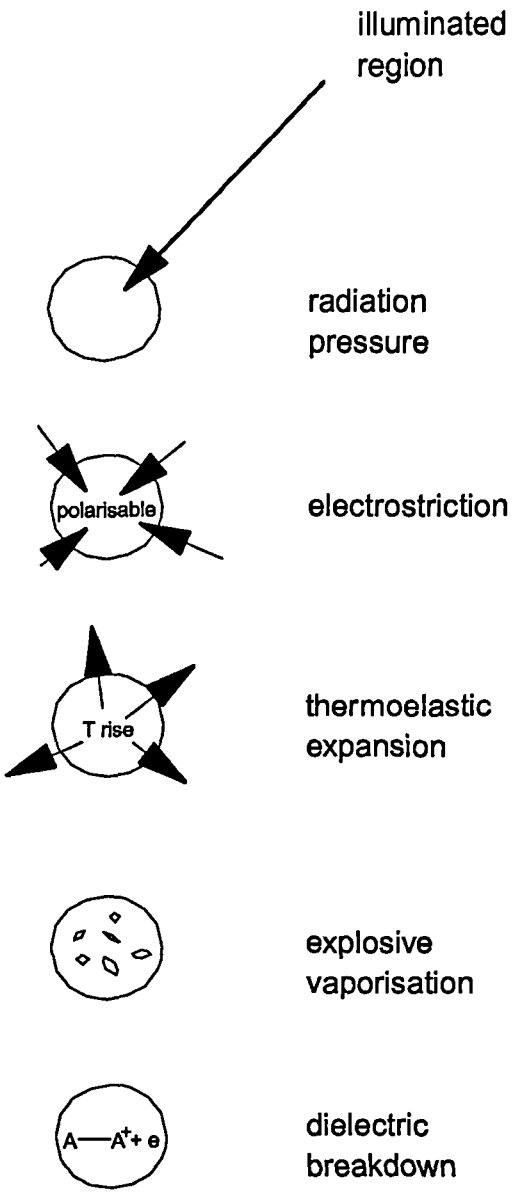

Fig. 2.1 Mechanisms of Acoustic Generation by Optical Illumination

different physical mechanisms that can, under differing circumstances be responsible for acoustic generation, in order of increasing efficiency of energy conversion (2.3).

Radiation pressure is assumed to be a very weak effect in all cases considered in this thesis. Electrostriction is also a weak effect in general, significant only in the particular circumstances of liquid samples with very weak optical absorption or with a high electrostrictive coefficient, and will be discussed briefly in due course. Thermoelastic expansion is the mechanism of prime importance in most photoacoustic applications and will be discussed fully in the next section. Vaporisation and dielectric breakdown are dominant in the realms of high intensity illumination, and of no further interest within the context of this thesis.

2.3.2. Thermoelastic Expansion

The dominant mechanism for acoustic generation by modulated optical illumination that is of particular relevance to analytical studies in liquids is thermoelastic expansion and this thesis will concentrate almost exclusively on the effects and applications of this mechanism. The fundamental processes involved in the conversion of optical energy to acoustic energy by this manner are shown in fig. 2.2. When an absorbing medium is illuminated by modulated (pulsed or chopped) optical radiation, a fraction of the incident optical energy is removed from the excitation beam. This energy is momentarily stored by the molecules of the sample through the population of excited energy levels. The energy may be released in a number of ways, and after different periods of time, depending upon the type of illumination and the sample. Fluorescence and phosphorescence are two radiative methods of energy release, but if the relaxation is non-radiative the absorbed energy usually manifests itself as heat. Such heating, in the vicinity of the illuminated volume, leads to an expansion of that volume. The expansion generates a pressure (or acoustic) wave emanating from the illuminated region, and can be detected as such with a suitable transducer.

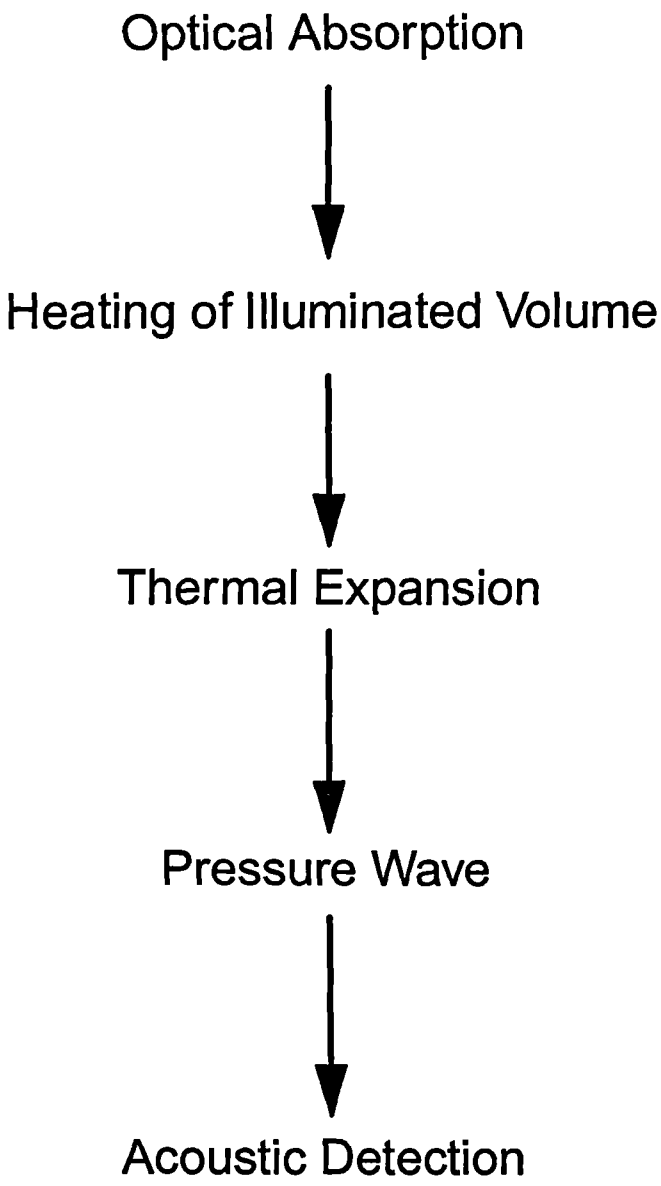

Fig. 2.2 The Photoacoustic Effect by Thermoelastic Expansion

2.3.2.1. Excitation Modes

Photoacoustic generation may be classified according to the excitation mode *i.e.* using a continuous wave (CW) or pulsed source. In the CW case, the duty cycle of the modulated beam is close to 50 %. Signal analysis is often performed in the frequency domain. The large duty cycle means that the boundary conditions of the sample cell are important in determining the response. It is sometimes possible to utilise the acoustic resonances of the cell to maximise the photoacoustic response. Thermal diffusion effects may be important when using CW mode excitation.

Pulsed mode excitation uses a high peak power, low duty cycle optical source. Since the optical energy is deposited in the sample in a relatively short time, thermal diffusion effects can largely be ignored. The peak pressure is usually greater than that generated using CW excitation. The acoustic propagation distance during the excitation pulse is typically smaller than the sample cell dimensions. As a consequence, the photoacoustic pulse shape is not usually affected by acoustic reflections from cell surfaces. Analysis is usually performed in the time domain and this means that gated techniques can be used to suppress noise, such as spurious acoustic signals from cell window absorption (2.3). Frequency domain analysis may provide useful information, for example to determine rate processes within the sample, especially when a broadband acoustic detector is used. Pulsed mode excitation can also be used more readily in the analysis of a flowing sample.

2.3.2.2. Early Developments

The first experimental studies, in which the thermoelastic expansion within a sample due to illumination by a modulated laser source was examined, were of gases, typified by Kreuzer's study of methane (2.4). This work highlighted the great potential that the photoacoustic effect had for making analytical measurements in samples containing very low concentrations of analyte. Shortly afterwards the photoacoustic effect was being used to study solids, with a chopped Xenon source (2.5). This work

led to the development of a pioneering theory known as R-G theory, describing photoacoustic generation by the CW excitation mode (2.6). The possibility of obtaining information about the optical properties of samples that could not easily be analysed using conventional transmission or reflection techniques, such as those with very low or very high absorption, became a powerful argument in favour of photoacoustics.

2.3.2.3. Qualitative Theory of Photoacoustic Generation in Liquids

A simple qualitative theory, such as that first outlined by Patel and Tam in 1981 (2.7), can lead to a very useful understanding of the physical processes that are involved in the generation of a PA signal in liquids. When radiation illuminates a sample, the amount of the incident energy transmitted by the sample, E_t is given by Beer's Law,

$$E_t = E_0 e^{-\alpha l} \qquad \{2.1\}$$

where E_0 is the incident optical energy, α is the optical absorption coefficient and l is the optical pathlength. The energy absorbed by the sample ΔE assuming no reflective or scattering losses is given by

$$\Delta E = E_0 - E_t \qquad \{2.2\}$$

In the case of weak optical absorption, where $\alpha l << 1$, as is often the case in near infrared experiments, the absorbed energy can be approximated to

$$\Delta E \approx E_0 \alpha l \qquad \{2.3\}$$

Strong optical absorption does occur in the near infrared and this leads to saturation effects, a topic dealt with in more detail in Chapter 3. As an example of weak absorption, consider a 1 μJ pulse incident on a sample of water contained within a 2 mm cell at a wavelength where the absorption coefficient = 1 cm^{-1}. In such a case the absorbed energy ~ 0.2 μJ. For the case of a collimated beam, this is absorbed within a volume V, given by

$$V = \pi R^2 l \qquad \{2.4\}$$

where R is a measure of the radius of the beam. Assuming that all of the absorbed energy goes into heat generation, there is a temperature rise ΔT given by

$$\Delta T = \frac{E_0 \alpha l}{\rho C_p V} \qquad \{2.5\}$$

where C_p is the specific heat capacity and ρ is the sample density. In the example given above, there is a temperature rise of approximately 1.2 x 10^{-2} C in water, assuming an optical spot radius of 25 μm. At this point in the discussion, the duration of the optical pulse, τ_p relative to the time for an acoustic wave to travel across the illuminated region, τ_a becomes an important consideration.

Small optical spot size (*i.e.* $\tau_p >> \tau_a$)

From the temperature rise estimate, the increase in the radius of the heated region ΔR, due to thermal expansion immediately after the laser pulse can be calculated, using the expression

$$\pi(R_s + \Delta R)^2 l - \pi R_s^2 l \approx \beta V \Delta T \qquad \{2.6\}$$

where β is the volumetric thermal expansion. In this case the acoustic source radius R_s is not equal to the illuminated radius R since the active source volume has had opportunity to expand for the duration of the optical pulse. In fact, R_s is determined by the laser pulse duration and is equal to $\upsilon.\tau_p$, where υ is the acoustic speed. Assuming that $\Delta R << R_s$, the expression for ΔR becomes:

$$\Delta R \approx \frac{E_0 \alpha \beta}{2\pi \rho \upsilon \tau_p C_p}. \qquad \{2.7\}$$

In the example considered above, an increase in the radius of the acoustic source of 3.5 x 10^{-12} m is predicted if τ_p = 150 ns. This expansion leads to a propagating acoustic displacement d, which at a radial distance r (where r >> R) from the beam axis is given by

$$d \approx \Delta R\left(\frac{Rs}{r}\right)^{\frac{1}{2}}. \qquad \{2.8\}$$

This expression is consistent with the acoustic energy following an r^{-1} law, as would be expected from a cylindrical source. The excess pressure p in a fluid caused by an acoustic displacement may be expressed in approximate form as

$$p \approx 2\pi f \upsilon \rho d \qquad \{2.9\}$$

where f is the frequency of the acoustic waveform. Assuming an acoustic frequency of 1 MHz, the excess pressure at a distance of 5 mm from the optical axis generated in the above example is approximately 7 $N.m^{-2}$. Combining equations {2.7} to {2.9}, a qualitative expression for the magnitude of the pressure pulse generated by thermoelastic expansion following the absorption of light is obtained, *viz*

$$|p| \approx k.\frac{\beta\alpha}{C_p}\left(\frac{\upsilon}{r}\right)^{\frac{1}{2}}.E_0 \qquad \{2.10\}$$

where k is a system constant which includes temporal factors important to the pressure waveform generation. As may be expected, the magnitude of the photoacoustic signal is proportional to the incident pulse energy and the optical absorption coefficient of the sample. The role of other physical parameters, in particular the thermal expansion coefficient and the specific heat capacity, in determining the PA signal amplitude is also made clear in equation {2.10}.

Large optical spot size (*i.e.* $\tau_a >> \tau_p$)

In the case of a large beam radius, the heated volume does not have time to expand during the laser pulse, with the result that there is a pressure increase p at the edge of the illuminated cylinder immediately after the laser pulse, given (from relating the stress and strain) by

$$p = \rho\upsilon^2\beta\Delta T. \qquad \{2.11\}$$

Substituting for the temperature rise {2.5} as before, and assuming that the peak acoustic pressure scales as $r^{-1/2}$, an expression for the peak acoustic pressure may be obtained :

$$|p| \approx \frac{1}{\pi R^{\frac{3}{2}}} \frac{\beta\alpha}{C_p} \frac{\upsilon^2}{r^{\frac{1}{2}}} . E_0 \qquad \{2.12\}$$

which is similar in form to that describing the case for a small optical beam. Equations {2.10} and {2.12} are essentially the same except that the effective acoustic source radius, given by $\upsilon\tau_p$ in the small beam case is replaced by the actual optical beam radius, R in the large beam case.

2.3.2.4. Rigorous Theory of Photoacoustic Generation in Liquids

The qualitative discussion presented above results in an expression that yields an insight into the magnitude only of the acoustic signal. There is no indication as to the nature of the time dependence of the waveform. The shape of the waveform in the time domain has important repercussions on the design of the acoustic detector through the frequency content of the signal. To gain an understanding of the time dependence requires a more rigorous approach to the theory of photoacoustic generation than that presented in Section 2.3.2.3. In the early eighties, two independent, key papers (2.8, 2.9) were published that explored in detail the mechanisms of photoacoustic generation in weakly absorbing liquids by pulsed laser excitation and that provided the formalism on which predictions of the time dependence could be made.

Beginning with the equation of motion,

$$\left(\frac{1}{\upsilon^2}.\frac{\partial^2}{\partial t^2} - \nabla^2\right) p = \left(\frac{\alpha\beta}{C_p}\frac{\partial}{\partial t} - \frac{\gamma}{2nc\upsilon^2}\frac{\partial^2}{\partial t^2}\right) I \qquad \{2.13\}$$

in which I is the optical intensity, γ is the coefficient of electrostriction, n is the refractive index, and c the velocity of light in a vacuum, and assuming a Gaussian

(temporal and spatial) optical beam, Lai & Young (2.8) arrived at the conclusion that the magnitude of the photoacoustic pressure pulse is given by

$$|p(r,t)| \propto \frac{\alpha\beta E_0}{8\sqrt{\pi}.C_p}.\left(\frac{\upsilon}{r}\right)^{\frac{1}{2}} \tau_e^{\frac{-3}{2}} \qquad \{2.14\}$$

where τ_e is an effective time parameter, made up of contributions due to the laser pulse duration and the acoustic transit time, such that

$$\tau_e = \left(\tau_p^2 + \tau_a^2\right)^{\frac{1}{2}}. \qquad \{2.15\}$$

The main conclusions to be drawn from equation {2.14} about the magnitude of the pressure waveform are :

i) the proportionality to α, β, E_0 and C_p^{-1},

ii) the -3/2 power dependence on the effective time parameter, τ_e, and

iii) the proportionality to $\upsilon^{1/2}$ and $r^{-1/2}$.

This extends the simple theory presented in Section 2.3.2.2 most significantly through item ii). The time parameter dependence indicates that short duration pulses in narrow beams yield the largest photoacoustic signals. This is intuitively appealing since:

a) a long optical pulse duration would reduce the rate of temperature rise and therefore the speed of thermal expansion, and

b) a large beam size would reduce the energy density in the acoustic source and result in non-coherent contributions from different regions of the beam arriving simultaneously at the detector, effectively smearing out the response.

The dependence of the magnitude of p on the acoustic velocity of the sample arises twice in equation {2.14}, directly as raised to the power 1/2, and also through

the effective time parameter. The acoustic transit time τ_a is inversely proportional to υ. For cases of small spot size, ($\tau_p >> \tau_a$), the magnitude of p follows $\upsilon^{1/2}$, in agreement with the conclusion of the simple theory summarised in equation {2.10}. In the situation where $\tau_p << \tau_a$, the acoustic transit time dominates the effective time parameter, with the result that the magnitude of p is proportional to υ^2, also in agreement with equation {2.12}. For cases of pulsed excitation and low absorption, it is reasonable to assume that the dependence of the magnitude of the photoacoustic signal can be summarised by the expression

$$|p| = k.\frac{\alpha\beta\upsilon^m}{C_p}.E0 \qquad \{2.16\}$$

where $1/2 < m < 2$ and k is a system constant.

The main significance of the work presented by Lai & Young was however a prediction of the temporal form of the photoacoustic waveform. Their theory predicts that the time between the compression maximum and the rarefaction minimum is $2.35.\tau_e$. Quan *et. al.* (2.10) have used a similar model to predict the PA waveforms generated in water and methanol. Typical waveforms are shown in fig. 2.3, as generated by the optical pulse shown in the lower trace. The smaller PA waveform is that generated in water. These display a bipolar nature, featuring a strong, short initial compression pulse, followed by a weaker, broader rarefaction.

A slightly different approach to obtaining an equation to describe the photoacoustic pressure waveform was employed by Heritier (2.9), but the result was essentially the same as that of Lai & Young. He also considered Gaussian beams, with the pulse duration defined in terms of the half width 1/e point, with the result that his effective time parameter, ε was related to τ_e by the expression

$$\varepsilon = \sqrt{2}.\tau_e. \qquad \{2.17\}$$

A further observation made by Heritier was that the full width half maximum (FWHM) of the compressive part of the pressure pulse had a duration of approximately 1.3ε.

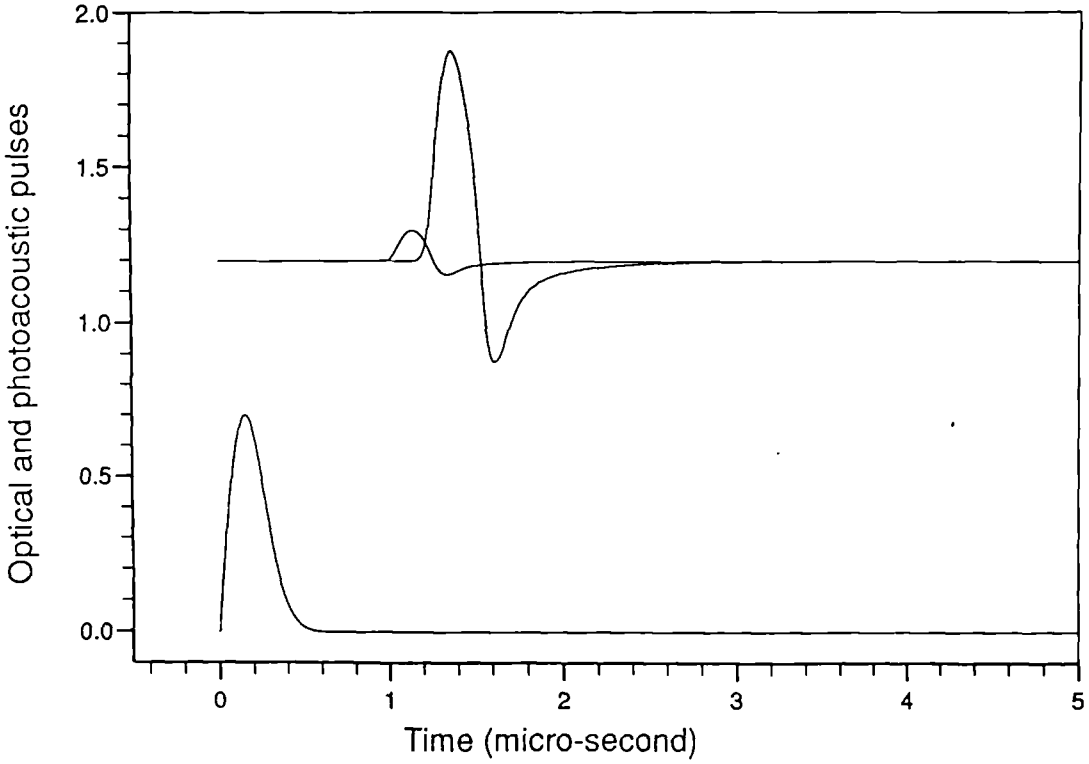

Fig. 2.3 Predicted Photoacoustic Waveforms in Water and Methanol

Included in both papers were attempts to compare the contributions to the pressure waveform generated in liquids due to electrostriction and thermal expansion. In water, electrostriction was predicted to yield an initial rarefaction, followed by a larger compressive pulse and a small, second rarefaction. However, the magnitudes of the electrostrictive pulses were only predicted to become comparable to those generated by thermal expansion in liquids of high electrostrictive coefficient (such as water), and at wavelengths at which the optical absorption was very weak ($\alpha < 1 \times 10^{-3}$ cm^{-1}). This thesis is predominantly concerned with near infrared interactions, where the optical absorption coefficients of liquids are typically at least two orders of magnitude higher than this limit. For this reason, effects due to electrostriction are assumed to be negligible for the further purposes of this thesis.

The first demonstration of the equivalence of the theories of Heritier and Lai & Young was reported by Sullivan and Tam (2.11), in a paper that also provided the first experimental evidence that the predictions were accurate. A broadband optical technique was used to measure the acoustic pulse profiles generated by short duration laser pulses in methanol. Very good agreement between the theoretical predictions and the experimental results over a range of pulse durations and beam sizes was reported, although some discrepancies were observed and attributed to the non-Gaussian nature of the optical beam.

2.3.3. Optical Scattering in Photoacoustics

The presence of scattering particles in a sample presents a major problem to trace analysis by optical means such as transmission spectroscopy. Any loss of the transmitted light due to scattering could be mis-interpreted as an increase in absorption. The effect of scattering particles on photoacoustic generation has been considered by several authors (2.12, 2.13, 2.14). The general consensus is that photoacoustic spectroscopy (PAS) is less sensitive to the presence of scatterers than transmission spectroscopy, since it is a direct measure of the absorbed rather than the transmitted energy. The precise effect that scatterers will have on PA generation will

depend on several parameters, such as the size, shape and concentration of the particles, the background optical absorption coefficient, α and the optical absorption coefficient of the scattering particles themselves. Detailed theoretical studies of the effects of different scatterers on a photoacoustic signal have been developed by Yasa (2.14) and Helander (2.15). Although these were based on CW mode photoacoustics, several of the arguments can be transferred to cases in which pulsed excitation is used.

In general, the addition of scatterers to an otherwise non-scattering sample changes the photon distribution within the sample such that the photon density becomes higher in the region close to the optical input surface. Predicted photon densities for several values of α and the scattering coefficient, K have been plotted in (2.12). The effect that this redistribution of photons has on the photoacoustic signal depends mainly on the magnitudes and ratio of αl and Kl, where l is the effective optical pathlength. Five different cases have been considered and are outlined below:

Case 1) $Kl \leq 0.1$, $\alpha l \leq 1$: scattering has negligible effect on the photoacoustic signal.

Case 2) $Kl \leq 0.1$, $\alpha l >> 1$: in this case, there is total absorption within the effective optical pathlength *i.e.* there is signal saturation, and the presence of scattering has little effect on the size of the photoacoustic signal.

Case 3) $Kl \approx 1$, $\alpha l \leq 1$: the scattering results in an increase in the mean photon path through the sample, and a corresponding increase in the number of absorbed photons. The scattering also results in an increase in the spatial dimension of the acoustic source. These effects have opposing influences on the size of the photoacoustic signal, such that the signal may remain largely unaltered from that generated in a non-scattering sample.

Case 4) $Kl > 1$, $\alpha l \leq 1$: if the scattering coefficient is much larger than the absorption coefficient, some photons will be scattered out of the sample before an absorption event can take place, in the same way as is utilised in diffuse reflectance spectroscopy. This will reduce the photoacoustic signal compared to that generated in a non-scattering sample.

Case 5) $Kl > 1$, $\alpha l > 1$: virtually total absorption will occur within the effective optical pathlength, but with an altered photon distribution compared to a weak scattering sample (Case 2)), with the result that the size of the photoacoustic signal will be slightly altered compared to that from a non-scattering sample of the same optical absorption.

Cases 1, 2 and 3 are those of most relevance to this thesis. Scattering experiments specific to the conditions likely to be encountered in an oil in water monitor are described and discussed in more detail in Chapters 3 and 4.

2.4. Acoustics

2.4.1. Acoustic Impedances and Reflections

The propagation of acoustic energy through a medium can be in the form of longitudinal or shear waves. Whilst both types of acoustic wave can exist in solids, liquids can only support longitudinal waves. The behaviour of acoustic waves at material interfaces is determined in part by the acoustic impedances of the materials, where the acoustic impedance, z is given by

$$z = \upsilon.\rho \qquad \{2.18\}$$

If the acoustic energy is to be transmitted efficiently at an interface, the acoustic impedances on either side of the interface should be well matched. If there is a large impedance mismatch, much of the acoustic energy will be reflected at the

interface. For the purposes of this thesis, I am most interested in two cases of acoustic propagation at an interface.

Firstly there is the case of an acoustic wave propagating in a liquid, impinging on a solid surface (*e.g.* a photoacoustic wave arriving at a ceramic based detector). For normal incidence of the acoustic waves, only longitudinal waves are excited in the solid. The power reflection coefficient, W is given by

$$W = \left(\frac{z_2 - z_1}{z_2 + z_1} \right)^2 \qquad \{2.19\}$$

where z_1 and z_2 are the acoustic impedances on either side of the interface. If however the incidence is not normal, the exact nature of the interaction becomes more complex. Depending upon the angle of incidence, the acoustic waves coupled into the solid can be longitudinal, shear, or a combination of both. Fig. 2.4 (2.16) shows the theoretical acoustic reflection and transmission coefficients for a plane acoustic wave propagating in water impinging on a flat aluminium surface. For an angle of incidence greater than approximately 30°, there is no coupling of the acoustic energy into the solid since it is all reflected. For angles of incidence greater than 14°, only shear waves are excited within the aluminium. At normal incidence, the reflection coefficient is 71%. The relevance of this to acoustic detector design is discussed in Section 2.5.3.

The second case is in the coupling of acoustic energy from one solid to another. A good impedance match is again necessary to ensure an efficient energy transfer from one material to another. This situation is relevant to the design of a backing arrangement for a ceramic transducer, used to provide some degree of damping of the acoustic signal and prevent excessive signal 'ringing', and will also be returned to in Section 2.5.3.

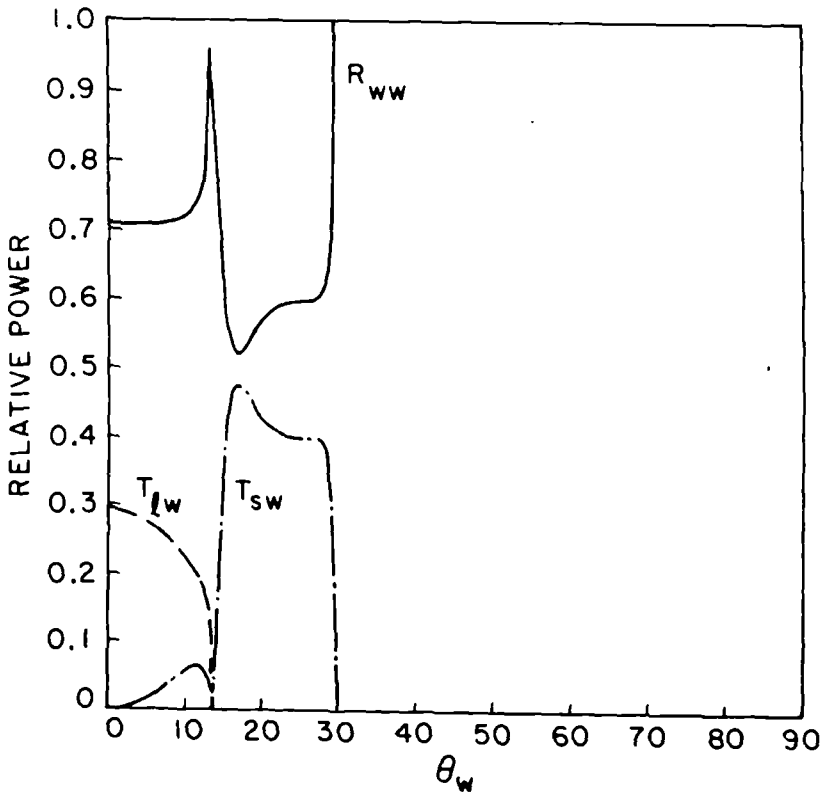

Fig. 2.4 Acoustic Transmission and Reflection Coefficients at an Aluminium / Water Interface : reproduced by permission of Prentice-Hall Inc., Englewood Cliffs, NJ

2.4.2. Acoustic Attenuation and Scattering

The rigorous theories described in Section 2.3.2.3 allow predictions of the frequency content of the generated acoustic waveform to be made. For the experimental conditions of interest in this thesis, the dominant acoustic frequencies are in the region 100 kHz to 5 MHz. At such frequencies, the attenuation of the acoustic waves in liquids has been assumed to be negligible, since the geometry of the photoacoustic detection schemes used was always arranged such that the acoustic detector was positioned within a few millimetres of the generation region.

An object that is large in cross-section compared to the acoustic wavelength and whose surface features are small in scale compared with the wavelength will tend to behave like a specular reflector. The scattering of acoustic waves by particles much smaller than the wavelength is weak, with scattering occurring in all directions, in much the same way as Rayleigh scattering in optics. The scattering intensity will depend upon the acoustic impedance mis-match at an interface in a similar manner to the reflection coefficient described above. Scattering by emulsion droplets will therefore be less severe than scattering by solid particles or air bubbles. The wavelength of a 1 MHz acoustic wave in water is approximately 1.5 mm. For the purposes of this thesis, all acoustic scattering has been assumed to be negligible.

2.5. Photoacoustic Detection

2.5.1. Piezoelectric Detection

Piezoelectricity, discovered by the Curie brothers in 1880, is a property of non-centro symmetric crystals by which a mechanical stress applied to a piece of the crystalline material results in the generation of an electric charge. This arises from the resultant strain altering the net dipole moment within the crystals.

Piezoelectricity has long been the basis of one class of photoacoustic detectors, used particularly as in-contact detectors of acoustic waves in solids

because of the good acoustic impedance match. They are also the most common in-contact detectors of photoacoustic waves in liquids, since the acoustic impedance match is very significantly better than that achieved with a gas buffered microphone system. To a first approximation, the voltage response, S of a thin piezoelectric element to a normal incidence plane pressure wave increases linearly as the thickness of the element increases, and is also dependent upon the piezoelectric constants of the element. For elements thicker than an acoustic wavelength, increasing the thickness of the piezoelectric element does not result in a proportional increase in the output voltage. The cross-sectional area of a piezoelectric element is an important consideration when the acoustic waves are not plane waves, since the pressure may not then be uniform over the entire area. The rise time, τ_r of a detector is often a further consideration. In the case of piezoelectric detectors, this is given by

$$\tau_r = \frac{t}{\upsilon} \qquad \{2.20\}$$

where t is the element thickness, and υ is the speed of sound in the piezoelectric.

Ceramic Detectors

Although several naturally occurring minerals (*e.g.* quartz) are piezoelectric, synthetic polycrystalline ceramics such as lead zirconium titanate (PZT) are the most widely used materials in the fabrication of piezoelectric elements. These may be fashioned into a wide variety of shapes before the process of poling determines the axis(es) of greatest sensitivity. A ceramic element has its own resonant frequencies, determined by its size, shape and composition. Mechanical stresses in the form of acoustic waves will be converted to electrical signals most efficiently if the acoustic frequencies match those of the ceramic resonances.

Thin Film Detectors

The electrical response from a ceramic piezoelectric is often dominated by its own frequency characteristic and it consequently may not yield a temporally accurate

reproduction of the acoustic waveform. This may be a drawback in studies where such a reproduction is important. A second class of piezoelectric material has been developed to meet this requirement. By utilising a thin piezoelectric foil, a detector free from resonances in the frequency range of interest can be made. Such a broadband detector faithfully reproduces the acoustic waveform. One such piezoelectric material is polyvinylidenefluoride (PVF_2), and this can readily be formed into films 10 μm thick. As may be expected, one drawback of such materials is a reduced sensitivity as compared to piezoelectric ceramics.

2.5.2. Optical Detection

Several optical methods have been used to detect acoustic waves in different media. These are techniques that in general offer broadband, non-contact detection. Three techniques that have been used to detect photoacoustic waves are described below.

Mechanical Beam Deflection

One technique for the detection of acoustic waves by optical means is that of a mechanical beam deflection. This is caused by the small acoustic displacements deforming a thin reflecting optical surface. A probe beam directed at the external surface of this mirror is deflected such that intensity variations at a detector may be observed. The technique has found application primarily in the photoacoustic analysis of gases (2.17). It has also been used in detecting temperature variations of 10^{-9} °C (2.18).

Beam Lensing

The principle behind the detection of photoacoustic waves by beam lensing is the change of the bulk refractive index of a sample via density or temperature variations. A probe beam is deflected such that intensity variations can be detected by a small area detector. Sullivan & Tam (2.11) used a probe beam parallel to the

excitation beam to obtain broadband data about PA waveforms generated in methanol. The intensity signal measured in this way is the time derivative of the photoacoustically generated pressure.

Interferometry

Optical interferometers detect changes in many physical parameters (e.g. temperature, pressure) through the effect these changes have on the optical pathlength of a beam. By comparing this beam with an unperturbed reference beam, an interference pattern, modulated by the physical changes, may be observed.

Interferometers of various types have found use in detecting acoustic waves, for example by measuring the sub-nanometre displacements (2.19) or phase modulation (2.20) these cause. This technique has found application particularly in the non-destructive testing (NDT) of solids, and combined with the laser generation of ultrasound forms an all optical, reproducible test-bed (2.19). The detection of acoustic waves in liquids by interferometry can work on the same principles, but the low optical reflection coefficient at an air / water interface is just one factor in lowering the sensitivity of the technique.

Interferometers can be made rugged by incorporating them into an optical fibre and this also allows the possibility of a portable system with considerable flexibility in the positioning of the measurement head. The use of a fibre optic interferometer to detect photoacoustic waves in liquids will be discussed more fully in Chapter 6.

2.5.3. Piezoelectric Detector Design

For reasons of sensitivity, size and cost, piezoelectric ceramic transducers have been used almost exclusively as the basis of the photoacoustic detectors used in this thesis. Several considerations must be taken into account when designing a detector of photoacoustic waves based on a piezoelectric transducer. The detector geometry to couple the acoustic signal most efficiently to a transducer depends upon the spatial profile of the acoustic source. The optical absorption coefficient of the

sample determines whether the acoustic source can be treated as a cylinder (low absorption) or as a disc (high absorption). Most cases presented in this thesis are of low optical absorption and an acoustic source approximating a cylinder. A hollow cylindrical piezoelectric transducer would form the most sensitive detector, to interact with the maximum acoustic signal. However an instrument based on such a detector geometry is difficult to achieve in a flowing pipeline system, in which the instrument is to be installed from the side. Thus most detectors used in this study have been based on a solid piezoelectric disc situated a few millimetres below the optic axis, oriented with its flat surfaces parallel to the optic axis.

In experiments using a cuvette to hold the sample, the length of the acoustic source is, in cases of low absorption, determined by the optical pathlength of the cuvette. As discussed in Section 2.4.1, only acoustic waves impinging within a shallow angle will be coupled into a solid from a liquid as longitudinal waves. This imposes an effective acoustic source length on the detector arrangement which is slightly larger than the dimension of the piezoelectric in the direction of the optic axis. For similar reasons of acoustic reflection, there is little point in increasing the lateral dimension of the piezoelectric transducer beyond the optical spot size.

In order to prevent excessive acoustic reflections at the rear face of the piezoelectric element, and consequent ringing, a backing material of acoustic impedance similar to that of the element should be used. Ideally this material should also provide attenuation of the acoustic energy. The resonances of a ceramic element mounted in this way will be modified by such damping.

The magnitude of the electrical signal, S developed by a piezoelectric transducer is proportional to the pressure, such that from equation {2.16},

$$|S| \propto |p| = k.\frac{\alpha\beta\upsilon^{m}}{C_p}.E_0 \qquad \{2.21\}$$

where in this thesis, the magnitude of S corresponds to voltage difference between the first maxima and first minima of the signal. In most cases of photoacoustic

spectroscopy, it is desirable to normalise the PA signal to the input optical energy. In this thesis, the parameter P is most commonly plotted, where

$$P = \frac{|S|}{E0}. \qquad \{2.22\}$$

P is presented as having no units since both S and E_0 are measured as voltages. Several piezoelectric detector designs have been used for the purposes of this thesis. The important features of the detector geometry are shown schematically in fig. 2.5.

2.6. Applications

2.6.1. Applications of Photoacoustics

Photoacoustic spectroscopy has long been recognised as a powerful technique in the analysis of the optical properties of materials that may be difficult to characterise by other optical methods. In particular, PAS finds application in the characterisation of samples of very low or very high optical absorption, as well as scattering and powdered samples. The low detection limits for the optical absorption coefficient leads to the technique finding many applications in trace analysis (2.21), including pollution monitoring in liquids (2.22) and gases (2.23). This thesis is concerned primarily with such an application.

The photoacoustic effect has however found a much wider scope of application, a little of which is presented here for completeness. A comprehensive review of photoacoustic techniques and applications has also been given by Tam (2.3). The measurement of physical parameters is a field in which the PA effect has found wide use. A measurement of the thermal conductivity and heat capacity of transparent liquids has recently been reported by Leite and Miranda (2.24), and lifetime measurements using a broadband acoustic detector have also been made (2.25). The energy relaxation pathways following optical absorption may be deduced from photoacoustic measurements. Simultaneous multiple wavelength photoacoustic

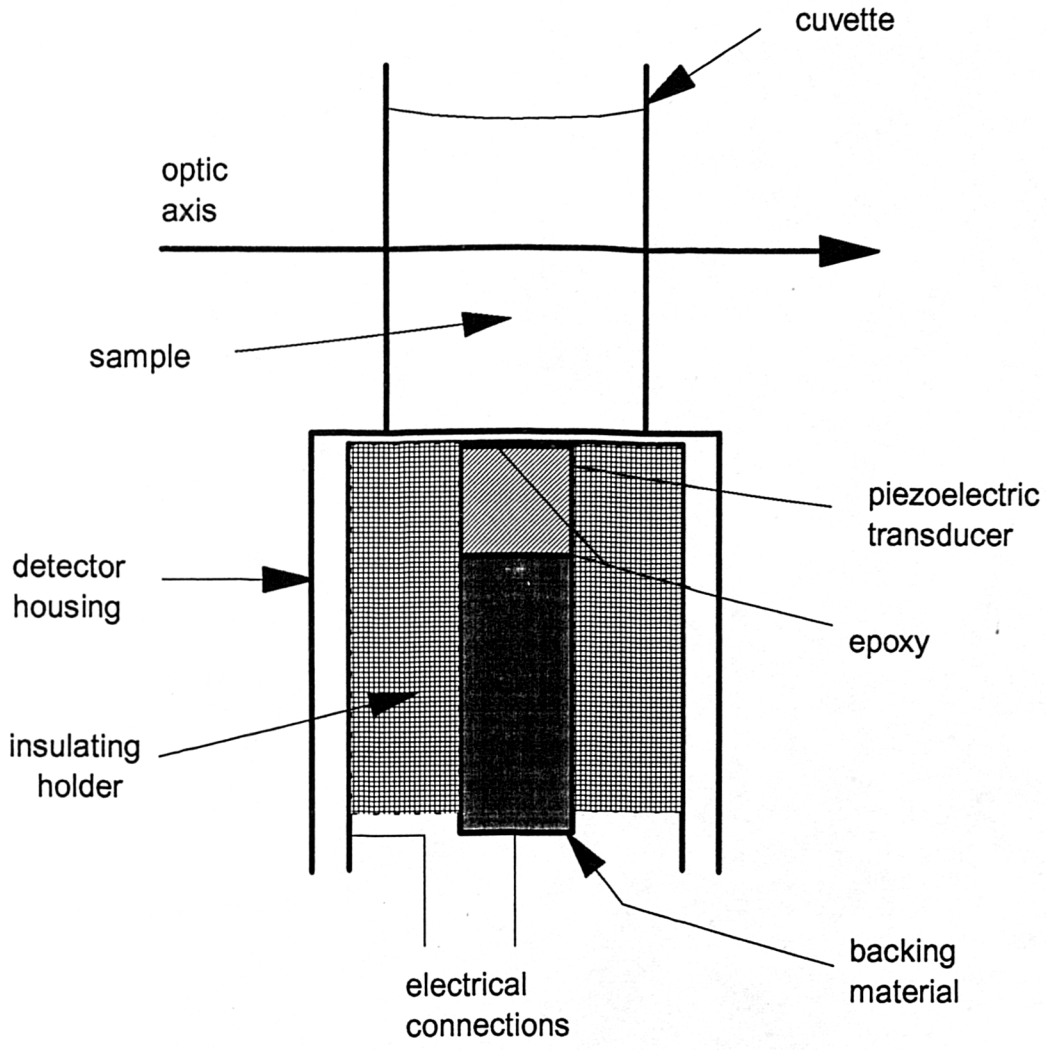

Fig. 2.5 Geometry of Cuvette Based Piezoelectric Photoacoustic Detectors

and luminescence measurements have recently been used to determine the fluorescent quantum efficiency (2.26). The nature of photoacoustically generated waves is very dependent upon the excitation source and the sample. Therefore a photoacoustic measurement can be used within feedback systems to aid process control, for example in laser ablation processes (2.27).

2.6.2. PAS of Hydrocarbons and other Organic Liquids

Photoacoustic spectroscopy has found use in the analysis of hydrocarbons and other organic liquids. The eighth harmonic of the C-H stretch in benzene has been spectrally characterised by Patel *et. al.* (2.28). This data was used to derive an improved anharmonic formula for spectral band assignment in benzene. The assignment of the near infrared bands of several other aromatic and aliphatic hydrocarbons by PAS has been reported by several authors (2.29, 2.30), showing that spectral selectivity is not diminished by the photoacoustic effect. Quantitative analysis of the aromaticity of organic mixtures, including crude oil diluted in benzene has also been presented in (2.29). The photoacoustic analysis of water and methanol has shown internal structural changes in the liquids at an interface with air (2.31), by utilising the ability of CW PAS to obtain a depth profile of a sample by the alteration of the modulation frequency.

Photoacoustic spectroscopy continues to find application in many areas, including trace analysis in liquids. The detection of oil in water is currently an important one, to which the photoacoustic effect is well suited. Experiments that show some of the key aspects of this are described in the following chapters.

2.7. References

(2.1) Bell A.G., *Am. J. Sci.*, 20, 305, 1880

(2.2) Askar'yan G.A. Prokhorov A.M., Chanturiya G.F., Shipulo G.P., *Sov. Phys. JETP*, **17**(6), 1463, 1963

(2.3) Tam A.C., *Rev. Mod. Phys.*, **58**(2), 381, 1986

(2.4) Kreuzer L.B., *J. Appl. Phys.*, **42**(7), 2934, 1971

(2.5) Rosencwaig A., *Opt. Comm.*, **7**(4), 305, 1973

(2.6) Rosencwaig A., Gersho A., *J. Appl. Phys.*, **47**(1), 64, 1976

(2.7) Patel C.K.N., Tam A.C., *Rev. Mod. Phys.*, **53**, 517, 1981

(2.8) Lai H.M., Young K., *J. Acoust. Soc. Am.*, **72**(6), 2000, 1982

(2.9) Heritier J-M., *Opt. Comm.*, **44**(4), 267, 1983

(2.10) Quan K.M., MacKenzie H.A., Hodgson P., Christison G.B., *Ultrasonics*, **32**(3), 181, 1994

(2.11) Sullivan B., Tam A.C., *J. Acoust. Soc. Am.*, **75**(2), 437, 1984

(2.12) Helander P., Lundstrom I., McQueen D., *J. Appl. Phys.*, **51**(7), 3841, 1980

(2.13) Oda S., Sawada T., Moriguchi T., Kamada H., *Anal. Chem.*, **52**, 650, 1980

(2.14) Yasa Z.A., Jackson W.B., Amer N.M., *Appl. Optics*, **21**(1), 21, 1982

(2.15) Helander P., *J. Appl. Phys.*, **54**(6), 3410, 1983

(2.16) Kino G.S., "Acoustic Waves: Devices, Imaging, and Analog Signal Processing", Prentice-Hall, Inc., © 1987

(2.17) Choi J.G., Diebold G.J., *Appl. Optics*, **21**(22), 4087, 1982

(2.18) de Paula M.H., Vinha C.A., Badini R.G., *Rev. Sci. Instrum.*, **63**(6), 3487, 1992

(2.19) Hoyes J.B., Shan Q., Dewhurst R.J., *Meas. Sci. Technol.*, **2**, 628, 1991

(2.20) Bucaro J.A., Dardy H.D., Carome E.F., *J. Acoust. Soc. Am.*, **62**(5), 1302, 1977

(2.21) Vargas H., Miranda L.C.M., *Phys. Rep.*, **161**(2), 1988

(2.22) Hodgson P., MacKenzie H.A., Christison G.B., Quan K.M., in "Near Infrared Spectroscopy: bridging the gap between data analysis in NIR applications", pg 407, Ellis Horwood, 1992

(2.23) Sigrist M.W., Bernegger S., Meyer P.L., *Infrared Phys.*, **29**(2-4), 805, 1989

(2.24) Leite N.F., Miranda L.C.M., *Rev. Sci. Instrum.*, **63**(10), 4398, 1992

(2.25) Heihoff K., Braslavsky S.E., *Chem. Phys. Lett.*, **131**(3), 183, 1986

(2.26) Rodriguez E., Tocho J.O., Cusso F., *Phys. Rev. B*, **47**(21), 14049, 1993

(2.27) Leung W.P., Tam A.C., *Appl. Phys. Lett.*, **60**(1), 23, 1992

(2.28) Patel C.K.N., Tam A.C., Kerl R.J., *J. Chem. Phys.*, **71**(3), 1470, 1979

(2.29) Adams M.J., Beadle B.C., Kirkbright G.F., *Anal. Chem.*, **50**(9), 1371, 1978

(2.30) Lewis L.N., *J. of Organometallic Chem.*, **234**, 355, 1982

(2.31) Haas U., *Can. J. Phys.*, **64**, 1063, 1986

CHAPTER 3

Near Infrared Spectroscopy

3.1. Overview

This chapter aims to clarify the similarities and differences between conventional transmission spectroscopy and pulsed photoacoustic spectroscopy, highlighting some of the advantages and disadvantages of each. The chapter commences with the pertinent fundamentals of molecular spectroscopy and outlines some of the most important resonances and their near infrared features that are of particular relevance to this thesis. A detailed description of the photoacoustic effect may be found in earlier chapters whilst a short resume of transmission spectroscopy techniques is given here. A brief section describes how a tunable near infrared source was created using Raman processes in an optical fibre, and how this source was used to perform photoacoustic spectroscopy. A comparison of the pure compound spectra of water and hydrocarbons obtained by transmission and photoacoustic techniques is then presented. Saturation effects on the resulting photoacoustic spectra are discussed before a presentation of results showing how the presence of scattering particles in the sample may affect the interpretation and analysis of data acquired by these methods.

3.2. Molecular Resonances

A molecule will interact with incident electromagnetic radiation in different ways, depending upon the photon wavelength λ, and the incident intensity I_0. Visible light (400 - 700 nm) leads to electronic transitions, whereas infrared (IR) radiation (2.5 - 100μm) excites vibrational and rotational (in gases) energy levels within a molecule. The near infrared (NIR) spectral region (0.7 - 2.5μm) falls between the visible and infrared, but has many absorption features (3.1), comprising overtones of fundamental infrared excitations, combination bands (the result of an interaction between two or more vibrations), and low energy electronic transitions, leading to a wavelength region rich in spectral information. Although the NIR spectral features tend to be of broad linewidth in liquids and are weaker than infrared excitations, the NIR is used in many varied applications. Indeed, one reason for this is the lower optical absorption coefficients typical of the NIR which allow a greater penetration depth into liquid and solid samples than could be achieved in the IR, and a measurement of the bulk material to be made.

3.2.1. Vibrational Modes

A simple multi-atomic molecule has in general several associated vibrational modes, the frequencies of which depend upon the masses of the individual atomic constituents of the molecule and the strength of bonding forces between the atomic constituents. Complex molecules may often be thought of as being made up of a particular combination of such simple functional groups. Although the presence of additional bonds and neighbouring functional groups in more complex molecules has an effect on the strength and frequency of the rudimentary vibrational modes, it is usually quite possible to assign the spectral features of such a complex molecule to its constituent functional groups.

O-H bonds

The O-H bond occurs in water (H_2O) and in alcohols, and plays an important role in determining the structure of these liquids through hydrogen bonding. O-H vibration modes are strongly dependent upon the neighbouring molecular structure. In the NIR, the strongest O-H resonances in water are found at 1.44 μm (second stretching harmonic) and 1.93 μm (combination of stretching and deformation vibrations). The O-H resonances in other molecules, for example alcohols, can occur at quite different wavelengths (3.2). The second harmonic of the O-H stretch in methanol occurs at 1.55 μm.

C-H bonds

An isolated C-H bond has a fundamental stretching frequency of approximately 3000 cm^{-1} (3.3 μm). The symmetric and anti-symmetric resonant stretching frequencies of CH_2 and CH_3 groups are also very close to this value and as a consequence many organic compounds display absorption features within a band centred on 3.3 μm. Higher harmonics of this vibrational mode occur in the NIR at wavelengths close to 1.7 μm, 1.2 μm and 0.9 μm. In addition C-H groups have bending (deformation) vibrations. The CH_2 group has a bending mode at 6.8 μm, the third and fourth harmonics of which are at 2.3 μm and 1.7 μm respectively (3.3). Benzene (C_6H_6) has relatively sharp NIR absorption features because of its unique ring structure; the resonance at 1.66 μm is particularly strong.

3.3. Pure Compound Spectroscopy

3.3.1. Transmission Spectroscopy

Conventional transmission spectroscopy is based on the comparison of the intensity of monochromatic light transmitted by a sample to the incident intensity, and through Beer's Law allows the determination of the optical absorption coefficient.

$$\frac{I}{I_0} = e^{-\alpha l} = T \qquad \{3.1\}$$

I = transmitted intensity I_0 = incident intensity

α = sample optical absorption coefficient l = sample path length

T = transmittance (also often expressed as a percentage).

Transmission spectroscopy is a very sensitive analytical technique, and well established commercially. All the transmission measurements included in this thesis were performed on a Shimadzu UV-3100 spectrophotometer. This is a dual beam instrument (sample and reference channel) which can compensate for fluctuations in ambient conditions such as temperature, and instrument deviations such as source intensity. The instrument measures the base 10 logarithm of the ratio of the two transmitted intensities (Abs), and a simple algorithm allows the calculation of the sample absorption coefficient from this measurement.

$$Abs = 0.434[\alpha.l - \alpha_r.l_r] \qquad \{3.2\}$$

where α_r and l_r relate to the reference channel. When α_r is zero, Abs is equivalent to the optical density, O.D.. The dual beam facility is especially useful when measuring small changes in α on large background signals.

Optical density plots of 1 and 2 mm of distilled water over a wavelength range 1.1 - 2.5 μm are compared in fig. 3.1, measured when using an empty cuvette as a reference. Noise in the instrument imposes an upper limit of 4 on the measurable O.D.. The 1 mm result has been converted to optical absorption coefficient in fig. 3.2. Over this region, the absorption coefficient of water varies by approximately three orders of magnitude, from 0.1 cm^{-1} to over 100 cm^{-1}. This large dynamic range is an important consideration when determining the optical path length of sample holders for photoacoustic as well as transmission spectral measurements and whether signal saturation may be occurring.

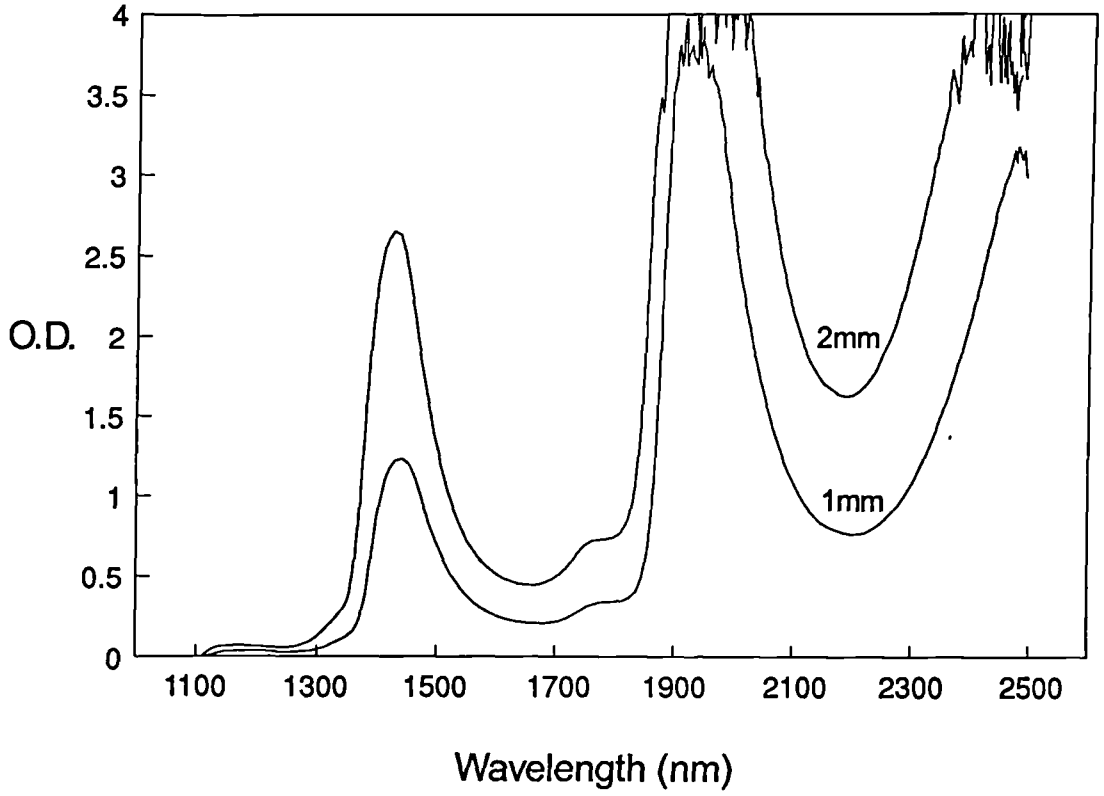

Fig. 3.1 Near Infrared Optical Density Plots of Distilled Water

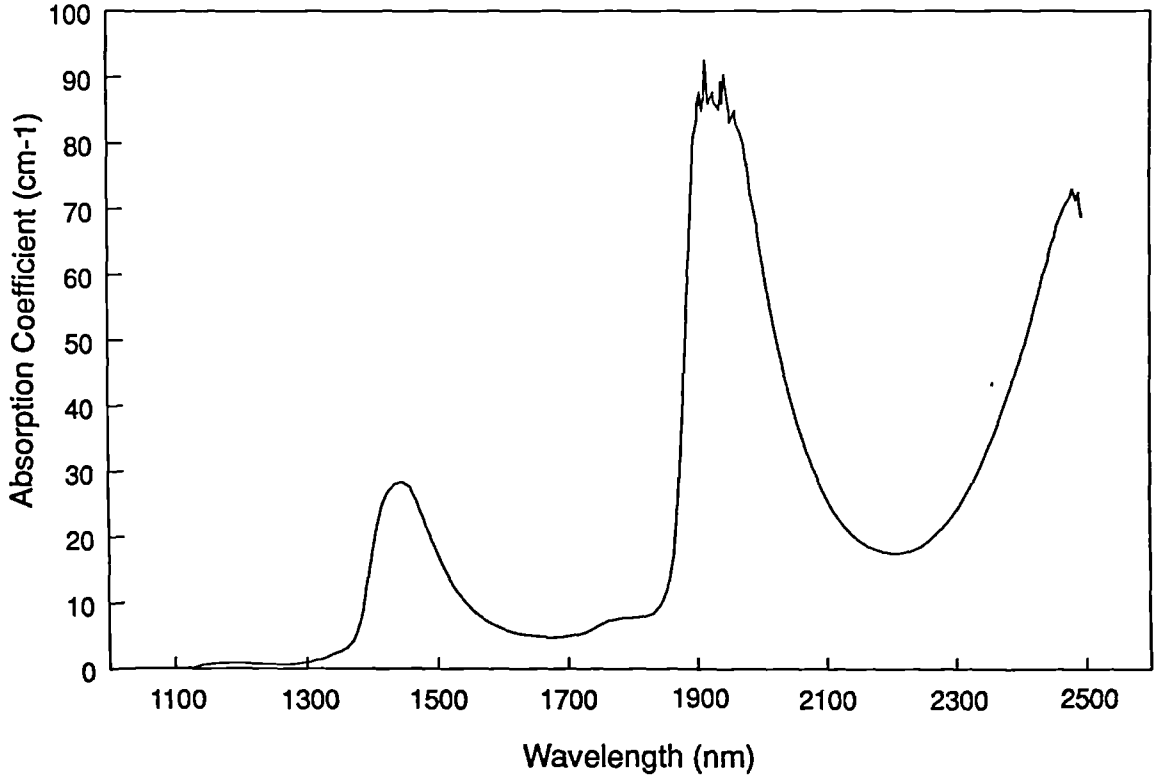

Fig. 3.2 Near Infrared Absorption Spectrum of Distilled Water

The Near Infrared Atlas (3.4) should be referred to as a comprehensive library of the transmission spectra of other liquids in this spectral region.

3.3.2. Photoacoustic Spectroscopy

Chapter 2 details the conventional theory of the photoacoustic effect by pulsed excitation in liquids. Photoacoustic spectroscopy is a direct measure of the optical energy absorbed by a sample, in contrast to transmission spectroscopy in which the transmitted energy is measured. The conversion efficiency from optical to acoustic energy is usually low (*e.g.* 10^{-6}) in cases where thermoelastic expansion is the dominant mechanism for acoustic generation. However, piezoelectric detectors are extremely sensitive, a fact that means acoustic measurements can be made with low input optical energies. Whereas transmission spectroscopy is most suited to the analysis of samples with intermediate absorption coefficients, photoacoustic spectroscopy can be used with both low and high absorbing materials.

3.3.2.1. Tunable NIR Radiation by Stimulated Raman Scattering

When high power radiation propagates in an optical fibre, the high intensities maintained in the core of the waveguide produce frequency shifted radiation of longer wavelength (the Stokes wave) by single pass Stimulated Raman Scattering (SRS) (3.5). The generated frequency shift and the critical pump power, P_c are material dependent, and may be calculated from the Raman gain coefficient, g_R. A plot of the gain coefficient against frequency shift for SiO_2 and a pump wavelength of 1.0 μm is shown in fig. 3.3 (3.6). Other glasses (or dopants in SiO_2) yield different gain coefficients. The critical pump power is given by (3.7)

$$P_c \approx \frac{16A}{g_R . L_{eff}} \qquad \{3.3\}$$

where A is the fibre core area, and L_{eff} is the effective fibre length, defined below. The confinement and low loss inherent in an optical fibre leads to a long interaction length and the possibility of many orders of Stokes radiation at the fibre output.

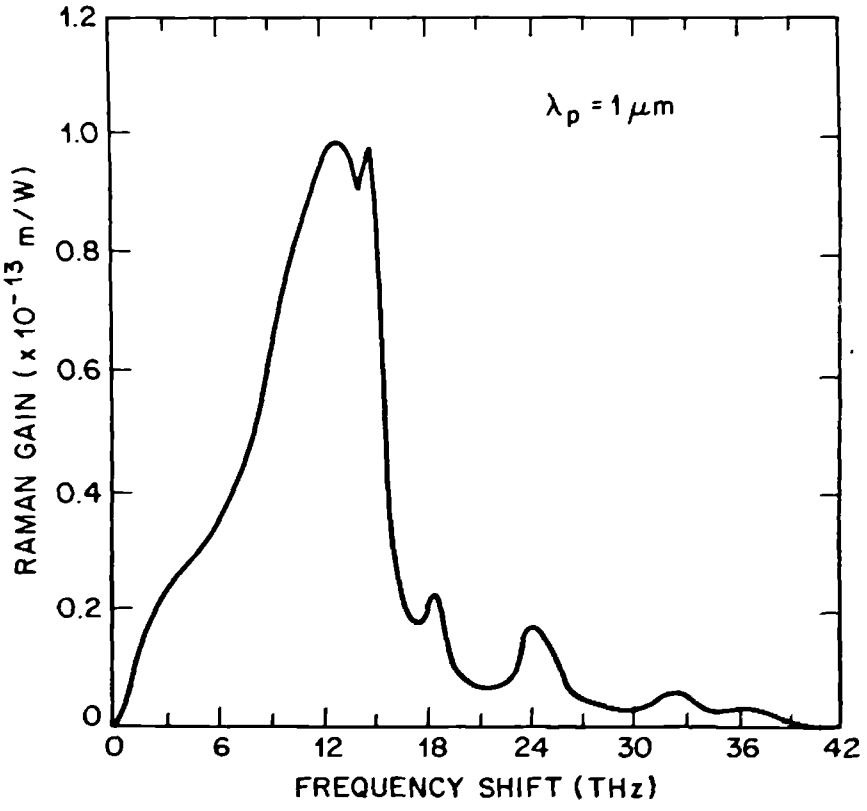

Fig. 3.3 Raman Gain Coefficient of SiO_2 © 1980 IEEE

Pulsed tunable radiation in the NIR for the purposes of photoacoustic spectroscopy was generated by pumping a 1 km length of graded index multimode optical fibre (STC CA1618/392F) with a Spectron Lasers Q-switched Nd:YAG laser (model SL50Q) emitting at 1.06 μm. The pulse duration of the pump (FWHM) was 180 ns and the pulse energy approximately 3 mJ. The pulse repetition rate was 200 Hz. The fibre attenuation at the pump wavelength was 1 dB/km, and the effective interaction length L_{eff}, given by (3.8)

$$L_{eff} = \frac{1}{\alpha_p}\left[1 - \exp(-\alpha_p L)\right] \qquad \{3.4\}$$

was 890m, a little less than the actual fibre length L due to the linear pump absorption α_p. Using equation {3.3}, the critical power for SRS was estimated to be 500 W, well below the peak power of 20 kW. The spectral output of the fibre is shown in fig. 3.4.

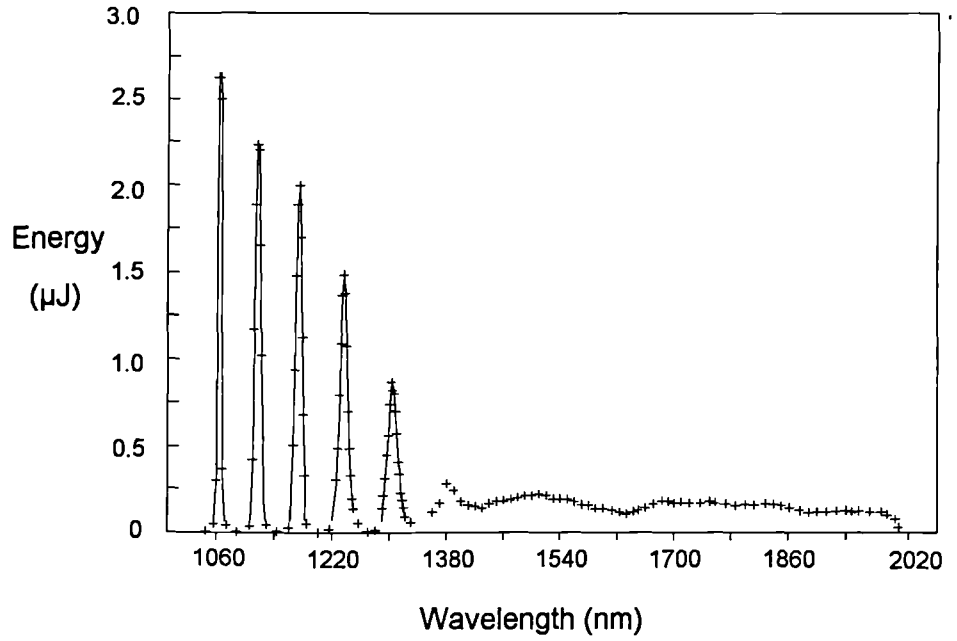

Fig. 3.4 Raman Fibre Output Spectrum

Eight Stokes orders were observed, the peak wavelengths being in good agreement with those predicted and previously observed for silica fibre (3.9). Through pump depletion effects the temporal profile of the output pulses displayed

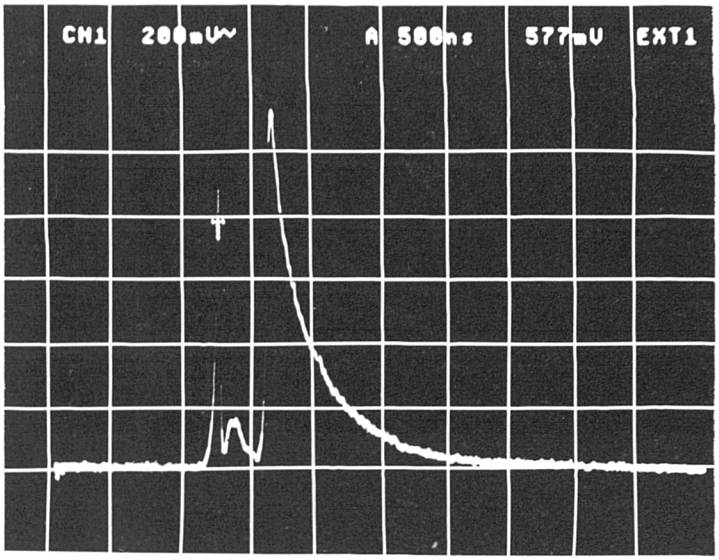

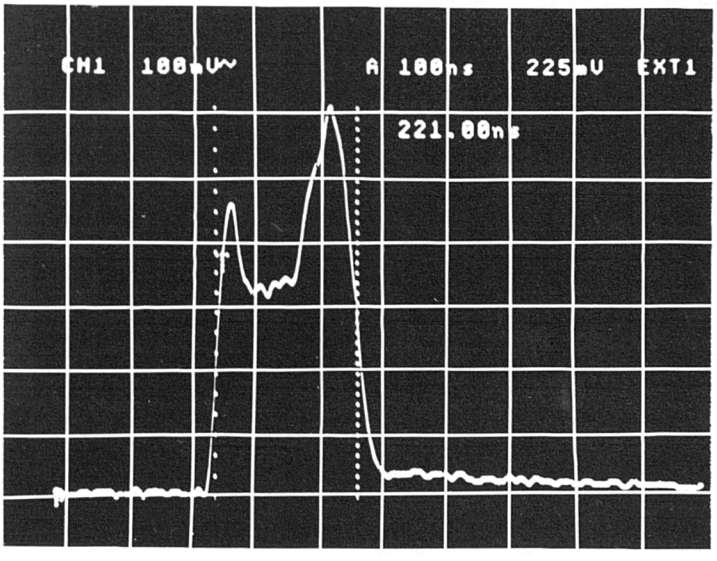

Fig. 3.5 Temporal Profile of Raman Fibre Output Pulses

at 1064 nm (upper trace) and 1550 nm (lower trace)

characteristic double peaks and narrow pulse envelopes (3.10) such that the output pulse duration varied between 190 ns and 600 ns depending on the wavelength. Fig. 3.5 shows the temporal profile of the Raman fibre output pulse at 1064 nm and 1500 nm. The output pulse energy varied by up to 30 % from the mean value, particularly at the shortest wavelengths of the range.

3.3.2.2. Generation of Photoacoustic Spectra

A SPEX MINIMATE monochromator was used to sequentially select wavelengths of the broadband fibre output for spectroscopic measurements. The linewidth determined by the monochromator in the long wavelength (continuum) region was 8 nm. The pump and the four lowest Stokes orders are of linewidths narrower than this. Fig. 3.6 is a schematic diagram of the tunable NIR source.

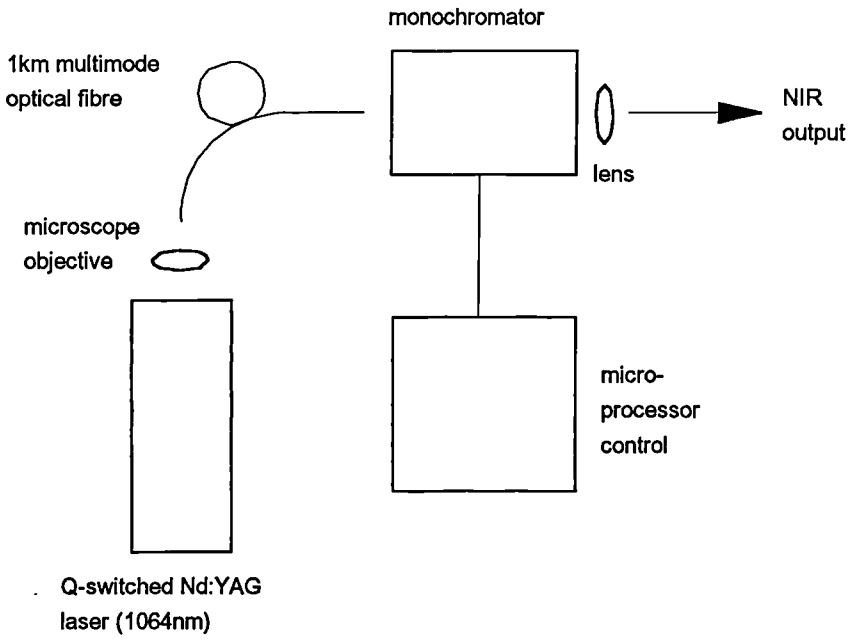

Fig. 3.6 Tunable NIR Source

A beam splitter was used to direct approximately 4% of the monochromator output to a Mullard A869 1503 pyroelectric detector with a 'flat' response at near infrared wavelengths, for pulse energy monitoring. A lens arrangement focussed the remainder of the optical beam into a quartz cuvette containing the sample. The spatial

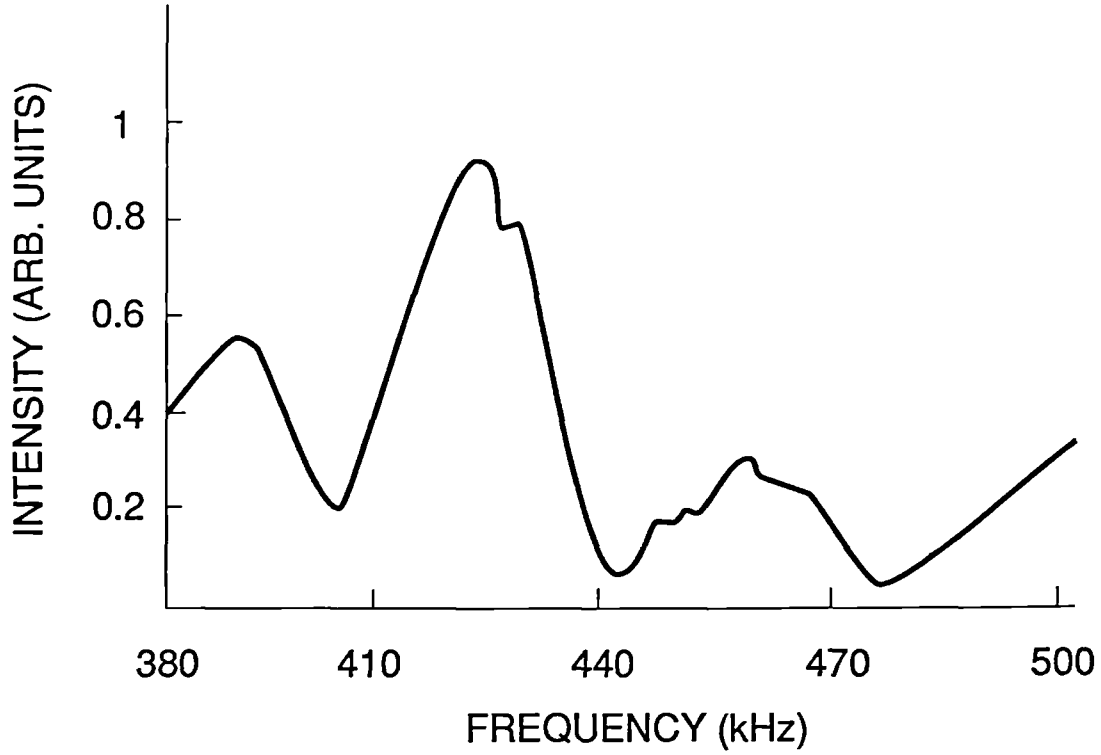

Fig. 3.7 Frequency Response of Piezoelectric Ceramic Detector

profile of the beam at the cuvette was approximately elliptical, the dimensions of which could be altered by choosing lenses of differing focal lengths. A typical focussed spot was 0.5 mm by 2 mm. Cuvettes with optical path lengths of 1, 2, 5, and 10 mm were used. A cylindrical piezoelectric ceramic (PZT 5A) element of diameter 4.8 mm and thickness 3.9 mm was fixed beneath the cuvette. The frequency response of this detector arrangement is shown in fig. 3.7 and highlights the detector resonance at approximately 420 kHz. 50 dB amplification of the photoacoustic signal was incorporated into the detector unit; the 3 dB points of the amplifier bandpass were at 30 kHz and 1.3 MHz.

A Tektronix 2430A digitising oscilloscope was used to acquire and display the photoacoustic and energy monitor signals. These could also be transferred to a PC via a GPIB interface for further analysis. In order to improve the signal to noise ratio, the averaging facility of the oscilloscope was employed, which allowed up to 256 averages to be analysed. The PC could also be used to select the wavelength of the monochromator output.

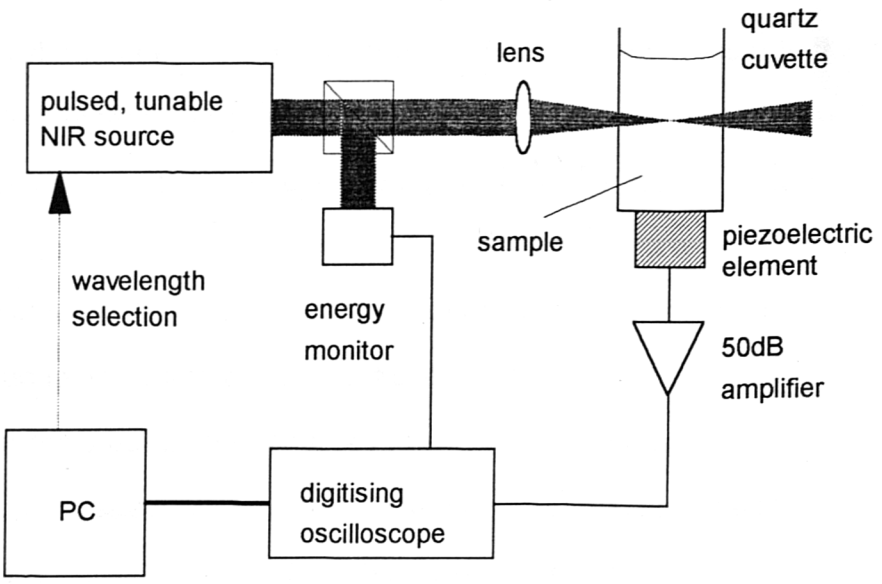

Fig. 3.8 Photoacoustic Spectrometer

Eighteen default wavelengths were generally used to generate photoacoustic spectra, chosen where appropriate to coincide with the fibre output peaks. The peak

to peak value of the piezoelectric transducer output (S) was ratioed to the optical pulse energy (E_0) at each measurement wavelength, to give the normalised signal P. The experimental arrangement is shown in figure 3.8.

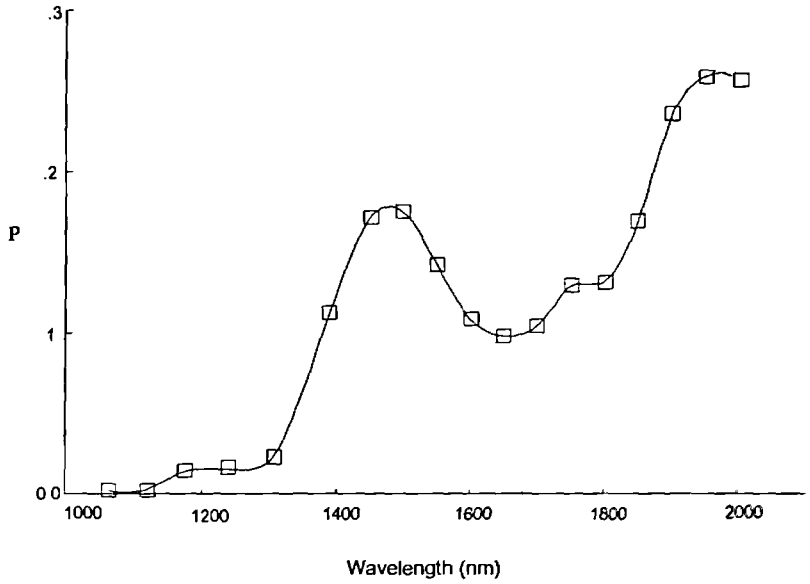

Fig. 3.9 Photoacoustic Spectrum of Distilled Water (1 mm)

The measured photoacoustic spectrum of water, obtained from a 1 mm cuvette, is shown in figure 3.9. The error estimate in P increases with the wavelength, and is given approximately by the symbol size. Comparison with figure 3.2 confirms that the photoacoustic spectrum is broadly similar to the corresponding absorption spectrum.

Photoacoustic spectra of two hydrocarbons and an alcohol have been acquired under the same conditions, as shown in fig. 3.10 and show clearly the same absorption features as are observed in conventional transmission spectroscopy. No loss of spectral selectivity due to the photoacoustic effect has been observed. This is further borne out in fig. 3.11, in which a comparison of the photoacoustic (sol'd curve) and absorption (dashed curve) spectra of benzene is made, centred on the second harmonic C-H stretch at 1660 nm. The spectral intervals were 10 nm and 1 nm, respectively.

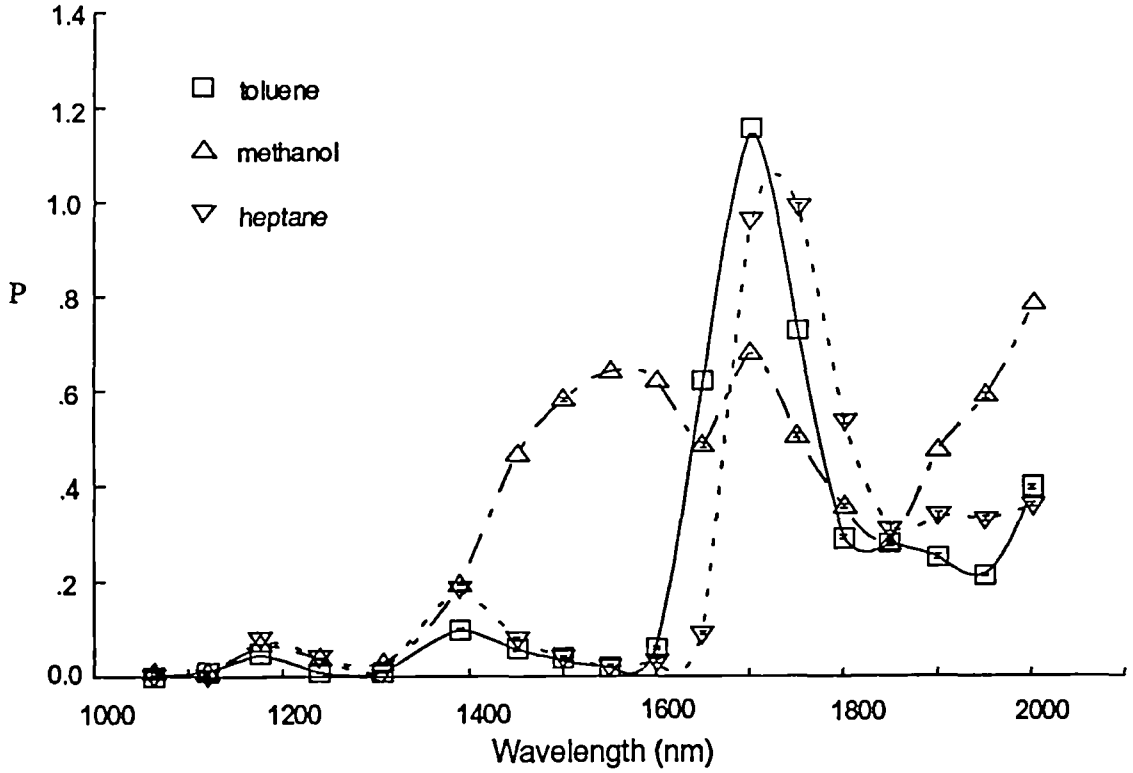

Fig. 3.10 Photoacoustic Spectra of Toluene, Heptane and Methanol

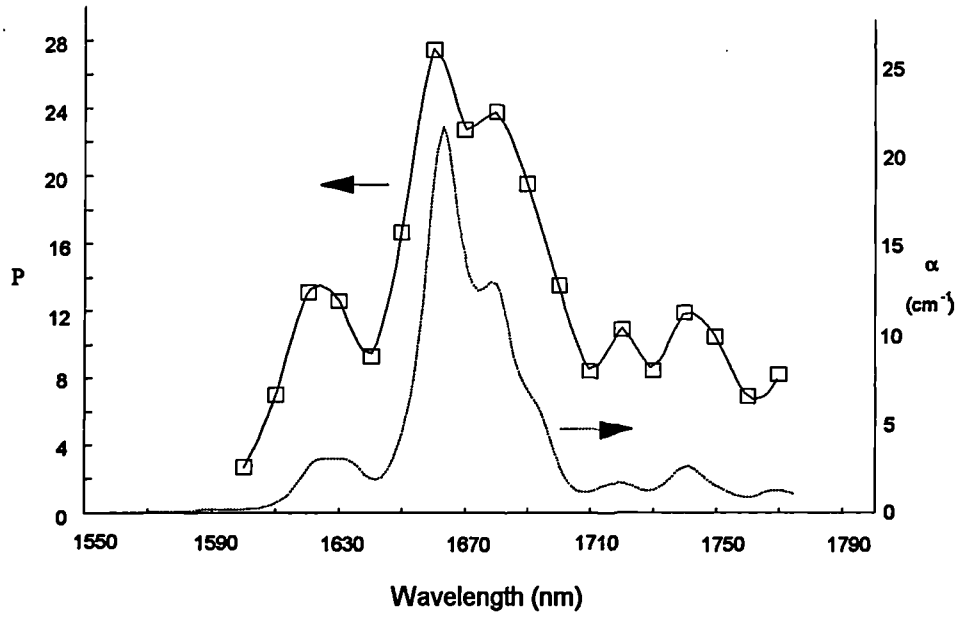

Fig. 3.11 Narrowband Spectra of Benzene (2nd C-H stretch)

3.3.2.3. Role of Physical Parameters

Chapter 2 formally describes the process by which acoustic waves are generated in liquids by the photoacoustic effect, and explains the dependence of the magnitude of the detected acoustic signal (normalised to the optical pulse energy) on several physical parameters of the sample, as summarised by equations {2.21} and {2.22} :

$$P = k.\left[\frac{\alpha\beta\upsilon^{m}}{C_p}\right] \qquad \{3.5\}$$

where β is the thermal expansion coefficient, C_p is the specific heat capacity, υ is the acoustic speed, k is a system constant and $1/2 < m < 2$.

Thus the differences between spectra due to sample absorption coefficients can be supplemented (or diminished) by the effect of these (non-wavelength dependent) physical parameters, and to a dramatic degree. This is particularly the case when comparing hydrocarbons and alcohols to water, since the thermal expansion coefficient and specific heat capacity in particular tend to result in much greater photoacoustic signals from such organic compounds. As an illustration of this, the factor in the square brackets in equation {3.5} has been calculated (m = 1/2) for

distilled water, methanol, benzene and pentane, at a wavelength where all the optical absorption coefficients are similar. This result has been compared to the magnitude of the experimental photoacoustic response at the same wavelength (normalised to water) in Table 3.1. A 5 mm cuvette was used.

Sample	α, cm^{-1} @ 1700 nm	C_p ($\times 10^3$) $Jkg^{-1}{}^{\circ}C^{-1}$	β ($\times 10^{-5}$) $^{\circ}C^{-1}$	υ ms^{-1}	PA factor (*c.f.* water)	PA measurement (*c.f.* water)
water	5.4	4.19	21	1483	1	1
methanol	9.2	2.52	119	1118	14	17
benzene	6.0	1.42	122	1321	18	16
pentane	9.2	2.36	155	1044	19	23

Table 3.1 Theoretical and Experimental Comparison of Photoacoustic Signals

There is excellent agreement between the predicted and measured values. The estimate of the error in each measured photoacoustic signal is $\pm$ 5%, due mainly to electronic noise in the acoustic detection unit. The remainder of the discrepancy is most likely due to differences in the acoustic source profile and the coupling efficiency of acoustic energy to the piezoelectric detector, as discussed in Chapter 2. At wavelengths where two different samples have the same optical absorption coefficient, and therefore the absorbed energy is the same, the photoacoustic effect can still distinguish between the two samples, because of the differences in optical to acoustic energy conversion efficiency.

Fig. 3.12 shows a broadband spectral comparison of distilled water and pentane. The upper plot is the absorption spectra, in which water is clearly the dominating species. Conversely in the photoacoustic spectra (lower plot), the response from pentane is overall far stronger than that from water. Thus photoacoustic methods have great potential in applications involving the detection of hydrocarbon / organic compound and water mixtures.

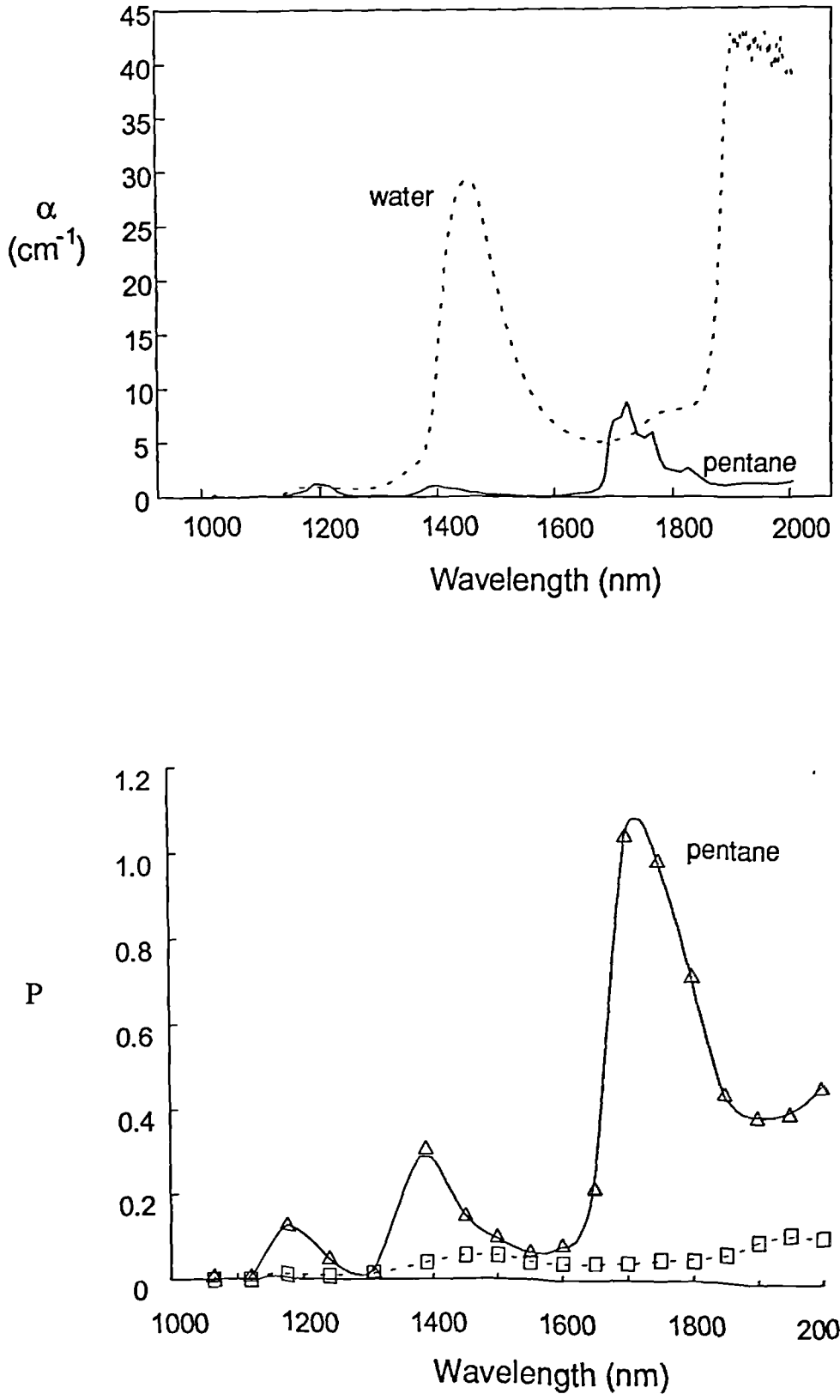

Fig. 3.12 Absorption (upper plot) and Photoacoustic Spectra of Water and Pentane

3.3.3. Saturation

In transmission spectroscopy, conditions of low optical absorption lead to the largest signal, whereas equation {3.5} leads to the conclusion that the photoacoustic signal is proportional to the optical absorption coefficient (at least for conditions where $\alpha.l << 1$). However, should $\alpha.l$ become so large that almost all the optical energy is absorbed within the confines of the sample holder, the photoacoustic signal will saturate. This effect is apparent in fig. 3.13, in which P has been plotted against α.

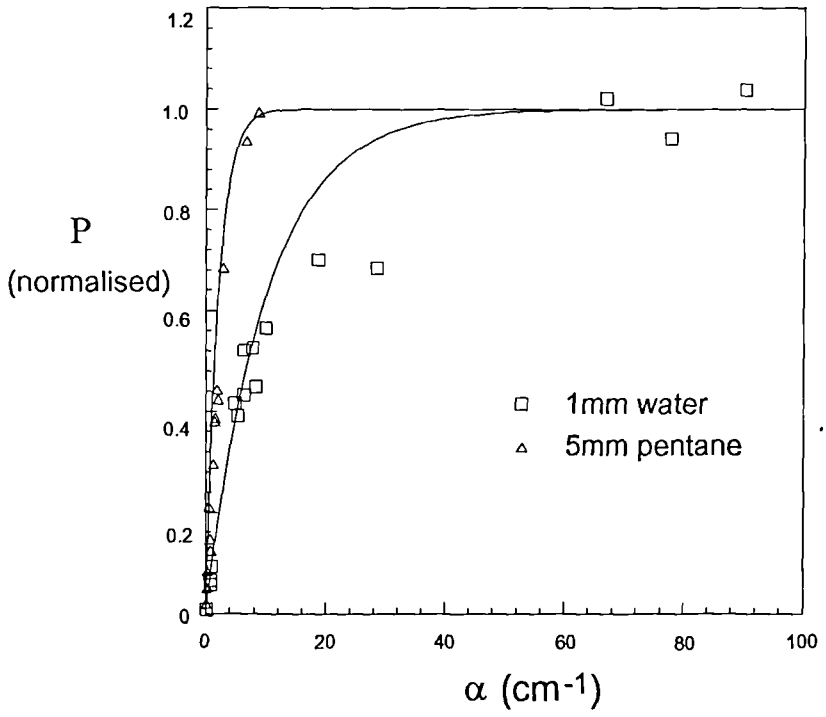

Fig. 3.13 Photoacoustic Signal Saturation

Experimental data from 1 mm water and 5 mm pentane are shown. The data have been normalised to the maximum photoacoustic signal generated in each sample. The large values (> 20 cm^{-1}) of some near infrared optical absorption coefficients of water, in particular those corresponding to the longer wavelengths, lead to photoacoustic signal saturation in a 1 mm path length cell. In the case of pentane, α < 10 cm^{-1} across the whole wavelength region. In a 5 mm cell, the effects of saturation are just becoming evident. The relative signal strength is greater than that obtained from a 1 mm cell, because of the greater interaction volume. The solid lines

are exponential curves representing the fraction of the input optical energy absorbed within the respective sample cells ($1-e^{-\alpha l}$) and show that the photoacoustic signal strength is to a large degree proportional to the absorbed energy.

The saturation effect leads to a familiar compromise between signal to noise ratio and signal contrast and a compromise must be made based on the sample optical absorption coefficients across the wavelength range of interest. For a 1 mm cuvette, optical absorption coefficients up to approximately 30 cm^{-1} display a satisfactory signal contrast.

3.4. Scattering

The presence of light-scattering particles in a sample under test can lead to considerable ambiguity in subsequent data analysis. In transmission spectroscopy, a loss of optical signal at the detector which is in fact due to scattering, may be mis-interpreted as an increase in the optical absorption coefficient. Any photon scattered off the optic axis is unlikely to impinge upon a detector positioned along it. Such a photon is still available for optical absorption, and may contribute to the generation of a photoacoustic signal. Thus in a sample containing scatterers, there is likely to be an increase in the number of photons absorbed. This increase in the total absorbed optical energy occurs concurrently with an increase in the illuminated volume. As discussed in Chapter 2, a larger illuminated region leads to a reduction in the peak to peak photoacoustic signal through a lower energy density and less localised heating. The relative magnitudes of these two opposing effects depends upon the ratio of α and the scattering coefficient K, and these consequently determine the overall effect on the generated photoacoustic signal. An experimental study to determine the effect on the photoacoustic spectra of the scattering likely to be encountered in an oil in water measurement is presented here.

3.4.1. Scattering Theory

Optical scattering results from inhomogeneities in the refractive index of a medium. The intensity and spatial distribution of the scattered light depends upon the size and shape of the inhomogeneities relative to the illuminating wavelength λ, and the refractive index disparity. Two cases are usually considered: Rayleigh scattering and Mie scattering, both of which are well established theories and covered in many texts (3.11, 3.12). Brief overviews of these theories are given here.

The effect of scattering in a sample can be thought of as a removal of a proportion of the incident intensity from the propagating beam, in much the same way as the effect of absorption. Beer's Law then becomes modified to

$$\frac{I}{I_0} = e^{-\alpha_{ex} l} \qquad \{3.6\}$$

where the extinction coefficient $\alpha_{ex} = \alpha + K$.

Rayleigh Scattering

In the case of the scattering particle having a major dimension, $a << \lambda$, the resultant scattering can be described by Rayleigh theory, which assumes that the instantaneous electric field is uniform over the extent of the particle. Thus an oscillating dipole moment is established within the particle, which radiates secondary waves of the same wavelength as the excitation isotropically. This forms the scattered radiation, and is of relatively low intensity. The most significant features of Rayleigh scattering are the λ^{-4} and a^6 dependencies of the scattered light intensity.

Mie Scattering

For larger particles the electromagnetic field across the particle can no longer be considered uniform and an alternative approach to determining the scattered light intensity must be taken. A beam incident upon a particle may be thought of as consisting of several individual rays which follow their own path. Scattering of the light occurs through reflection, refraction and diffraction. Mie theory may be used to

determine the fields at any point inside and outside the particle and thus the distribution of the scattered light. The scattered intensity tends to be greater than in Rayleigh scattering, but more forward directed.

3.4.2. Scattering Experiments

A comparison of the effect that the presence of scattering particles has on the spectra obtained in both transmission and photoacoustic experiments has been conducted, under a variety of scattering and absorbing conditions.

Sample Preparation

Particles of aluminium oxide (Al_2O_3) were used as the scattering particles in these experiments. The refractive index, n of Al_2O_3 is 1.76 at 1.0 μm, leading to a reflection coefficient in water (n = 1.33) of approximately 2 %. It was assumed that the particles were non-absorbing in the near infrared. Concentrations of scatterers up to 1000 milligrams per litre (≡ 1000 ppm by mass) were prepared in the sample liquid. A range of particle sizes was used in order to investigate the effect for different values of λ/a. Fig. 3.14 shows a photograph of nominally 3 μm Al_2O_3 particles. An indication of the actual size distribution and the range of shapes in one scattering sample can be obtained from this photograph.

Spectroscopy

A comparison of the effect that Al_2O_3 scatterers had on the transmission and photoacoustic spectra of pure methanol has been conducted. A concentration of 720 ppm 1 μm particles in methanol was used as the scattering sample. Fig. 3.15 (upper plot) shows the transmission spectra from 1 - 2 μm of the pure and scattering samples in a 1 mm pathlength cell. The presence of scatterers at this concentration clearly has a large effect on the transmission spectrum at all wavelengths in this range.

The photoacoustic spectra of the same samples measured under the same conditions are shown in fig. 3.15 (lower graph). Within the bounds of the experimental

Fig. 3.14 Electron Microscope Photograph of Al_2O_3 Particles

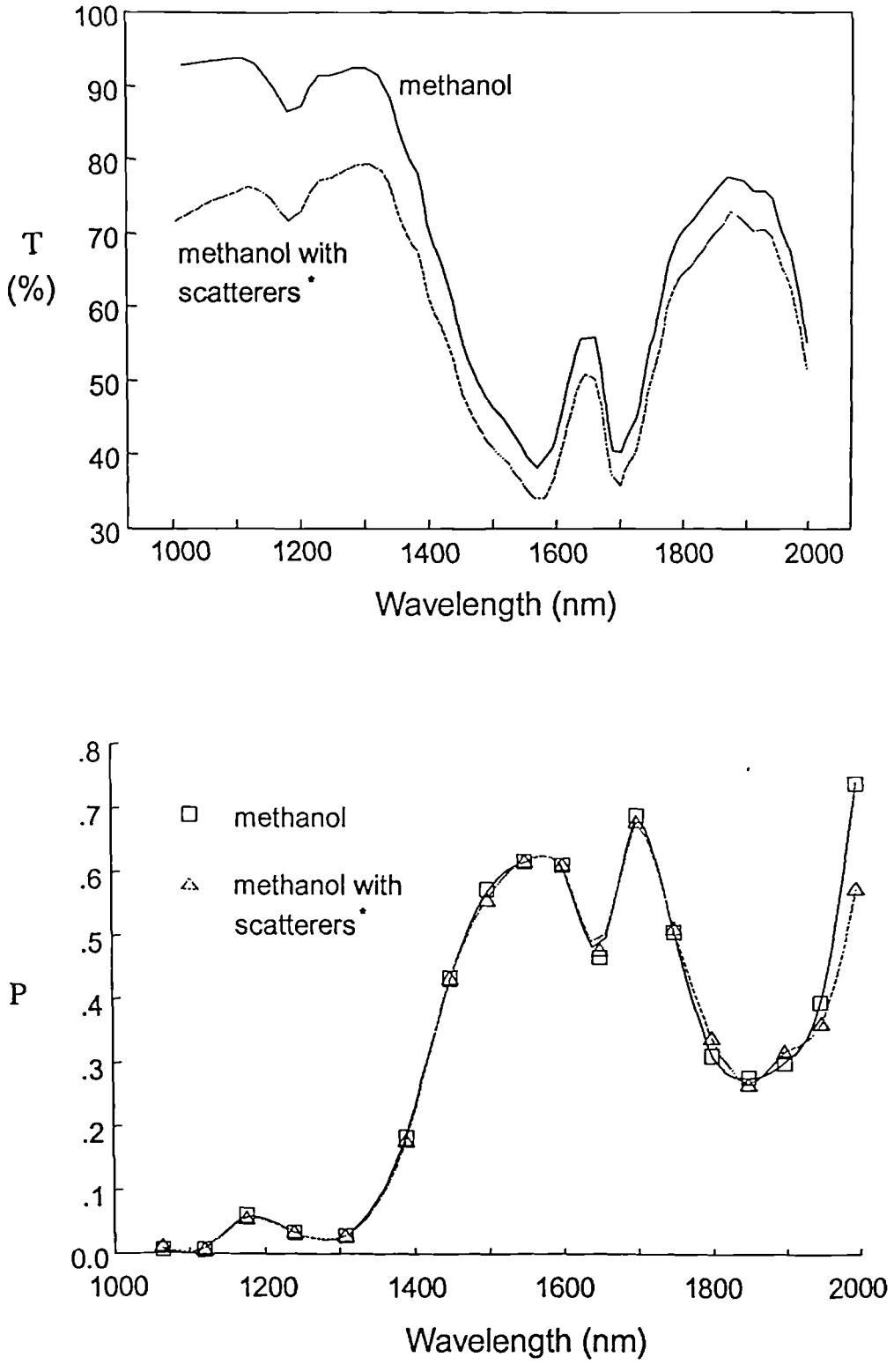

* 720 ppm 1μm Al_2O_3

Fig. 3.15 Effect of Scattering Particles on the Transmission (upper plot) and Photoacoustic Spectra of Methanol

error, there was no difference in the peak to peak photoacoustic signals obtained from the clear and scattering samples.

The effect of different scattering particle sizes and concentrations on the photoacoustic and transmission signals at 1450 nm in water (high optical absorption) has also been compared. Fig. 3.16 shows the signal loss (as a percentage of the signal from the pure water sample) as a function of the scattering concentration for particles of nominal size 0.3 and 3.0 μm. The transmission results show that the presence of scatterers can result in greater than a 25 % signal loss. In contrast, the photoacoustic signal magnitude is not affected by concentrations of scatterers up to 1000 mg/l, within the bounds of experimental error.

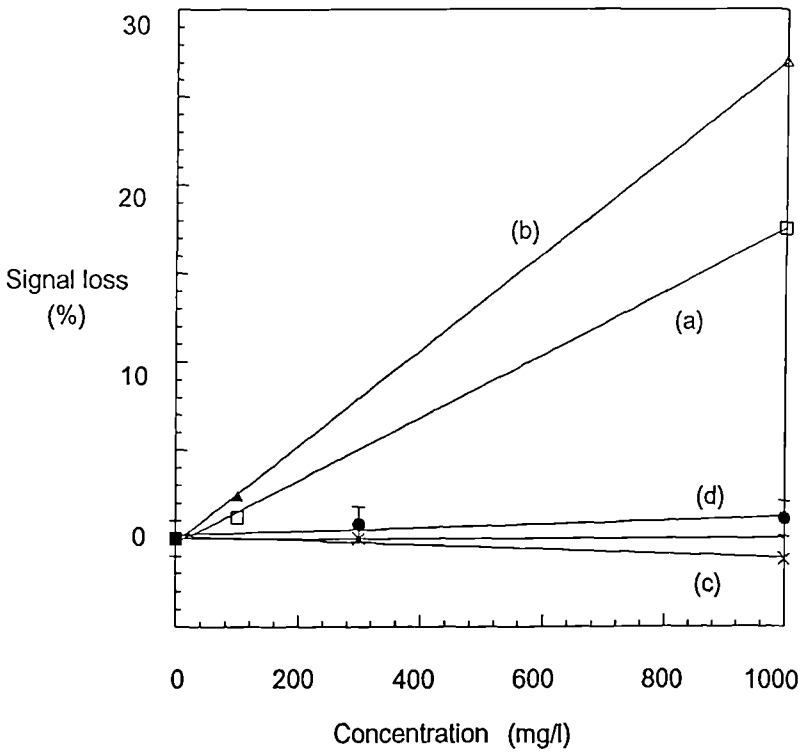

a) transmission loss (0.3μm)
b) transmission loss (3μm)
c) photoacoustic signal change (0.3μm)
d) photoacoustic signal change (3μm)

Fig. 3.16 Effect of scatterers on water signal at 1450 nm

Further experimental work has investigated more comprehensively the effect of scattering particles on the transmission spectroscopy of 2 mm of distilled water (3.13). The particle sizes were 0.05, 0.3, 1.0, 3.0, 9.0, and 15 μm and the concentrations were 100, 300, 500, 750, and 1000 mg/l. The wavelength range chosen for this study was 400 - 900 nm, since over this region the absorption coefficient of water is low (3.14) and the extinction coefficient was therefore dominated by the scattering processes within the sample. Thus the parameter λ/a was variable between 0.027 and 18. This study showed that the loss in the transmission signal was most severe when the parameter λ/a was close to unity. Subsequent photoacoustic experiments, in which oil droplets acted as scattering particles, are described in Chapter 4.

3.5. Discussion

Spectroscopy, in its many forms, is a vitally important scientific tool in numerous applications. The particular type of spectroscopy most suited to a specific application depends upon the measurand, the sample and its properties, as well as the measurement environment. Near infrared photoacoustic spectroscopy is well suited to applications of trace analysis, in which there is a large disparity in the optical absorption coefficient, the thermal expansion coefficient, the specific heat capacity and / or the speed of sound of the analyte and the background medium.

Transmission spectroscopy is most useful for samples of intermediate optical absorption. For high values of αl, the transmitted signal to noise ratio is low, whereas a low value of αl may mean there is little contrast between similar samples. Photoacoustic spectroscopy is most commonly used for the analysis of samples with either low or high values of αl, although it too may be used for intermediate samples. The conversion efficiency of optical energy to acoustic energy due to thermoelastic expansion is low. As a consequence, the detected signal in transmission spectroscopy is usually of higher energy than a photoacoustic signal. However, the

availability of very sensitive acoustic detectors in the form of piezoelectric ceramics means that low energy optical sources can be used as sources for analytical PAS.

Since many hydrocarbons have a high expansion coefficient, a low heat capacity and considerable differences in the absorption coefficient in the NIR compared to water, photoacoustic spectroscopy has great potential in the measurement of hydrocarbon and water mixtures. The thermal expansion, heat capacity and speed of sound of a sample are properties that are not wavelength dependent and their effect can be considered as an amplification (or attenuation) of differences in the optical absorption coefficient (3.15). In many hydrocarbons, these terms lead to a photoacoustic response more than an order of magnitude greater than the response from water, in regions where the optical absorption coefficients are similar.

A further key feature of photoacoustic spectroscopy is the performance in conditions of optical scattering. In samples where transmission spectroscopy has been shown to be subject to large signal changes with the presence of scattering particles, the photoacoustic response is largely unaffected. This occurs primarily because the photoacoustic signal is a measurement of the absorbed energy rather than the transmitted energy. Differences in the spatial profile of the acoustic source caused by scattering can be balanced by an increase in the mean photon path through the sample, and therefore an increased number of absorption events.

3.6. References

(3.1) Wheeler O.H., *Chem. Reviews*, **59**, 629, 1960

(3.2) Badger R.M., Bauer S.H., *J. Chem. Phys.*, **5**(11), 839, 1937

(3.3) Bellamy L.J., The Infrared Spectra of Complex Molecules Vol. 1, Chapman and Hall, 1975

(3.4) Sadtler, Atlas of Near Infrared Spectra, Sadtler Research Laboratories, Philadelphia, USA

(3.5) Agrawal G.P., Nonlinear Fiber Optics, Academic Press, London, 1989

(3.6) Stolen R.H., *Proc. IEEE*, **68**(10), 1232, 1980

(3.7) Smith R.G., *Appl. Optics*, **11**(11), 2489, 1972

(3.8) Stolen R.H., Ippen E.P., *Appl. Phys. Lett.*, **22**(6), 276, 1973

(3.9) Cohen L.G., Lin C., *IEEE J. Q. Elec.*, **QE-14**(11), 855, 1978

(3.10) Lin C., Cohen L.G., Stolen R.H., Tasker G.W., French W.G., *Opt. Comm.*, **20**(3), 426, 1977

(3.11) van de Hulst, H.C., Light Scattering by Small Particles, Wiley, New York, 1957

(3.12) Kerker M., The Scattering of Light, Academic Press, London, 1969

(3.13) Campbell A., Scattering in Photoacoustic Spectroscopy, 4th Year Project, Dept. of Physics, Heriot-Watt University, 1991-92

(3.14) Hale G.M., Querry M.R., *Appl. Optics*, **12**(3), 555, 1973

(3.15) Quan K.M., Christison G.B., MacKenzie H.A., Hodgson P., *Physics in Med. & Biol.*, **38**, 1911, 1993

CHAPTER 4

The Detection of Crude Oil Emulsions

4.1. Overview

This chapter describes experiments designed to investigate the feasibility of the photoacoustic technique as a method for detecting low concentrations of an analyte in an aqueous solution, with particular emphasis on the detection of crude oil emulsions at legislatively important limits in water. This study begins with an investigation of methanol concentrations in water, since this is a relatively simple system to analyse. The preparation and characterisation of oil in water emulsions is described and is followed by descriptions of the photoacoustic experiments performed on oil emulsions, to determine the feasibility and sensitivity of the technique. A detailed study of the acoustic waveforms generated by the photoacoustic effect in oil in water emulsions is then presented. The chapter concludes with a discussion on the merits of the photoacoustic technique for making an oil in water measurement.

4.2. Detection of Low C-H Concentrations in Water

The initial stages in the feasibility study of the relevance of the photoacoustic technique to the detection of oil in water were undertaken using samples of water and methanol. This system was chosen because of the complete miscibility of these two liquids. They therefore form a relatively simple system for a study of the detection of C-H bonds in an aqueous solution, free of difficulties in analysis arising from effects

such as scattering. Samples of methanol in distilled water were prepared, of concentrations ranging from 0.1% to 80% methanol by volume. Both conventional transmission and photoacoustic experiments were performed on these samples, to determine the nature of the spectroscopic responses at low concentrations of an analyte in water. For reference purposes the absorption spectra of distilled water and methanol are shown in fig. 4.1.

Transmission measurements of the methanol / water mixtures indicate that the optical absorption coefficient at 1700 nm increases linearly with methanol concentration, as shown in fig. 4.2. This optical activity may be attributed to excitation of the C-H bonds in the methanol. At wavelengths where water is the dominant absorbing species, such as 1420 nm, the optical absorption coefficient displays a linear decrease with increasing methanol concentration, as might be expected. This may be considered to be a substitution of the water molecules by larger methanol molecules (4.1). Since the peak water absorption is much greater than that of methanol, such regions of absorption coefficient reduction may be the most sensitive indicators of analyte concentration in aqueous solutions when using absorption spectroscopy. As discussed in Chapter 3, the dependence of the photoacoustic effect on other physical parameters can lead to a modification of the response from this singular dependence upon the optical absorption coefficient.

Photoacoustic spectra of methanol / water mixtures were obtained using the experimental system based on the Raman fibre source described in Chapter 3 and using a 1 mm pathlength cell. The spectrum of distilled water, together with the spectra of 10, 20 and 30% methanol by volume in distilled water are shown in fig. 4.3. The larger optical absorption coefficient of methanol at 1700 nm (due to C-H bonding) combined with the more favourable physical parameters of methanol for photoacoustic generation lead to an increasing response with increasing methanol concentration at that wavelength. At wavelengths where the optical absorption coefficient of water is dominant, such as 1450 nm, the decrease in the sample absorption coefficient as the methanol concentration is increased acts in opposition to

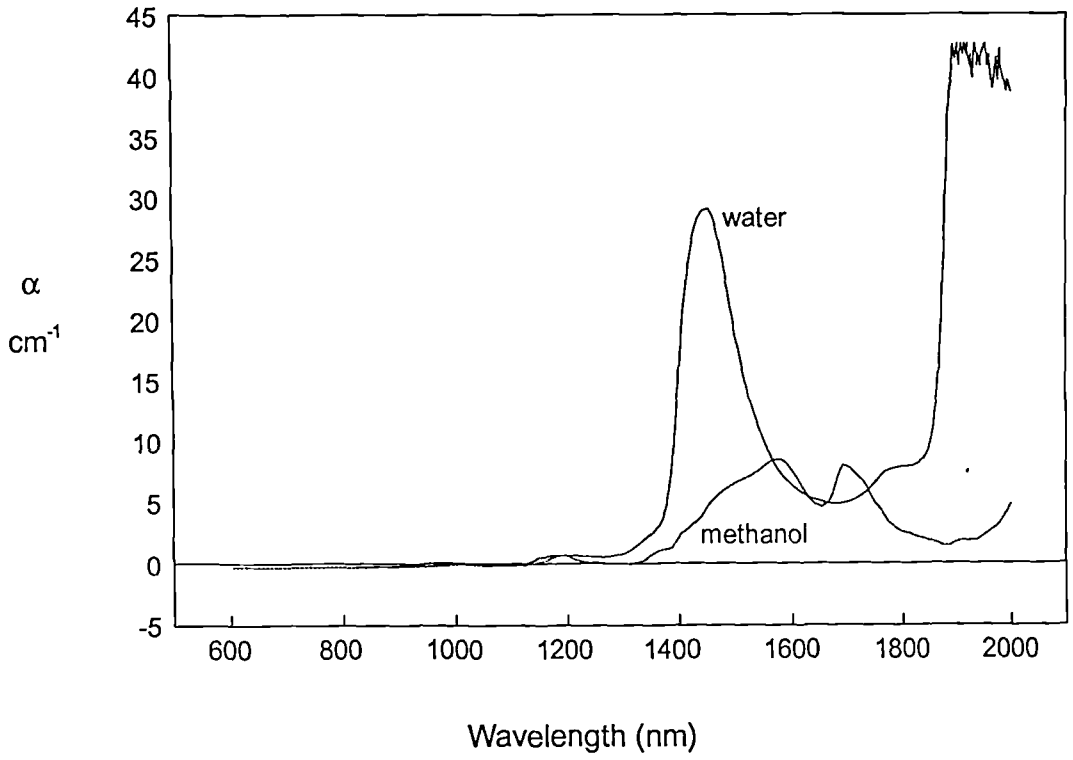

Fig. 4.1 Absorption Spectra of Distilled Water and Methanol

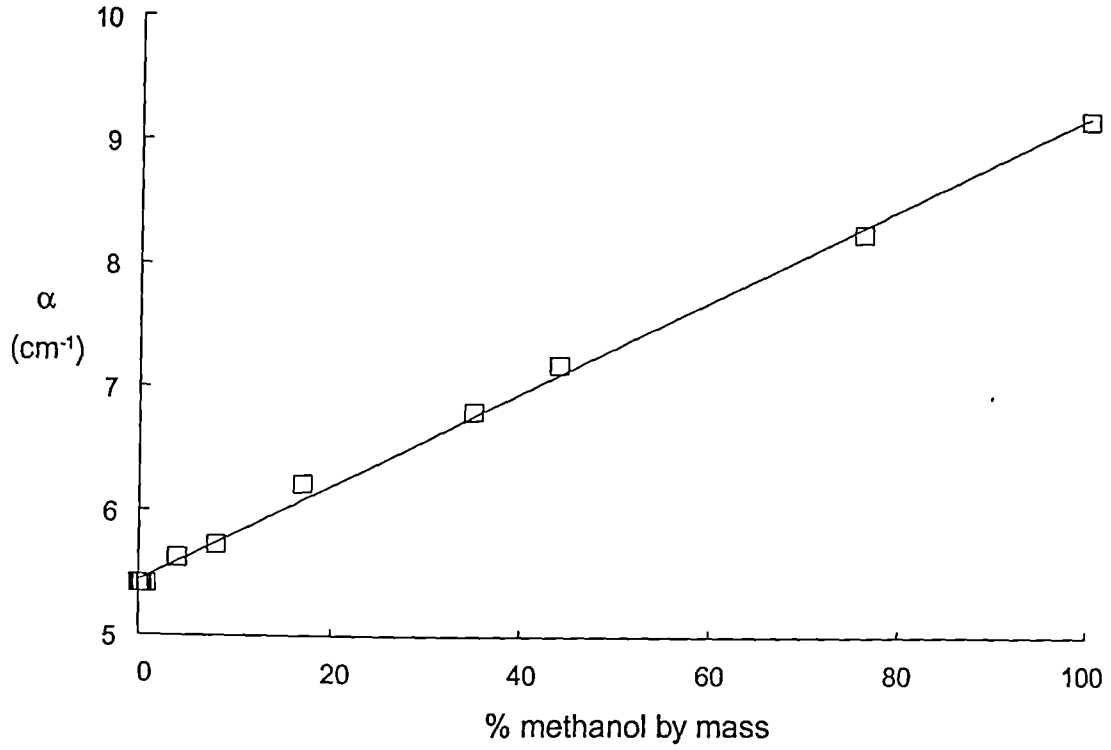

Fig. 4.2 Absorption Coefficient of Water / Methanol Solutions at 1700 nm

the positive effect of the other physical parameters of the sample. The physical parameter effects are stronger and lead to an increasing photoacoustic signal at these wavelengths too.

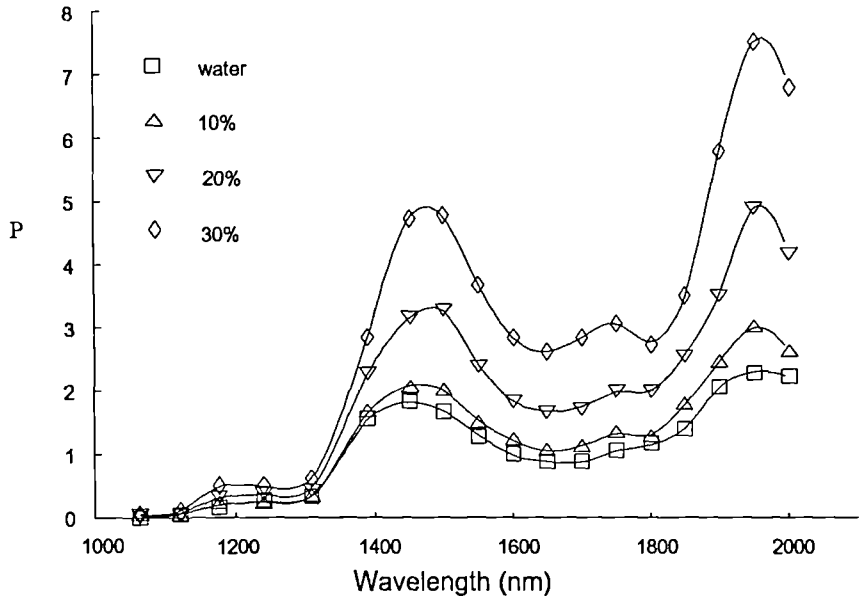

Fig. 4.3 Photoacoustic Spectra of Methanol Concentrations

The experimental results at 1700 nm have been compared with the theory summarised by equation {2.16} in fig. 4.4. The theoretical curve has been normalised to the experimental results at the value for a distilled water sample. It has been assumed that the thermal expansion coefficient and specific heat capacity of the sample varied linearly with concentration between the limits of distilled water and pure methanol. Burton has shown the variation in the velocity of acoustic waves with methanol concentration to be non-linear (4.2). A fourth order polynomial was fitted to the experimental data of Burton and used in the curve-fitting to the photoacoustic data. The polynomial used is plotted in fig. 4.5. It has been proposed that the peak in the acoustic velocity characteristic at around 30% alcohol is caused by a molecular arrangement in which an alcohol molecule is completely surrounded by water molecules, a configuration leading to a minimum in compressibility (4.3).

The methanol concentrations shown in fig. 4.4 have been converted from volume to mass percentages using the relationship

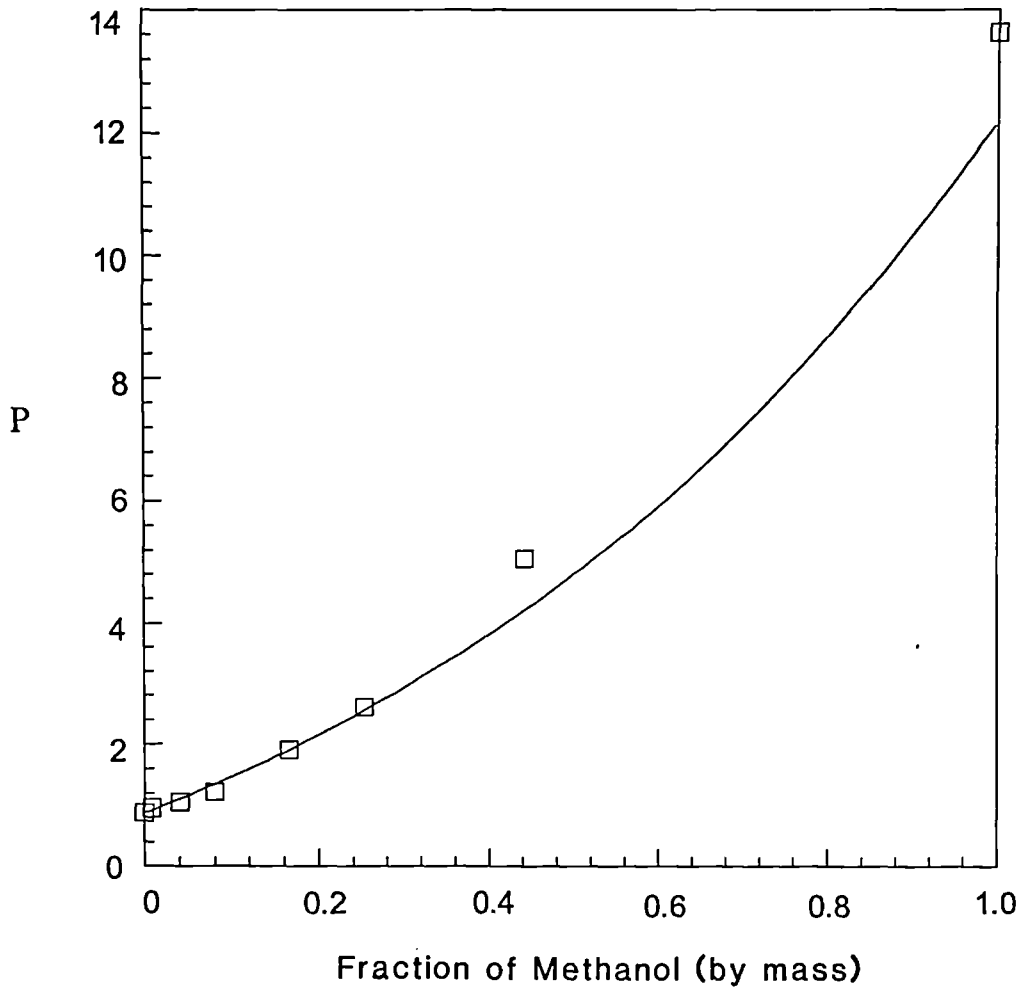

Fig. 4.4 Variation of Photoacoustic Signal with Methanol Concentration at 1700 nm

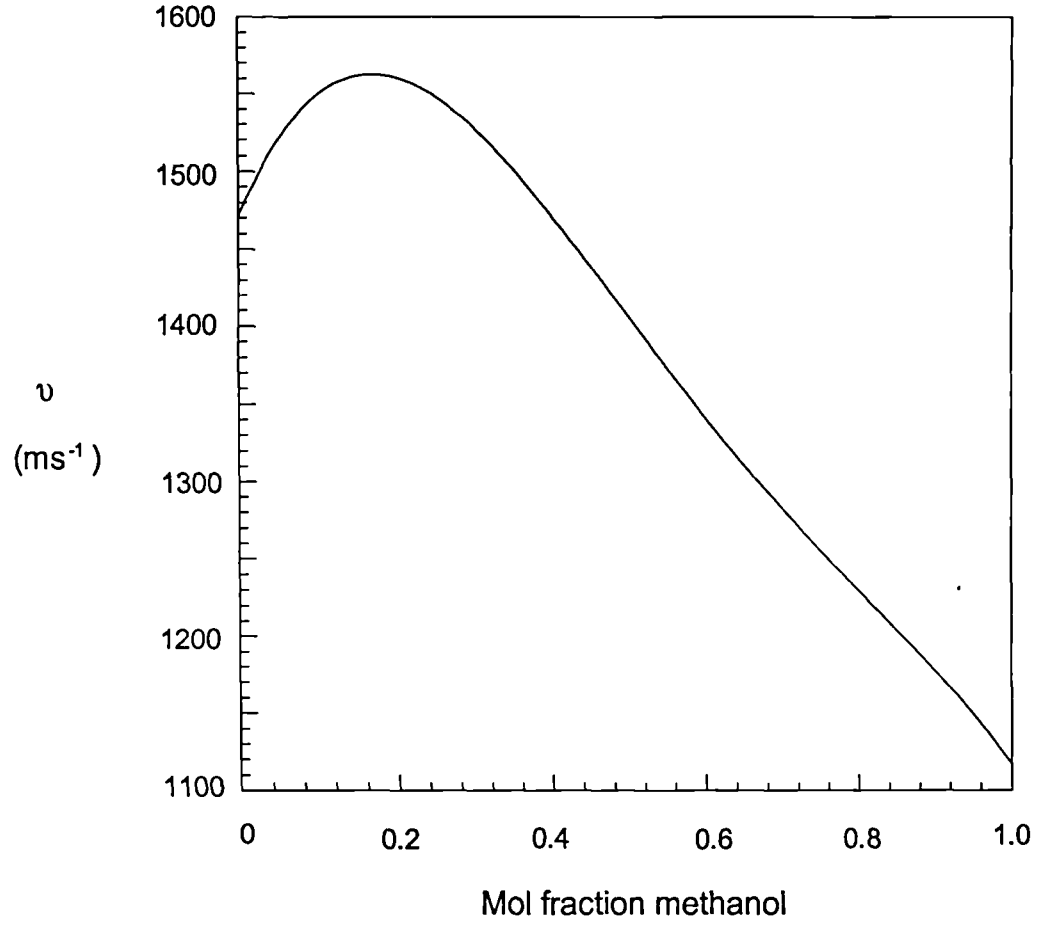

Fig. 4.5 Acoustic Speed as a Function of Methanol Concentration

$$\%(m) = \frac{\%(v).\rho}{\%(v).\rho + 100 - \%(v)}.100 \qquad \{4.1\}$$

where ρ = analyte density (g/cc), and the density of water is 1 g/cc, to enable a more direct comparison with the oil concentrations discussed later to be made.

The theoretical curve in fig. 4.4 displays good agreement with the experimental data points, highlighting a slight deviation from a linear relationship between the photoacoustic signal and analyte concentration under these experimental conditions. This is because the photoacoustic response is not solely dependent upon a single linearly varying parameter (*i.e.* α). Since the other physical parameters important to the photoacoustic process also vary with concentration, the overall effect of concentration is that the photoacoustic response follows a more complex functionality. These experiments were conducted with relatively large analyte concentrations. A prediction of how the photoacoustic signal would change with increasing methanol concentration at the more significant hundreds of ppm levels is compared to the predicted change in the optical absorption coefficient in fig. 4.6. In this figure, the predicted signal change at 1700 nm generated in a sample containing methanol is expressed as a percentage increase and compared with the predicted signal generated in a pure water sample. The prediction of the increase in the photoacoustic signal is derived from the same expression as used for the theoretical curve in fig. 4.4. Although the gradient of the theoretical curve for the photoacoustic response decreases with decreasing concentration, it does not tend to zero at zero concentration. A photoacoustic signal increase of 0.62% (over a water signal) is predicted for a 1000 ppm methanol in water sample as compared to a 0.08% increase in the optical absorption coefficient.

4.3. Oil and Oil Emulsions

Crude oil, by its very nature, is a substance of great complexity and variety. The chemical composition of an oil sample depends not only upon the well from which

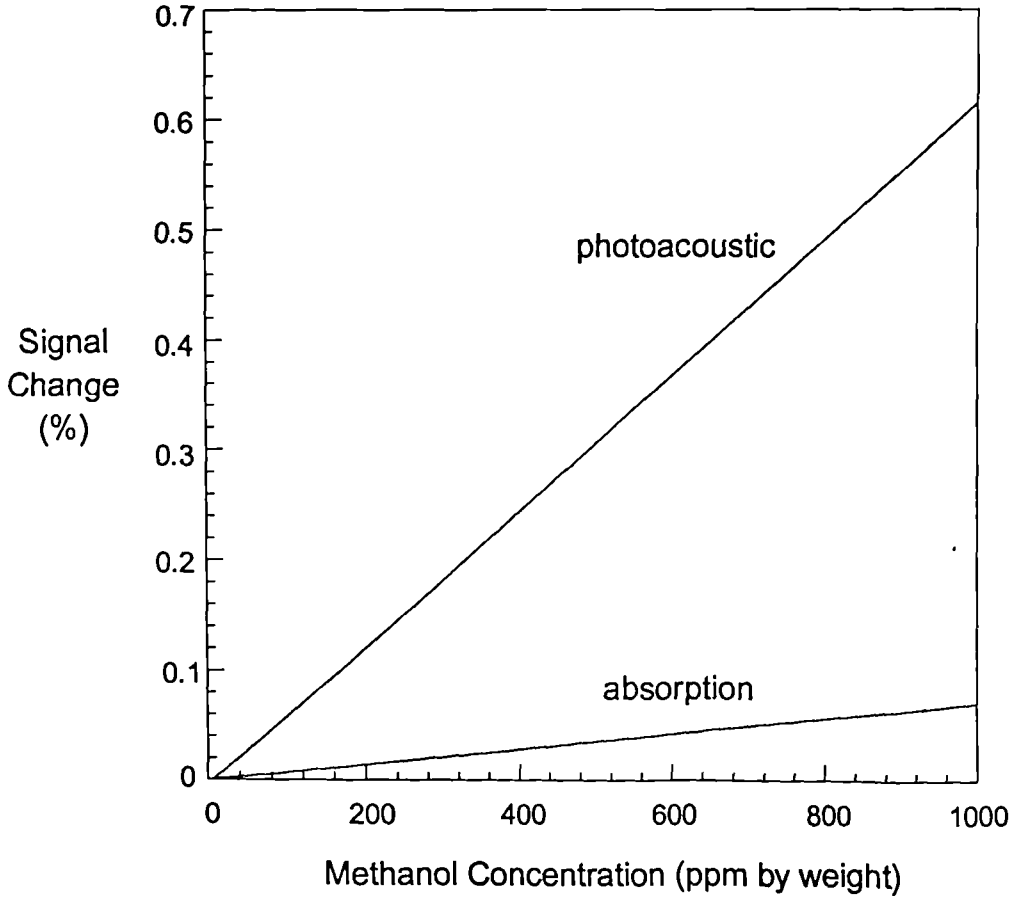

Fig. 4.6 Predicted Increases in the Photoacoustic Signal and Absorption Coefficient at 1700 nm

it originated, but also the position within the deposit from which a particular sample was obtained. Whilst it is difficult to determine exactly the constituents of crude oil, and thereby to have good control over an experimental sample, the applied nature of the project deemed that it was important to advance from making measurements on simple systems such as alcohols in water. In order to achieve this it was necessary to perform photoacoustic experiments on a real crude oil emulsion sample, as an important step in determining the feasibility of the photoacoustic technique to measuring oil in water concentration.

4.3.1. Properties of Crude Oil

Three crude oil samples, to be known as oils A, B, and C, have been used in various experiments conducted as a part of this thesis. Crude oil A was used in the majority of the experiments to determine the sensitivity limits of the photoacoustic measurement technique for oil in water. Oils B and C were used together with oil A in studies to characterise oil emulsion samples. The different viscosity of the oils allowed a greater range of emulsion droplet sizes to be created, than if one oil type had been used.

Crude oil is a complex substance and one that is difficult to categorise generally since its composition varies a great deal depending upon the source field. Mid-range values of some of the relevant physical properties of a crude oil sample are detailed below.

specific heat capacity $C_p = 1.7 \times 10^3$ J.kg^{-1}.°C^{-1} (4.4) viscosity = 5 centistokes (4.5)

thermal expansion coeff. $\beta = 1.1 \times 10^{-3}$ °C^{-1} (4.4) bulk modulus $B = 1 \times 10^9$ Pa (4.5)

acoustic velocity $\upsilon = 1.1 \times 10^3$ m.s^{-1} (4.6) density $\rho = 870$ kg/m^3 (4.7)

refractive index n (@ 589 nm) = 1.45 (4.6)

The acoustic velocity is related to the bulk modulus and the density through the relationship

$$\upsilon = \sqrt{\frac{B}{\rho}}. \qquad \{4.2\}$$

The near infrared absorption spectrum of crude oil A, as measured in a 0.2 mm pathlength cell is shown in fig. 4.7. Activity due to the C-H stretch is clearly visible at 1720 nm, and the C-H deformation mode is evident at 2320 nm and also at 1200 nm. There is also evidence for some vibrational bond activity at 1390 nm. At wavelengths less than 1.1 μm the absorption coefficient increases dramatically. This is the long wavelength (low energy) edge of the region in which electronic transitions within the oil are excited, and which extends through the visible and into the ultraviolet region of the spectrum. Although the initial absorption of the photon energy goes into promoting an electron to an excited energy state, the relaxation pathways for the absorbed energy can include non-radiative as well as radiative (*e.g.* fluorescence) processes. The fluorescence intensity is to some extent determined by the lifetime of an excited electron in a state from which the relaxation may be by fluorescence. If the lifetime is long, there is an increased chance that the energy relaxation will occur through non-radiative processes. Relaxation by fluorescence tends to become more significant at visible and UV excitation wavelengths, but experiments have shown that near infrared excitation of crude oil at 776 nm also yields fluorescence at 855 nm (4.8).

4.3.2. Preparation of Crude Oil Emulsions in Water

Crude oil emulsions were prepared by ultrasonically agitating at 43 kHz a known mass of oil in 20 ml of distilled water to produce a base concentration, usually in the range 100 to 1000 ppm oil in water (by mass). Lower concentrations of oil were then derived from the base solution by volume dilution with distilled water.

4.3.3. Emulsion Characterisation

When preparing the base oil emulsion, it was clear from visual inspection that not all of the measured oil droplet contributed to the formation of the emulsion, but

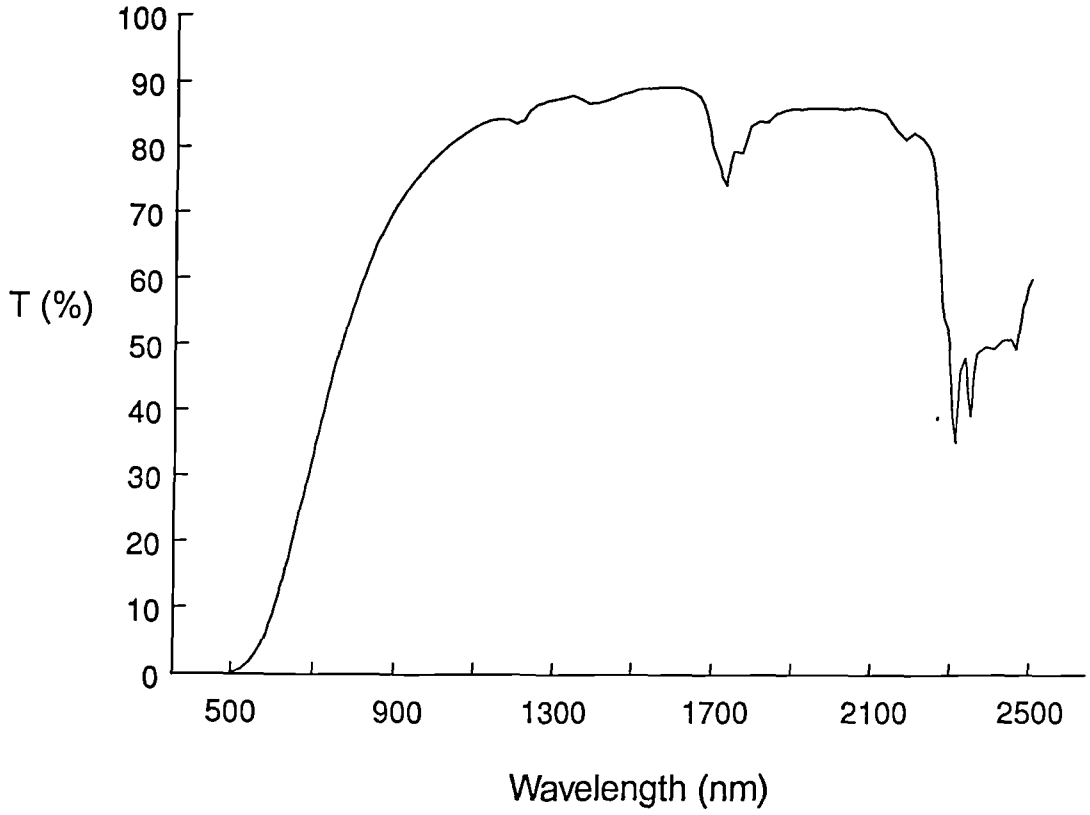

Fig. 4.7 Near Infrared Transmission Spectrum of Crude Oil

remained separate, usually as a thin layer on the water surface. A calibration check of the emulsion preparation procedure employed was therefore necessary. This was achieved by infrared transmission measurements at the C-H stretch fundamental (~ 3.3μm) or at the third harmonic of the C-H deformation (~ 2.3μm), after the oil had been extracted from the water by a solvent such as CCl_4 or 1,1,2-trichloro-1,2,2-trifluoroethane. Fig. 4.8 shows calibration plots at two wavelengths for oil A in emulsion, obtained after extraction of the oil with 1,1,2-trichloro-1,2,2-trifluoroethane. 10 mm cuvettes were used in the spectrophotometer. The solvent was used as the reference, so that the ordinate is a measure of the absorption coefficient difference, where α is equal to $\alpha_S - \alpha_T$.

An independent calibration test by solvent extraction and infrared transmission of a sample containing a nominal oil concentration of 100 mg/l was performed. The test found the sample concentration to be 79.4 mg/l. Since there was a delay of several days between the sample preparation and testing, such a discrepancy was not unexpected. The measured value was however close enough to the expected value to give confidence that the emulsion preparation technique provided emulsions of sufficient accuracy for experimental purposes.

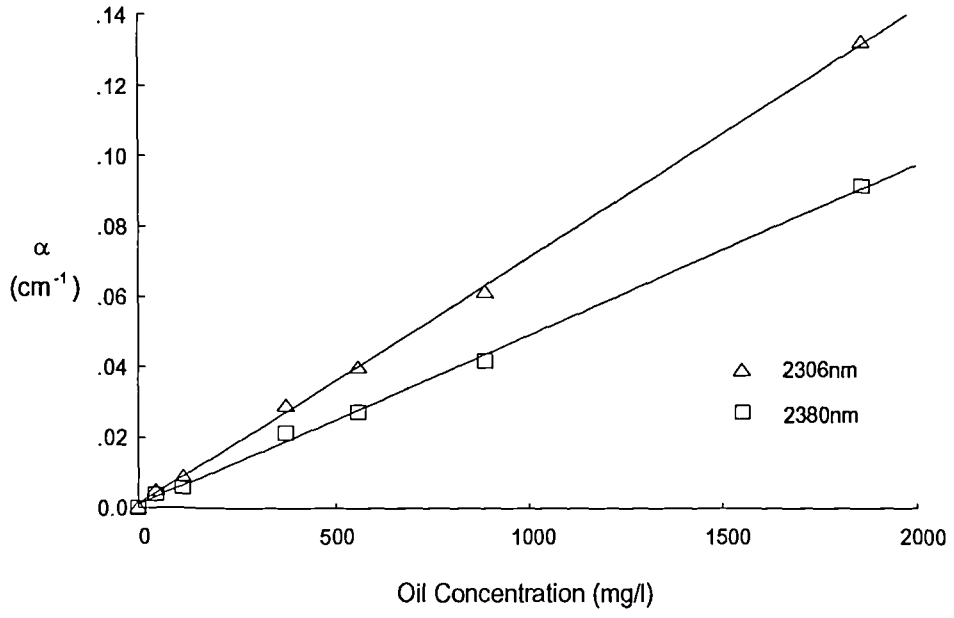

Fig. 4.8 Calibration Curve for Oil Emulsion Samples

Emulsion Stability

The droplet size distribution is just one of the important parameters to be considered in the characterisation of an oil emulsion. It is likely that scattering effects in particular would be largely dependent upon the size and shape of the oil droplets and that these may lead to ambiguities in the data analysis, in particular in transmission spectroscopy. Any field trial of an instrument to measure oil concentration would have to perform within specification over a wide range of droplet sizes. Characterisation of the oil emulsions prepared by ultrasonic agitation was necessary in order to have some degree of control on the experimental conditions.

Analysis of the droplet size in the prepared emulsions was achieved using a Galai CIS-1. This instrument uses a scanning He-Ne laser beam to perform transit time calculations which are the basis of particle sizing. Estimates of oil concentration and particle shape can also be derived from this instrument. Using oil A, an emulsion of nominal value 60 mg/l was prepared by subjecting the oil and water mixture to 18 minutes ultrasonic agitation. The droplet size distribution of this sample is shown in fig. 4.9, and highlights that particles of between 1 and 10 μm diameter were created.

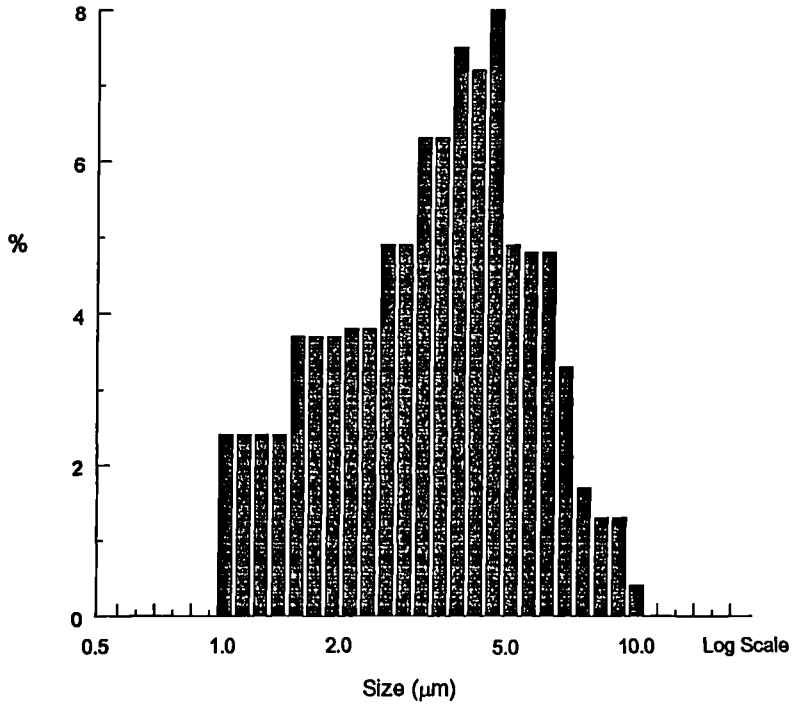

Fig. 4.9 Emulsion Droplet Size Distribution

Every 30 minutes droplet size and concentration data from this sample was obtained (1 minute acquisition time) for a period of 15 hours. The sample was left undisturbed for this period. After a further period of approximately 7 hours, the sample was analysed once more, without having been disturbed. The sample was immediately agitated in the ultrasonic bath for 10 minutes, before three final measurements were made over a period of 10 minutes. The mean particle size and concentration data obtained is shown in figure 4.10. The main feature is a steady decrease in both the mean particle size and oil concentration with increasing time after emulsion formation. Since oil is less dense than water the oil droplets rise, largest droplets fastest, to the liquid surface. Thus the concentration of oil remaining in emulsion within the bulk of the liquid becomes lower. Since the largest droplets are lost to the surface most rapidly, the mean particle size also decreases. As time progresses, oil droplets coming into contact with one another may merge to form larger droplets, affecting the rate of change of concentration and particle size.

After 22 hours the mean particle size had decreased from 3.5μm to 2.6μm and the measured concentration had reduced from approximately 50 mg/l to 22 mg/l. After re-agitation in the ultrasonic bath, the emulsions regained to some extent their initial characteristics. The mean particle size after re-agitation was within 10% of its initial value, at 3.2μm, and the oil concentration was approximately 36 mg/l. This concentration was a little lower than the initial value probably because a significant amount of the original oil remained on the liquid surface. Further experiments have established that longer re-agitation times reconstitute the oil in emulsion concentration at levels much closer to its initial value. Thus the samples could be reconstituted and used over a period of several days.

The oil droplet sizes that generally occur in the field application for which this study has been conducted range from approximately 3 μm to 15 μm. Larger oil droplet sizes could be created in the laboratory emulsions by using a shorter initial ultrasonic agitation time and using a more viscous oil. Emulsions were prepared using oil C, and agitations of several durations up to 1 minute. The dependence of the mean particle

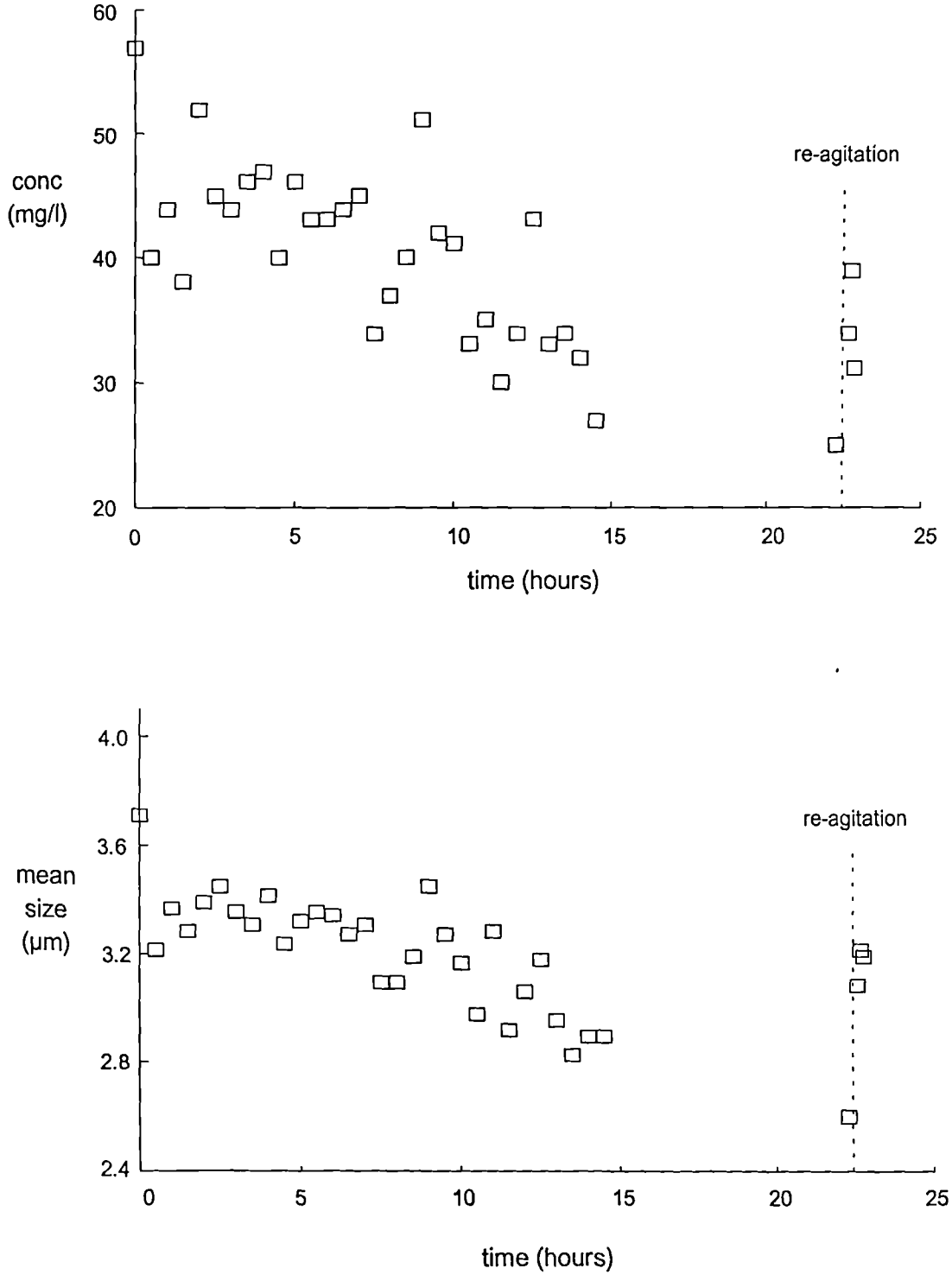

Fig. 4.10 Oil Concentration and Droplet Size Stability

size on agitation time is plotted in fig. 4.11, showing that a range of mean droplet sizes between 5 μm and 9 μm were created.

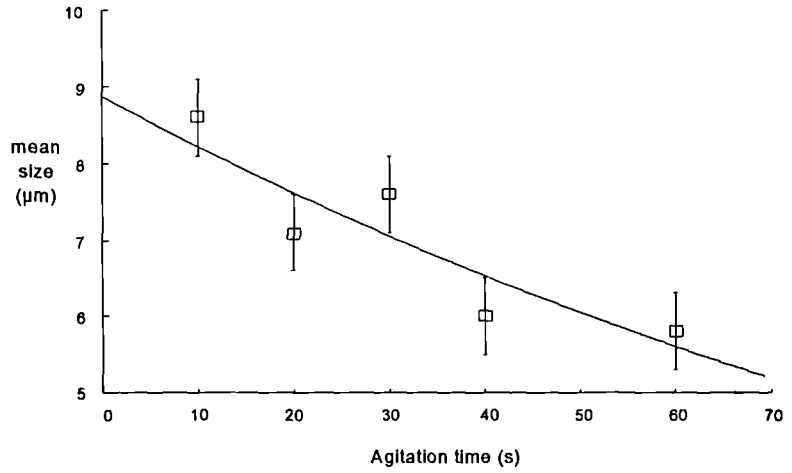

Fig. 4.11 Mean Droplet Size as a Function of Agitation Time

A further consideration is the water in which the oil is to be measured. For most of the investigations into the feasibility of the photoacoustic technique it was desirable to maintain a simple and controlled sample, by using distilled water. However the real situation requires the measurement of oil in a salt water environment. Simulated produced water brine (PWB) can be used to represent the discharge water from a sea based oil platform. The composition of the simulated PWB is shown in Table 4.1.

Compound	Quantity (g / 20 litres of distilled water)
NaCl	526.428
KCl	11.482
$CaCl_26H_2O$	65.286
$MgCl_26H_2O$	39.93
$NaHCO_3$	17.81
$MgSO_47H_2O$	63.00

Table 4.1 Produced Water Brine Composition

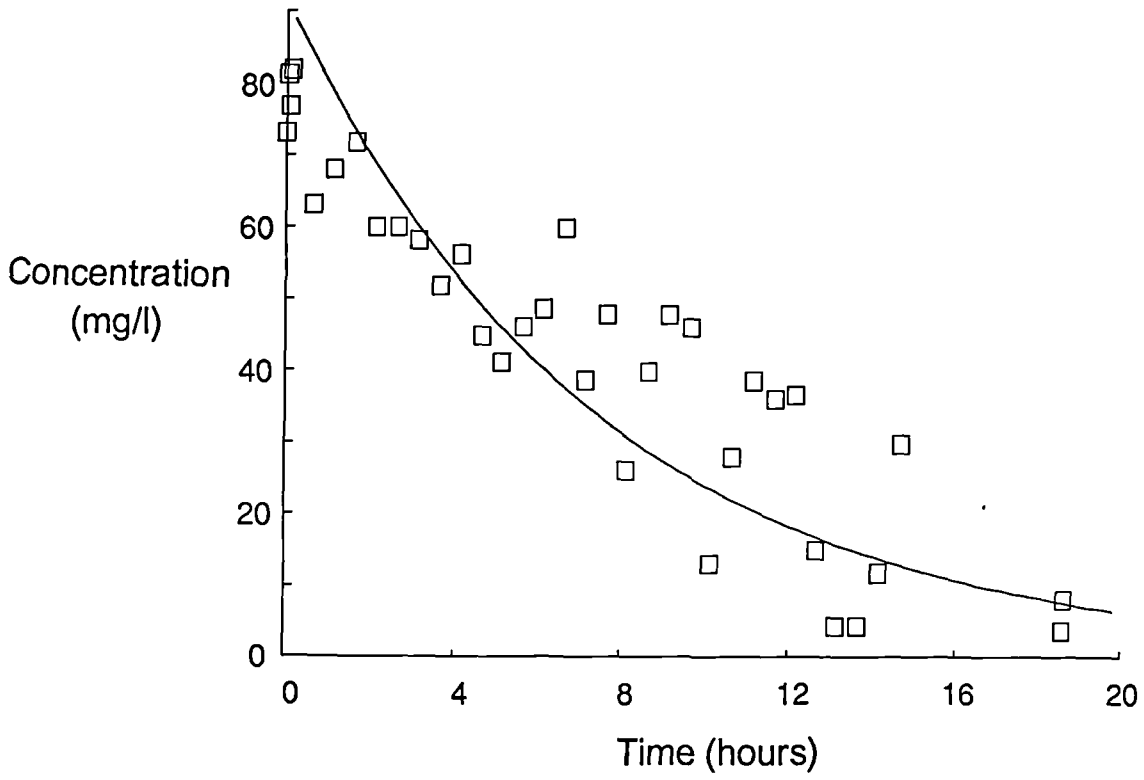

Fig. 4.12 Stability of PWB Based Oil Emulsion Concentration

Experiments to determine whether the ultrasonic technique used successfully for producing stable oil emulsions in distilled water was capable of doing the same in salt water were performed. Figure 4.12 shows the variation in the measured oil concentration in a brine based emulsion over a period of almost 20 hours. Although not as stable as a distilled water emulsion, the PWB based emulsion was found to be stable enough for experimental purposes. However, in order to maintain the most accurately controlled experimental samples, emulsions based only on distilled water were used to determine the photoacoustic response to oil.

4.4. Oil Emulsion Photoacoustics

4.4.1. Temperature Dependence of the Photoacoustic Effect

The photoacoustic effect is dependent upon the sample temperature in a number of ways. The optical absorption coefficient, α, is temperature dependent through shifts in the shape and position of spectral absorption features. In addition to this, the other physical parameters important to the photoacoustic effect (β, υ and C_p) also vary with temperature. In aqueous systems the thermal expansion coefficient in particular is strongly temperature dependent, especially so at low temperatures, and changes polarity around 4°C. This leads to a temperature at which the photoacoustic response is zero, below which the heating caused by optical absorption leads to an initial rarefaction rather than an initial compression (4.9, 4.10).

Empirically determined relationships for the temperature dependencies of the parameters β, υ, and C_p of water have been used to predict the combined effect due to these parameters on the photoacoustic signal caused by temperature changes, based on equation {2.16}. The predicted change in the signal for a 0.1 °C temperature increase at three ambient temperatures has been calculated. The results are shown in Table 4.2.

This strong dependence upon temperature, (especially strong at low temperature) meant that in conducting photoacoustic experiments in which small signal changes between samples were to be resolved, there was a need for temperature control of the sample and / or accurate monitoring of the sample temperature and subsequent correction. A stabilising temperature jacket for the photoacoustic cell together with an algorithm to correct for the temperature variation in β, C_p, and υ, previously described (4.1), were used in the oil emulsion spectroscopy experiments described here.

Ambient Temperature (°C)	Signal Increase (%)
10	1.6
19	0.6
40	0.2

Table 4.2 PA Signal Increase in Water due to a 0.1 °C Temperature Rise

4.4.2. Photoacoustic Spectroscopy

Emulsions used for the majority of the photoacoustic spectroscopy experiments were formed from oil A in distilled water, under long ultrasonic agitation times. This combination provided emulsions that had characteristics that changed very little over several hours, and that could be reconstituted to their original form by further ultrasonic agitation.

The spectra of such emulsions, of nominal concentrations 100, 200, 400, 800, and 1000 mg/l, as well as that of distilled water were measured using the Raman fibre based photoacoustic spectrometer described in Chapter 3. As might be expected for such low concentrations of oil, the spectra were all similar in magnitude and form to the distilled water spectrum shown in fig. 3.9. The photoacoustic response to oil concentration at two near infrared wavelengths generated by the fibre system, 1390 nm and 1750 nm, is shown in fig. 4.13, together with the response from similar oil emulsions when using the Q-switched Nd:YAG laser directly as the source for

photoacoustic generation at 1064 nm. The solid lines are best fit linear regressions, and there is also a significant error estimate in the oil concentration. At all three wavelengths the photoacoustic signal increased systematically with oil concentration. At 1750 nm, where the response to hydrocarbons in water was predicted to be strong because of the C-H absorption and a minimum in the water absorption, an increase in the photoacoustic signal of 6.1 % for an oil concentration of 1000 mg/l was observed. The response at 1390 nm had a lesser but still positive gradient with oil concentration (4.2 % over 1000 mg/l). Reference to fig. 4.7 indicates that the 1064 nm radiation was interacting initially with electronic transitions in the oil, which nevertheless resulted in a strong photoacoustic signal (7.2 % signal increase for a 500 mg/l emulsion). This aspect, of short NIR wavelength excitation, will be discussed further in the diode laser experimentation of Chapter 5.

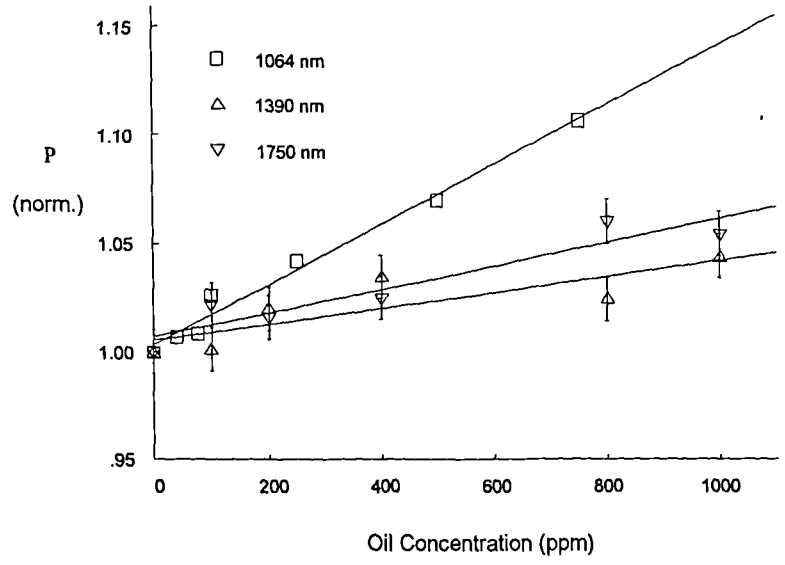

Fig. 4.13 Normalised Photoacoustic Response to Oil Emulsion Concentration

Estimates of the limits of detection (l.o.d.) of the photoacoustic measurements made with this system can be made. A signal to rms noise ratio of 1.5 has been used as the criteria. Despite the low sample absorption coefficient at 1064 nm, the large pulse energy available results in an l.o.d. of approximately 4 mg/l. The results at 1390

and 1750 nm suffer from reduced oil to water absorption contrast at those wavelengths, low optical pulse energy, and poor optical pulse reproducibility. As a consequence, an l.o.d. of approximately 160 mg/l is achieved.

4.5. Dissolved and Dispersed Components

Hydrocarbons may exist in water in dissolved or dispersed (emulsion) form and it is desirable that a sensor to detect hydrocarbons should be sensitive to both components. A test of the capability of the photoacoustic technique to meet this requirement has been conducted, in which the Nd:YAG laser (operating at 1064 nm) was used as the optical source for acoustic generation. The photoacoustic responses from distilled water, a sample containing dissolved C-H bonds (4% (≡ 40,000 mg/l) methanol in water), a sample containing dispersed C-H bonds (nominally 500 mg/l crude oil in water), and a combined sample of 4% methanol and 500 mg/l crude oil in water have been compared. The percentage increase of the photoacoustic signals relative to that generated in water are summarised in Table 4.3.

sample	percentage increase in photoacoustic signal
distilled water	0.0
4% methanol	7.4
500 mg/l oil	4.7
combined sample	11.7

Table 4.3 Photoacoustic response to dissolved and dispersed components, normalised to water

A signal increase of 11.7% was observed when the combined sample was analysed, in good agreement with the sum of the two individual increases (12.1%). This agreement is evidence only that these two particular components are acting independently of each other, and that photoacoustic techniques are capable of

simultaneously detecting dissolved and dispersed components. At these concentrations, the sensitivity per mg/l of analyte is however clearly very different for the two cases, being approximately 2 x 10^{-4} % for methanol and 0.01 % for the crude oil. This is mostly a reflection of the different physical parameters associated with the dissolved and dispersed components, in particular the optical absorption coefficient, which is approximately two orders of magnitude greater for the oil sample. In this case the absorption feature in methanol coincident with the wavelength of the laser can be assigned to the O-H bond. However it is likely that the photoacoustic response due to dissolved and dispersed C-H bonds will depend in a complex manner on the particular molecular composition of the analyte and be related to the bonds it makes with water. For this reason and others, there will be a need for a multi-wavelength approach to the problem of monitoring the C-H content in water.

4.6. Acoustic Frequency Studies

Information about the acoustic frequencies generated by the photoacoustic effect is important for two main reasons. Firstly, effective acoustic detector design depends upon an accurate knowledge of the frequencies to be detected, in order to achieve an efficient transfer of acoustic energy into an electrical signal. Secondly, an analysis of the generated frequencies may contain valuable information about the sample, in particular the rates of the non-radiative de-excitation processes that follow photoexcitation (4.11).

In order to perform acoustic frequency or time resolved studies of the acoustic waveform, it is necessary to employ a broadband detection technique. This can be achieved through the use of a broadband piezoelectric transducer, or alternatively by optical detection of the acoustic wave. Optical techniques are discussed in Section 2.5.2. Broadband piezoelectric techniques demand the use of a non-resonant piezoelectric material. These are usually in the form of a thin film such as polyvinylidenefluoride (PVF_2) or a miniature ceramic probe.

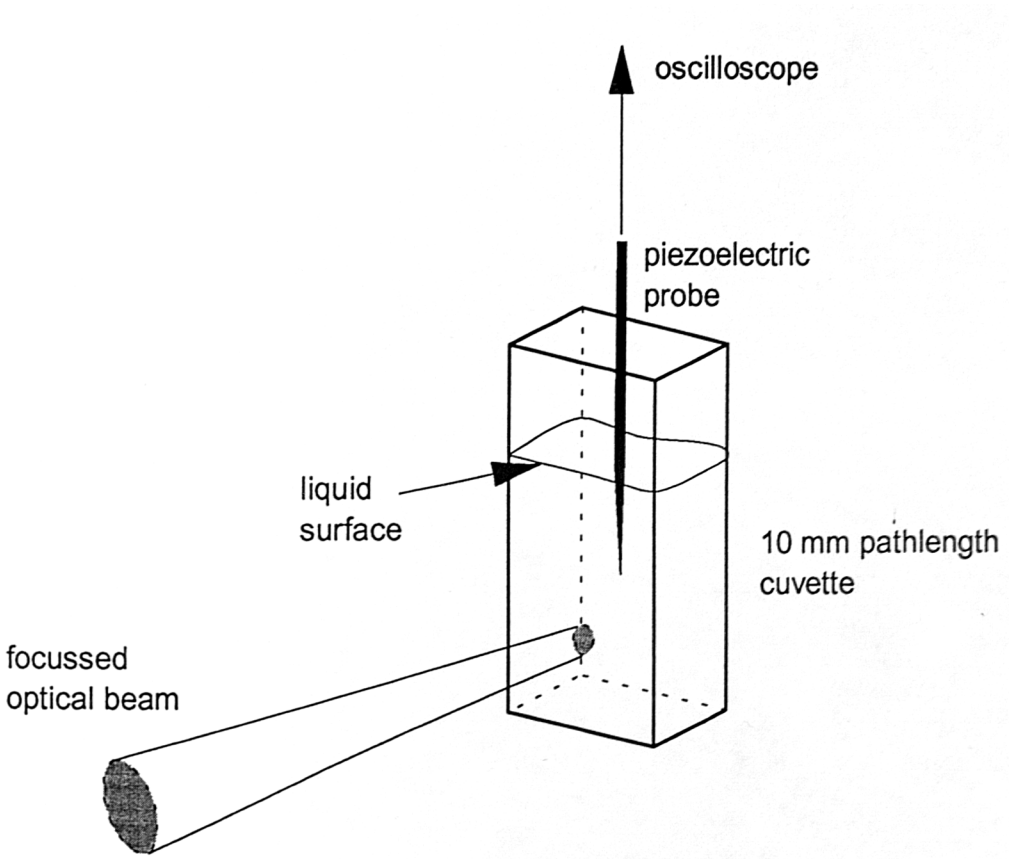

Fig. 4.14 Cuvette Arrangement for Acoustic Frequency Studies

A study of the acoustic waveform generated by pulsed Nd:YAG excitation at 1064 nm has been conducted using a miniature piezoelectric probe, manufactured by J.P. Weight (4.12), of diameter 150 μm and thickness 40 μm. The responsivity of the probe varied by less than 2dB up to a frequency of 20 MHz. The experimental arrangement is shown schematically in fig. 4.14. Pulses of 150 ns (FWHM) duration were focussed into a 10 mm pathlength quartz cuvette, so that at the centre of the cuvette, the beam diameter was estimated to be 40 μm. The optical pulse used in these experiments as detected by a fast silicon photodiode is shown in fig. 4.15.

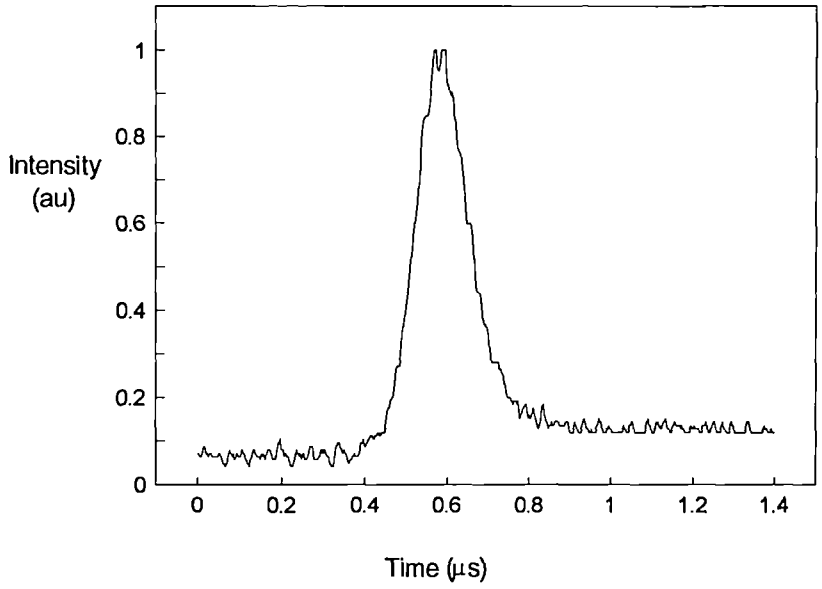

Fig. 4.15 Q-switched Nd:YAG Laser Pulse

4.6.1. Optical Alignment

The cuvette was mounted upon an x-y translation stage so that the beam could be positioned within the cell. In order to optimise the coupling of the acoustic waves to the detector, the probe was mounted in an x-y-z translation stage. In this way, the probe could be accurately positioned relative to the generation region. Since the probe has a fast response, it was possible to resolve acoustic signals from cell walls and other boundaries, as well as the direct signal. Fig. 4.16 shows the acoustic signal (upper trace) generated by a single optical pulse (lower trace), each component of the acoustic signal having taken a different path to reach the detector. The first and

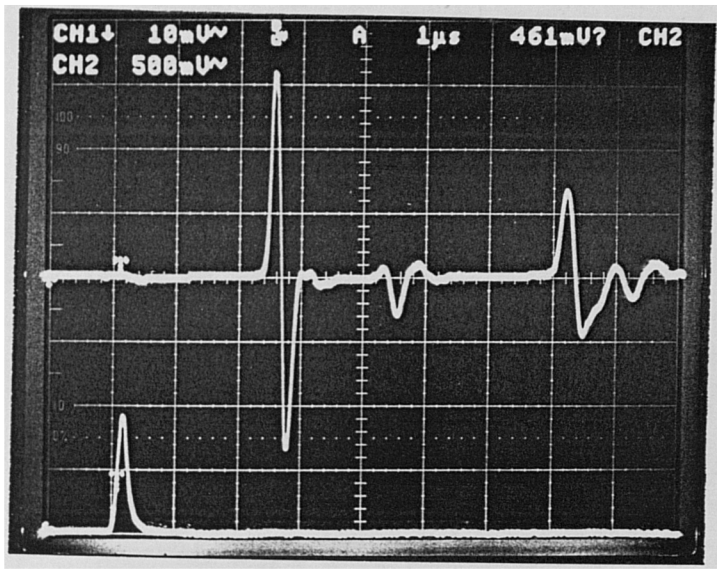

Fig. 4.16 Acoustic Signals Detected by Miniature Piezoelectric Probe

largest bipolar pulse is the pressure pulse direct from the optic axis in the liquid. Approximately 2 μs later (corresponding to an extra pathlength of 3 mm), the first additional signal reached the detector. This was most likely due to acoustic generation at the front and / or back cell wall, either through absorption in the wall itself, or via some contamination on the wall surface. A further acoustic signal was observed 7 μs (≡11 mm) after the optical pulse, corresponding to the reflections off the side walls of the cuvette. By altering the position of the probe relative to the cuvette, the reflections off the two side walls could be resolved from one other. The relative sizes of the signals could be used to determine the centrality of the laser beam in the cuvette. Further acoustic reflections from the liquid / air interface and the liquid / base interface could also be observed.

Equation {2.14} predicts that the peak acoustic pressure follows an $r^{1/2}$ relationship, where r is the distance from the optical axis. Thus it was important to place the probe as close to the illuminated volume as possible, to obtain the maximum signal without risking damage to the probe through exposing it to the high optical intensities at the focus of the beam. The distance of the probe from the optic axis can be determined by measuring the time delay between the optical pulse and the arrival of the acoustic signal at the detector if the speed of sound, υ in the medium is known.

A distilled water sample (υ = 1483 ms^{-1}) was used for the optical alignment procedure. Fig. 4.17a shows the direct photoacoustic signal beginning approximately 1.8μs after the start of the optical pulse. The corresponding distance from the edge of the optical beam to the detector was thus 2.7 mm.

4.6.2. Time Domain Results

Following the optical alignment outlined above, the photoacoustic signals generated in oil emulsion in water samples were measured using the broadband probe. Fig. 4.17 shows the acoustic signal from six samples, *viz.* distilled water (a), and concentrations of 20 (b), 250 (c), 500 (d), 750 (e) and 1000 mg/l (f) oil in water. Several interesting trends are evident. Firstly, as the oil concentration was increased,

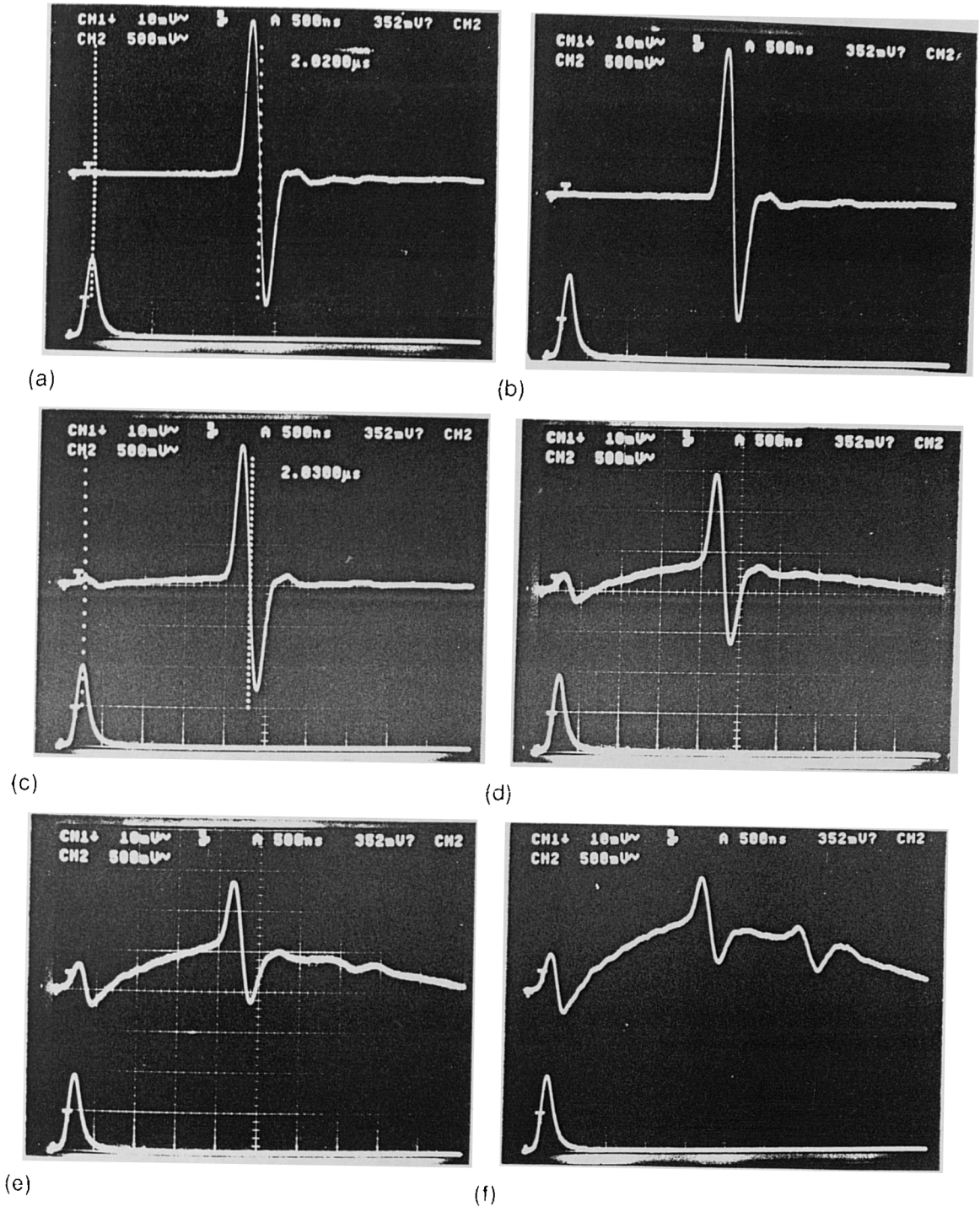

Fig. 4.17 Acoustic Signal Generated in (a) Distilled Water and in Oil Emulsions of Concentrations 20mg/l (b), 250mg/l (c), 500mg/l (d), 750mg/l (e), and 1000mg/l (f)

a growing acoustic signal coincident in time with the optical pulse was observed. This was most likely due to optical scattering off the oil droplets. There is a slight mis-match in the refractive indices of water (1.33) and oil (≈ 1.45) in the near infrared, which results in a reflection coefficient of 0.2 % at an oil / water interface and consequent scattering. The scattered photons that impinged on the piezoelectric detector generated a signal similar in character to that observed due to a photoacoustic wave. A plot of the peak value of the piezoelectric signal due to scattering as a function of the oil concentration is shown in fig. 4.18 and shows a linear response at these low concentrations.

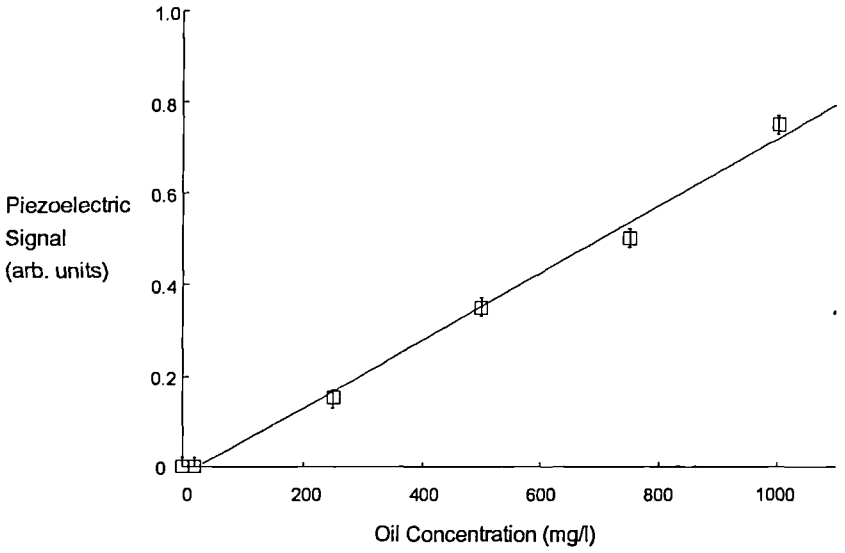

Fig. 4.18 Scattered Light Intensity as a Function of Oil Concentration

Secondly, a relatively slow rise in the pressure signal was increasingly apparent with increasing oil concentration, reaching a peak at the same time as the arrival of the direct acoustic signal, after which a slow decrease was observed. This is also a likely manifestation of optical scattering. Photons scattered from their original path may still be absorbed in the sample and contribute to a photoacoustic signal. If such a photon is absorbed in the region between the optic axis and the acoustic detector, the acoustic signal generated there will arrive before the acoustic signal generated on the optic axis, since the velocity of light is greater than the acoustic

velocity in water. This process is repeated throughout a volume of sample surrounding the optic axis, with the result that contributions to the acoustic signal originate within a volume somewhat larger than that defined by the beam size in a non-scattering sample. These acoustic contributions arrive at the detector at times which are determined by the location of the absorption event and can be before or after the pulse of acoustic energy originating on the optic axis.

A further feature of note as the oil concentration increased was the decrease in the peak to peak size of the direct pulse. Following the argument outlined above for the origin of the slower rising pressure front, the increase in scattering results in a decrease in the number of photons available for photoacoustic generation on the optic axis and a corresponding decrease in the direct acoustic signal. Analysis of these features of the acoustic waveform can be used to provide an insight into the relation between the absorption coefficient α, scattering coefficient K, and extinction coefficient α_{ex} of the sample. In the case of these oil emulsions, the results indicate that both optical absorption and scattering have significant roles in determining the form of the photoacoustic pressure pulse.

In the case of the most concentrated oil emulsions, a further feature in the waveform began to emerge, occurring approximately 3.2 μs after the optical pulse. This was attributed to optical absorption at the cell wall, probably caused by an oil droplet becoming attached to the glass. This highlights a problem of oil in water monitoring which is common to most optical methods; that of maintaining a clean optical window in a dirty environment.

The acoustic waves generated in samples of water and a 500 mg/l oil in water emulsion under the same excitation conditions were detected using a resonant piezoelectric detector. The signals are shown in fig. 4.19, the smaller trace originating from the water sample. The traces show a higher degree of similarity than the corresponding traces detected by the broadband probe, as the piezoelectric ceramic frequency response dominates. However the 500 mg/l sample does yield a signal that begins earlier than that from water, a feature that is most likely due to scattering.

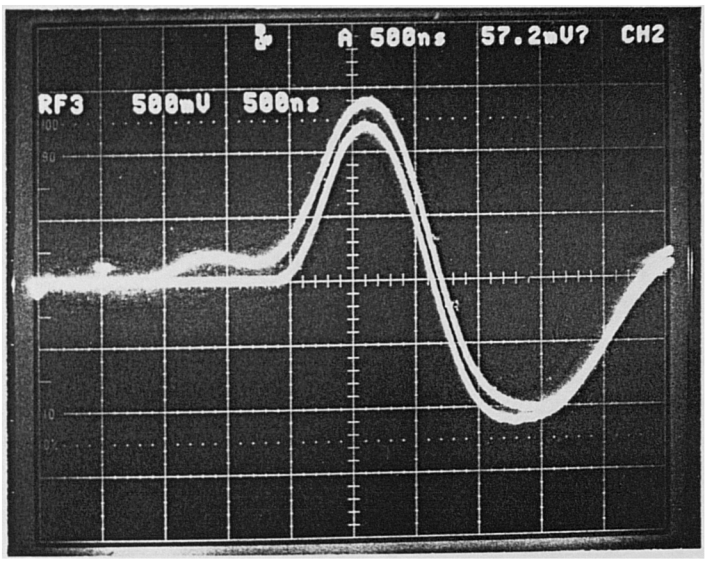

Fig. 4.19 Photoacoustic Signals Generated in Water and 500 mg/l Oil in Water

There is also a larger peak to peak value from the oil emulsion, which is attributed to changes in the physical parameters of the sample. One further consideration is that a shift in the frequency of the photoacoustic waveform caused by a larger acoustic source could result in more efficient coupling of the acoustic energy to the detector. However this is not borne out by the scattering results presented in Chapter 3.

4.6.3. Frequency Analysis

Frequency analysis of the acoustic waveforms detected by the broadband probe and the resonant ceramic detector was achieved using a Hewlett Packard 8590A Spectrum Analyser. Fig. 4.20 (upper plot) shows the spectrum of the waveform generated in distilled water measured with the probe. The horizontal scale is 0 to 5 MHz and the envelope peaks at approximately 1.5 MHz. There is however significant frequency content up to 4.5 MHz. The spectrum of the signal produced by the resonant ceramic detector under the same experimental conditions is also shown in fig. 4.20 (lower plot). The response of the detector dominates the spectral content in this case, which displays a peak at approximately 350 kHz and no significant content beyond 1.6 MHz. The narrow peaked structure to the spectra was largely due to the transient nature of the waveform.

The essentially equivalent theories of Lai & Young (4.13), and Heritier (4.14) describe predictions regarding the shape and amplitude of the photoacoustic waveform generated by pulsed excitation in liquids. Experimental verification of these predictions has been reported by Sullivan & Tam (4.15), Komorowski & Eyring (4.11) and by Quan *et al* (4.16). The time domain characteristics of the acoustic pulse are largely determined by two temporal parameters, the laser pulse duration, τ_p and the acoustic transit time across the illuminated region τ_a. An effective time parameter, τ_e is common to both theories and is defined as:

$$\tau_e = \left(\tau_a{}^2 + \tau_p{}^2\right)^{\frac{1}{2}} \qquad \{4.3\}$$

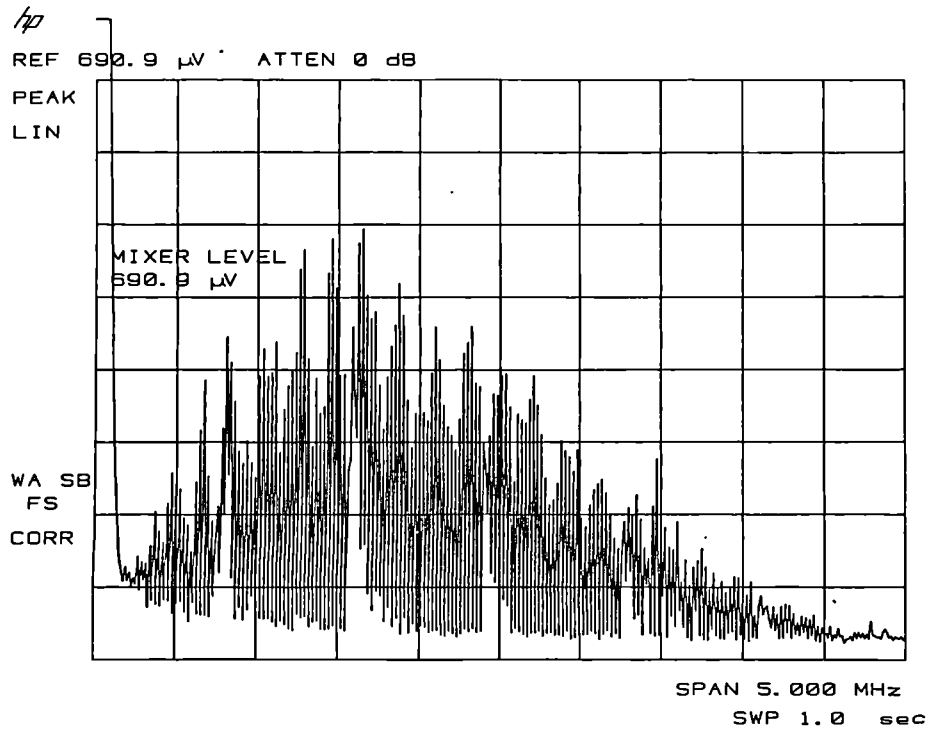

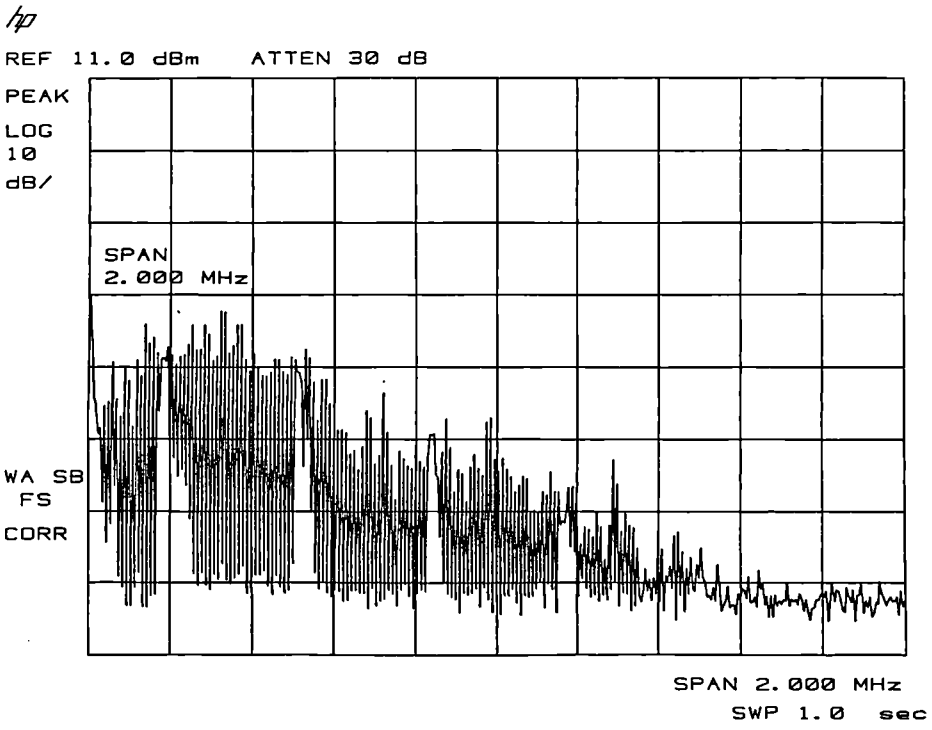

Fig. 4.20 Frequency Content of a Photoacoustic Pressure Pulse (upper plot) and the Signal Detected by a Resonant Ceramic Detector (lower plot)

If τ_p is defined as being the FWHM duration and τ_a the time for an acoustic wave to travel across the radius of the beam, the time between the pressure maximum and the pressure minimum is calculated to be $2.35\tau_e$ according to Lai & Young. The FWHM of the first pressure compression is also predicted to be proportional to τ_e by Heritier. The FWHM of the optical pulse used in these experiments was 150ns, and since τ_a was estimated to be approximately 20ns, $\tau_e \approx \tau_p$. Thus the predicted duration between the peak compression and rarefaction of the acoustic wave was 350 ns. In a qualitative manner, it is possible to double this duration and arrive at an approximation for the period, and consequently make an estimate for the dominant frequency of the acoustic signal from a measurement of the optical pulse duration. In this manner the dominant frequency was estimated to be 1.4 MHz, in excellent agreement with the measured value of 1.5 MHz. For a more quantitative approach, the theoretically predicted waveforms have been Fourier transformed to reveal very good agreement with the experimentally measured spectra (4.16) as shown in fig. 4.21.

4.7. Discussion

Much of the emphasis of this thesis is on performing experiments to determine the feasibility of photoacoustic spectroscopy as a technique to measure oil concentration in water. The results presented in this chapter have shown that the photoacoustic response to certain analytes in water is greater than in transmission spectroscopy, as a result of the physical parameters that determine the magnitude of a photoacoustic waveform. Significantly, the indications are that this enhancement of changes in the optical absorption coefficient persists at very low concentrations of analyte. Experiments on crude oil emulsions in water have revealed a systematic increase in the photoacoustic signal with low levels of oil concentration at several near infrared wavelengths. At a source wavelength of 1064 nm and 2 mJ input energy, a 500 mg/l emulsion resulted in a signal 7.2 % greater than the response from distilled water, corresponding to a limit of detection of approximately 4 mg/l of oil.

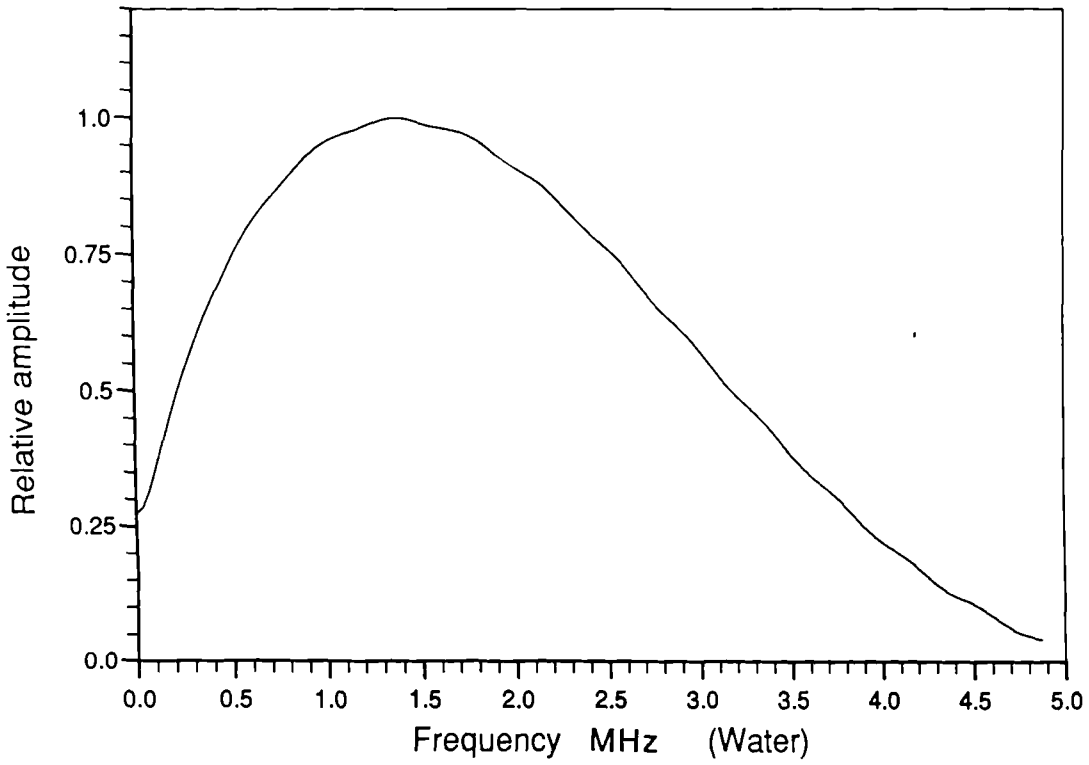

Fig. 4.21 Theoretically Predicted Frequency Content of Photoacoustic Pressure Pulse

Broadband studies of the acoustic waveform have shown that optical scattering from oil droplets has a significant effect on the shape of the optically generated acoustic waveform through the alteration of the acoustic source spatial profile. The additional absorption events that occur because of the increased mean photon path more than compensate for the increase in the volume of the acoustic source, resulting in an increasing magnitude of the photoacoustic signal with oil concentration. Scattering can also result in photons impinging directly on the acoustic detector, causing additional signals to be observed.

The nature of the oil in water monitoring problem means that it is desirable to be able to identify C-H bonds in different oils as well as C-H bonds existing within dissolved and dispersed components. Experiments have shown a much greater sensitivity per mg/l of analyte for dispersed oil (0.01%) compared to dissolved methanol (2×10^{-4}%). This can be attributed primarily to the much greater optical absorption coefficient of oil at the excitation wavelength (1064 nm). The absorption coefficient of crude oil tends to increase with decreasing wavelength at visible and short NIR wavelengths, as transitions in the electronic 'sea' become significant, in contrast to the absorption coefficients of the individual components of oil, which tend to decrease with decreasing wavelength. At the longer NIR wavelengths (1.2 μm to 2.0 μm), the absorption coefficients of oil are similar to those of the components of oil (*e.g.* pentane) that dissolve in water at low concentrations. Consequently the photoacoustic responses of dissolved and dispersed hydrocarbons are similar at those wavelengths. Thus it may be possible to distinguish between the presence of dissolved and dispersed components, using a range of excitation wavelengths that covers these two regions.

Thus photoacoustic spectroscopy has several aspects that make the principle of the detection well suited to the problem of monitoring oil in a water pipeline. Further aspects, involved more with the construction of an instrument based on the photoacoustic effect, are introduced in the next two chapters.

4.8. References

(4.1) Christison G.B., "The Determination of Blood Glucose Concentrations by Infrared Laser Photoacoustic Spectroscopy", Ph.D. Thesis, Dept. of Physics, Heriot-Watt University, 1992

(4.2) Burton C.J., *J. Acoust. Soc. Am.*, **20**(2), 186, 1948

(4.3) Parshad R., *Indian J. Phys.*, **15**, 323, 1941

(4.4) Maxwell J.B., "Data Book on Hydrocarbons", D. Van Nostrand Co., London, 1950

(4.5) Jamieson A.W., Shell U.K. Expro, private communication

(4.6) Kaye G.W.C., Laby T.H., "Tables of Physical and Chemical Constants and some Mathematical Functions", 15th ed., Longman, 1986

(4.7) "Petroleum Measurement Manual", Institute of Petroleum, Wiley & Sons, London, 1983

(4.8) Overton S., "Picosecond Time Resolved Single Photon Counting of Crude Oils", 4th Year Project, Dept. of Physics, Heriot-Watt University, 1992

(4.9) Tam A.C., Patel C.K.N., *Appl. Optics*, **18**, 3348, 1979

(4.10) Meier R., Arnesson J., Sigrist M.W., *Helv. Phys. Acta*, **57**, 262, 1984

(4.11) Komorowski S.J., Eyring E.M., *J. Appl. Phys.*, **62**(7), 3066, 1987

(4.12) Weight J.P., Hayman A.J., *J. Acoust. Soc. Am.*, **63**, 396, 1978

(4.13) Lai H.M., Young K., *J. Acoust. Soc. Am.*, **72**(6), 2000, 1982

(4.14) Heritier J-M., *Opt. Comm.*, **44**(4), 267, 1983

(4.15) Sullivan B., Tam A.C., *J. Acoust. Soc. Am.*, **75**(2), 437, 1984

(4.16) Quan K.M., MacKenzie H.A., Hodgson P., Christison G.B., *Ultrasonics*, **32**(3), 181, 1994

CHAPTER 5

Photoacoustics with New Laser Sources

5.1. Overview

There are several new developments in tunable near infrared laser technology that are of particular interest when considering the application of photoacoustic techniques to pollution monitoring. This chapter begins with a summary of the principles of operation and the characteristics of the relevant lasers. Photoacoustic experiments on oil in water samples conducted with two of these laser types, OPOs and diode lasers, are then described. A detailed analysis of the results obtained with diode laser sources is presented, including an estimate of the detection limit. The performance of near infrared diode lasers, as sources for photoacoustic generation for an oil in water measurement, is discussed as part of a wider discussion in which the suitability of the other new laser sources to instrumentation is considered.

5.2. Near Infrared Pulsed Laser Sources

5.2.1. Optical Parametric Oscillators

An optical parametric oscillator is based upon a non-linear optical process in which the energy of a pump photon of frequency ω_p is divided between two generated photons, called the signal and idler, such that the total photon energy is conserved. This is summarised by the equation

$$\omega p = \omega s + \omega i \qquad \{5.1\}$$

where ω_s and ω_i are the signal and idler frequencies respectively. Converting this to photon wavelengths, the idler wavelength λ_i is given by

$$\lambda i = \frac{\lambda s . \lambda p}{\lambda s - \lambda p} \qquad \{5.2\}$$

These equations show that there is a point at which the signal and idler photons are of equal frequency (half the pump photon frequency). This is known as the degenerate point. It is also apparent that to generate a signal photon of wavelength close to that of the pump photon, an idler photon of comparatively large wavelength is also generated. Thus there is the potential for very wide and continuous tunability in these systems. Equations {5.1} and {5.2}, the statements of energy conservation, do not give any indication as to which pair of photons are produced in any given system configuration. This is determined by a second conservation consideration, that of photon momentum and leads to the phase-matching condition that must also be satisfied.

$$kp = ks + ki + \Delta k \qquad \{5.3\}$$

k_p, k_s and k_i are the wave vectors of the pump, signal and idler photons respectively, and Δk is the momentum mis-match. For the most efficient operation of the OPO, Δk is zero.

The selection of one particular pair of generated photons is typically achieved by rotating the non-linear optical medium relative to the propagation axis of the pump beam, thereby altering the pump photon momentum within the medium and altering the second conservation criterion. Temperature tuning of the medium has also been used to vary the output wavelengths (5.1).

Crystals such as beta barium borate (BBO) usually form the non-linear medium, satisfying the theoretical requirements of large birefringence and d-coefficient, and the practical requirements of a high optical damage threshold and large crystal length. The pump requirements for BBO are met typically by XeCl

excimer or frequency tripled or quadrupled Nd:YAG lasers. Such systems can yield a tuning range extending from the near UV to beyond 3 μm in the near infrared. The theoretical tuning curve of a BBO OPO pumped at 308 nm is shown in fig. 5.1 (5.2), in which almost continuous tuning from the pump wavelength to 2.5 μm by rotation of the crystal is demonstrated. The linewidth of the tunable output has been one problematic area in the development of OPOs, especially at and near the degenerate point, where a linewidth of 10 nm was common. However in performing near infrared spectroscopy of liquids, where the absorption features are generally a few tens of nanometres broad, this is not a significant problem. Recent advances have nevertheless reduced the output linewidth to 0.14 cm^{-1} (0.013 nm @ 960 nm), such that spectroscopy of gases by the photoacoustic technique has been achieved (5.3).

Commercially available OPOs have recently begun to appear with output pulse energies of several tens of millijoules across the tuning range. These are currently based on flashlamp pumped Nd:YAG lasers. However diode pumped Nd:YAG lasers for pumping OPOs are the subject of much current interest (5.4, 5.5) and are likely to result in the development of commercial all solid-state tunable sources in the foreseeable future.

5.2.2. Diode Lasers

Diode lasers in their most usual form are not considered to be tunable sources. However they are important sources for spectroscopic applications, since as a result of their compact nature, several different devices may readily be combined into an instrument to provide a degree of wavelength coverage. True tunability may also be achieved with diode lasers, a topic discussed briefly in Section 5.2.3.

The operation of a diode laser is based upon the recombination of electrons and holes and the associated release of energy in the form of a radiated photon. This may be achieved at a simple p-n junction when electrons in higher energy levels (usually in the conduction band of a semiconductor) combine radiatively with holes in

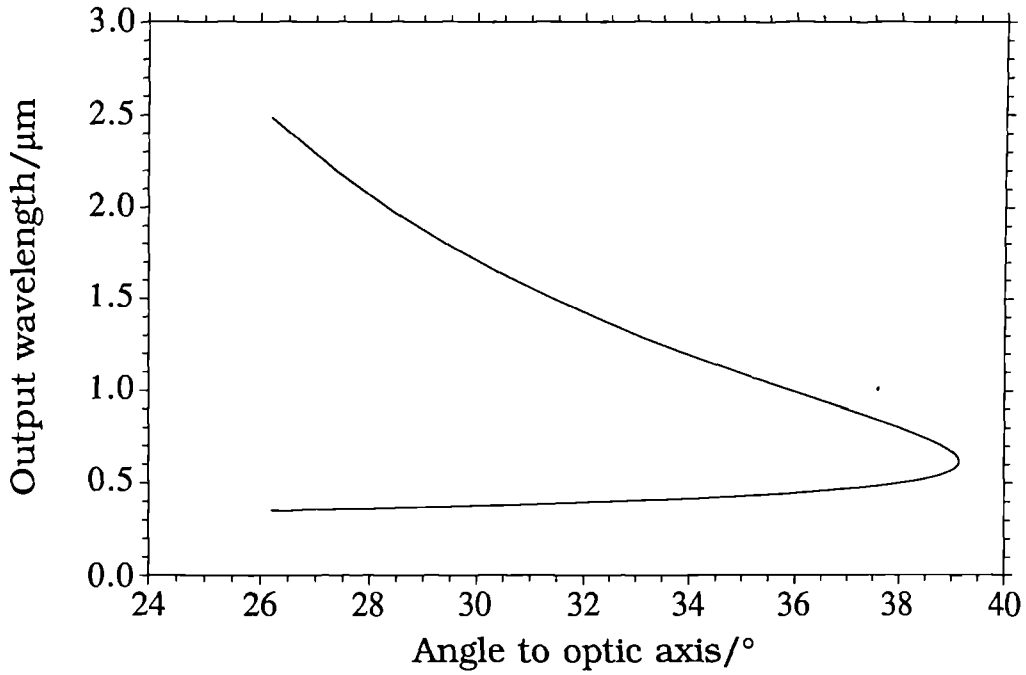

Fig. 5.1 Theoretical OPO Tuning Curve

lower levels (in the valence band). In order to achieve the necessary population inversion for efficient laser operation, doping of the n-type and p-type materials and the application of a forward current is required. The wavelength of the radiated emission is determined primarily by the bandgap of the active semiconductor layer. Polishing the ends of the semiconductor chip forms the reflectors of the laser cavity, that maintain the high photon density necessary for stimulated emission to dominate the optical transition processes.

The emphases of advances in diode laser design have tended to be towards reducing the threshold current density for lasing and narrowing the linewidth of the lasing emission. These have often taken the form of new semiconductor structures, such as double heterostructure devices, in which the injected charge carriers forming the population inversion are confined within the active layer, and buried heterostructure devices in which the active layer takes the form of a narrow stripe of semiconductor material. A further desirable feature is an active region of slightly higher refractive index than the surrounding semiconductor material, so that the confinement of photons is aided, increasing the photon density in the active region, also leading to a reduction in the threshold current density.

Much diode laser development has been driven by the need for sources for optical communications, as a result of which a few diode laser wavelengths, corresponding to the absorption minima of optical fibres (880 nm, 1300 nm and 1550 nm), are very common. The availability of diode lasers emitting at other wavelengths is currently patchy but improving. For example, new devices emitting at 1475 nm for the pumping of erbium doped fibre amplifiers, and 1650 nm for methane sensing are now available. There is also increasing interest in developing semiconductor devices that emit at wavelengths close to and longer than 2 μm (5.6, 5.7). These devices are typically based on III-V compounds such as InGaAsSb, and are targeted at applications such as environmental monitoring and molecular spectroscopy. The 3 - 4 μm region is of particular interest because the fundamentals of several vibrational transitions fall in this region.

High Pulsed Power Diode Lasers

Many diode lasers may be considered as weak emitters for the requirements of photoacoustic generation. However there is a class of diode lasers that can provide the necessary pulse energy. These devices have a relatively large volume active region and are driven by peak currents of several Amperes, in pulses of a few hundred nanoseconds duration. Table 5.1 shows a selection of some of the diode lasers belonging to this class.

All but the LD-163 are single diode devices. The LD-163 consists of three diodes (emitting regions) forming a stacked diode array on a single substrate. This type of device results in increases in the optical pulse energies that may be achieved although it becomes more difficult to combine the energy from such devices into a good quality beam.

λ (nm)	Manufacturer	Model	Pulse Energy (μJ)
640	LDP Inc.	CVD-640	0.1
810	SDL	2100	0.1
850	Northern Telecom	LP8M10C	0.2
880	Hamamatsu	L4356	4.0
904	LDP Inc.	LD-163	5.0
905	Northern Telecom	LA10	2.0
1300	EG&G	C86045	1.0
1475	Anritsu	FP-LD	0.2
1550	EG&G	C86091E	0.8

Table 5.1 High Pulse Energy Diode Lasers

5.2.3. Others

Wavelength tuning of diode laser output can be achieved in two ways; temperature tuning and via an external cavity. Lead salt diode lasers have been temperature tuned to emit over the range 8.5 μm to 15.9 μm (5.8) and the new quaternary compound lasers may be tuned by approximately 200 nm. External cavity tuning was first described in 1973 (5.9). By reducing the reflectivity of one end facet of a diode laser to a minimum and introducing a rotatable dispersive element positioned such that it forms a longer, external cavity with the remaining high reflectivity facet of the diode laser, a narrow band of the laser gain profile can be selected. The most recent developments have concentrated on broadening the tunable range, such that tuning ranges in excess of 200 nm using this technique have been reported (5.10). Commercially available instruments based on this technology are becoming common.

Fibre lasers are a further interesting source of tunable near infrared laser radiation. Optical fibre doped typically with a rare earth element such as erbium or neodymium forms a three or four level laser system (5.11). This may be pumped with one of a variety of sources, including laser diodes. Because the fluorescence spectrum of the rare earth doped fibre often extends over several tens of nanometres, so can the tuning range of the fibre laser. A typical arrangement is shown in fig. 5.2.

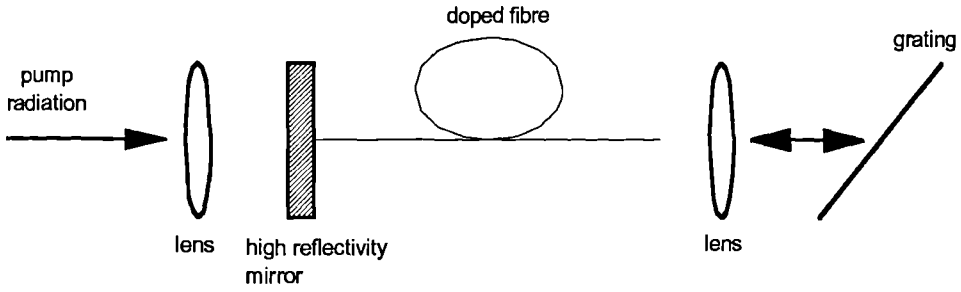

Fig. 5.2 Tunable Fibre Laser

The pump radiation is coupled into the doped fibre, approximately 1m in length, through a high reflectivity mirror forming one end of the laser cavity. The tuning of the fibre laser may be achieved in a number of ways, but is typically accomplished

by rotating a diffraction grating which forms the other end of the laser cavity. The narrow linewidth output may be accessed by inserting a pellicle in the cavity (not shown). Different dopants and fibres yield laser ouput in different regions of the spectrum. Erbium doped silica fibre lasers continue to be of great interest as they generate tunable radiation around the optical fibre 'window' of 1550 nm. Thulium doped silica fibre emits in the 2μm region and such a fibre laser has been tuned over a wavelength range of 276 nm (5.12). A tuning range of 86 nm centred at 1048 nm has been demonstrated from a Pr^{3+} silica based fibre laser (5.13). CW output powers are in the region of tens of mW.

The Ti:Sapphire laser is the most common of a class of solid state, four-level laser systems in which the laser operation is based upon a vibronic transition, whereby the active species undergoes a change in both electronic and vibrational state. Ti^{3+} ions are impurities formed within a crystal of sapphire and optical pumping excites these ions to a vibrationally excited state of an excited electronic state. From this level the ion relaxes to the upper laser level, before the laser transition reduces the ion to an excited vibrational level of the ground state. There is a broad laser transition linewidth in this system, leading to a wide tunable range. A final relaxation returns the ion to the ground state. Ti:Sapphire lasers are pumped by laser radiation of approximate wavelength 500 nm, such as is provided by a frequency doubled Nd:YAG laser. The emission covers the very near infrared region of the spectrum, typically from 660 nm to 1180 nm. Ti:Sapphire lasers are capable of delivering 100 mJ in 10 ns pulses and can also be used to generate extremely short (100 fs) pulses. Recent work has also used a Ti:sapphire laser as the optical source in high resolution photoacoustic spectroscopy of the vibration-rotation structure of C-H and C-C bonds in acetylene (5.14).

Colour centre (or F-centre) lasers are solid state tunable lasers with different crystal systems providing coverage of a wide range of visible and near infrared wavelengths. The active media are crystals into which point defects, in the form of impurities, have been deliberately introduced. These defects tend to absorb light in

the visible or near infrared and this absorption forms the pump transition for laser action. On absorption of a pump photon the atoms at the defect site become excited, and reconfigure themselves. The rearrangement, accompanied by a radiationless relaxation puts the defect site in to the upper laser level. This level has a lifetime long enough for stimulated emission to occur. From the lower energy level of the laser transition, the atoms at the defect site can relax back to the original configuration. Within the crystal, there exists a continuum of vibrational states, leading to broadening of the laser transition and the possibility of tuning of the emission wavelength. The emission wavelength itself can be made very narrow, making such lasers very good sources for spectroscopy.

5.3. OPO Experiments

The Physics and Astronomy Department at St. Andrews University, Fife, U.K. has expertise in designing optical parametric oscillators of many types. Preliminary near infrared photoacoustic measurements have been conducted with one of their OPO systems.

5.3.1. Experimental Arrangement

A XeCl excimer pumped OPO, previously described (5.15), was used as the optical source for photoacoustic measurements. A schematic of the OPO is shown in fig. 5.3.

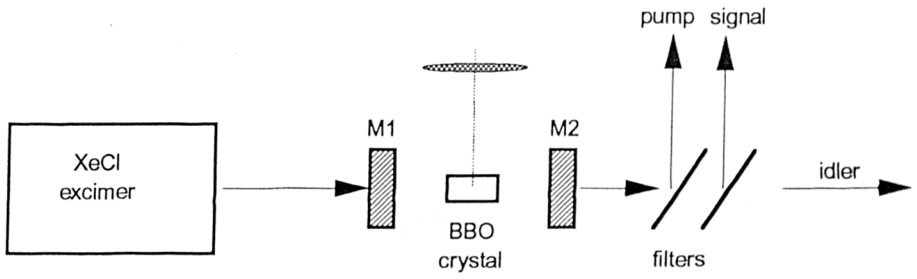

Fig. 5.3 Excimer pumped OPO

The XeCl excimer produced 17 ns, 100 mJ pulses at a wavelength of 308 nm. The pump laser linewidth was controlled to better than 0.25 cm^{-1} by injection seeding the power oscillator with a narrow linewidth master oscillator. M1 and M2 were mirrors forming the OPO cavity, and the BBO crystal could be rotated as shown to provide the tuning. Reflective filters removed the residual UV pump beam and the dominantly visible signal beam from the optic axis, leaving the idler beam for near infrared spectroscopic experiments. The idler pulse duration was typically 10 ns with a pulse energy of 5 mJ and a linewidth of approximately 3 nm at wavelengths much greater than the degenerate point (616 nm), at which point the linewidth was > 14 nm.

5.3.2. Results

Since the optical pulse energies available with the OPO source were three orders of magnitude greater than those available with either the Raman fibre system or diode lasers, it was necessary to investigate the linearity of the photoacoustic signal generated by the OPO. Fig. 5.4 is a plot of the photoacoustic signal magnitude versus the optical pulse energy and indicates that no non-linear effects in the photoacoustic generation were significant. The sample was 2 mm distilled water and the excitation wavelength was 1330 nm.

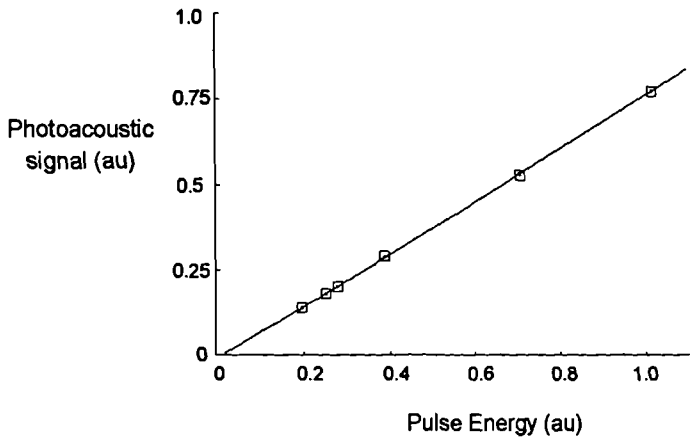

Fig. 5.4 Photoacoustic Signal Linearity

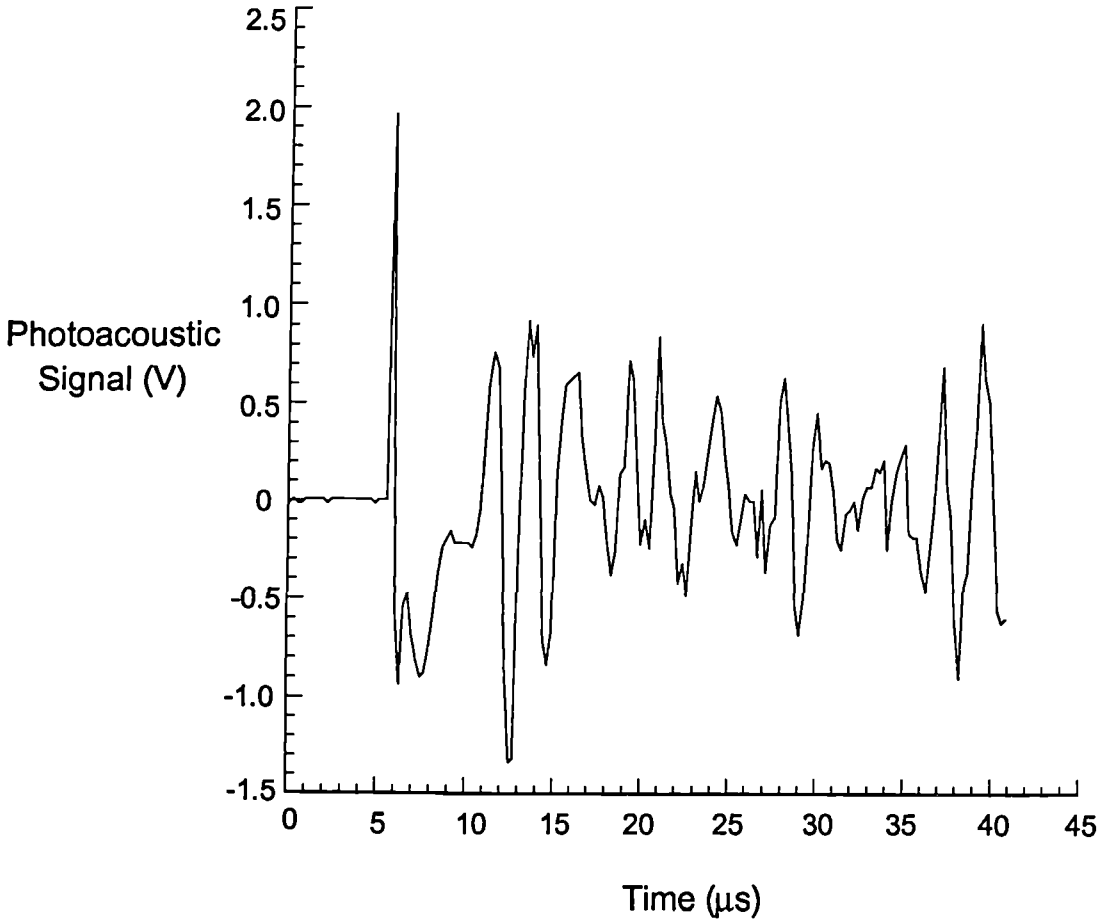

Fig. 5.5 Detected Waveform due to Photoacoustic Generation by an OPO

Photoacoustic experiments were conducted at several wavelengths in the near infrared. A typical waveform generated in 2 mm distilled water at 2260 nm is shown in fig. 5.5. The large spike at 6 μs (coincident with the optical pulse) was a consequence of the large electrical discharge required to operate the excimer OPO pump. The photoacoustic signal is evident, beginning just after 10 μs. There was considerable noise associated with the discharge spike which interfered with the true acoustic signal, making quantitative analysis difficult. A 200 ppm oil in water emulsion yielded a signal 1.1 ± 0.5 % greater than that generated in water at a wavelength of 1700 nm, averaged over 96 acquisitions, in reasonable agreement with the results achieved with the Raman fibre system. Much of the ringing visible in the latter stages of the photoacoustic signal was attributed to the use of a piezoelectric detector with a backing of poor acoustic impedance match.

5.4. Diode Laser Experiments

Diode lasers are of interest in photoacoustic experiments primarily because they constitute cheap and compact sources of intense optical radiation. In addition they are generally reliable over long operating lifetimes and rugged. Primarily because of the telecommunications industry, the technology to align diode lasers to efficiently launch light into optical fibres is well developed. Since the optical pulse energy, even from the most powerful devices is considered to be low for pulsed photoacoustic generation, a study to determine the feasibility of using diode lasers for photoacoustic measurements of oil content has been carried out.

5.4.1. Commercial Diode Lasers

Two of the commercially available diode lasers listed in Table 5.1, the LD-163 and C86091E, have been used to generate photoacoustic signals in various liquids. The LD-163 was chosen as a source for photoacoustic experiments because its emission wavelength of 904 nm coincides well with a small absorption feature present in both methanol and pentane. The emission wavelength of the C86091E (1550 nm)

is in the wings of the strong water absorption feature centered at 1445 nm. Each diode laser was driven by a Laser Diode Products Inc. LP-11, capable of supplying up to 80 A peak current in pulses of typically 200 ns duration. Investigation of the optical pulse energy from the diode lasers was performed by butting a Gentec pyroelectric joulemeter against the window of each diode laser. For the LD-163, the average pulse energy measured over 2560 pulses was 2.320 ± 0.001 μJ / pulse for a peak drive current of 30 A. The pulse energy from the C86091E was 1.03 μJ / pulse for a peak drive current of 16 A. These values were highly repeatable, after cycling the peak drive current through levels below the threshold of the laser and in terms of the pulse to pulse stability. The experimental arrangement for photoacoustic studies was as shown in Fig. 5.6. Because of the optical pulse stability, energy monitoring and normalisation of the acoustic signal to pulse energy was not required. In long term operation however, energy monitoring of the diode laser output would very likely be necessary.

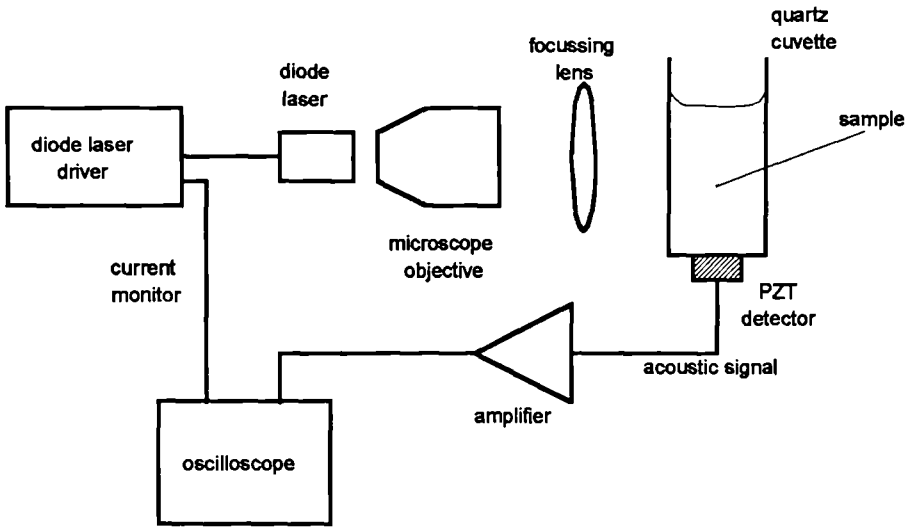

Fig. 5.6 Diode Laser Photoacoustic Experiments

A microscope objective (x 20, 0.4 NA) was used to collimate the diode laser beam and a 19 mm focal length lens was used to bring the beam to a focus. The profile of the LD-163 beam at the focus clearly showed the structure of the stacked

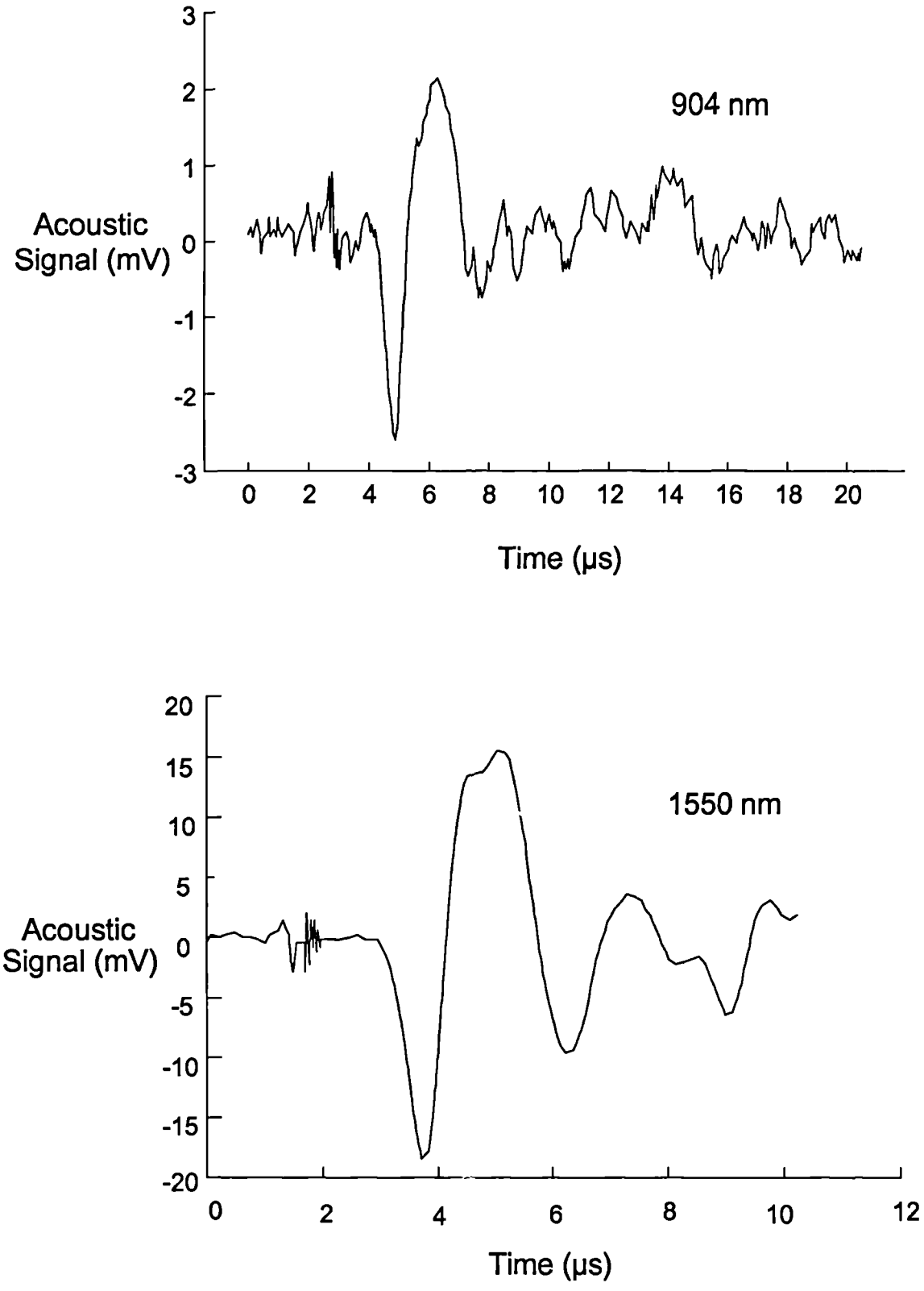

Fig. 5.7 Photoacoustic Waveforms Generated by Diode Laser Excitation

array, three bright regions being visible. The overall profile was 350 μm by 300 μm at the $1/e^2$ points of the focus, from an emitting area on the diode facet of 230 μm by 200 μm.

The photoacoustic response from oil in water emulsions prepared using the techniques described in Chapter 4 was measured using the two diode lasers. The acoustic detector was based on a well damped piezoelectric ceramic with a natural resonant frequency of 890 kHz. 50 dB of amplification was used before the acoustic signal was displayed on the digitising oscilloscope. Typical photoacoustic waveforms (256 averages) generated in distilled water at 904 nm and 1550 nm are shown in fig. 5.7. The response to oil concentration at the two wavelengths is shown in fig. 5.8. Each point is the result of 1280 acquisitions.

At 904 nm there is clearly a systematic increase in the amplitude of the photoacoustic signal with increasing oil concentration. An oil concentration of 890 mg/l results in a signal 12 % larger than that from distilled water. This corresponds to a detection limit of approximately 400 mg/l of oil. Increasing the number of acquisitions to 4096 should improve this to 200 mg/l. At 1550 nm, such a clear response is not evident and there is only a marginal increase in the photoacoustic signal over a concentration range up to 890 mg/l. The reasons for this are discussed later.

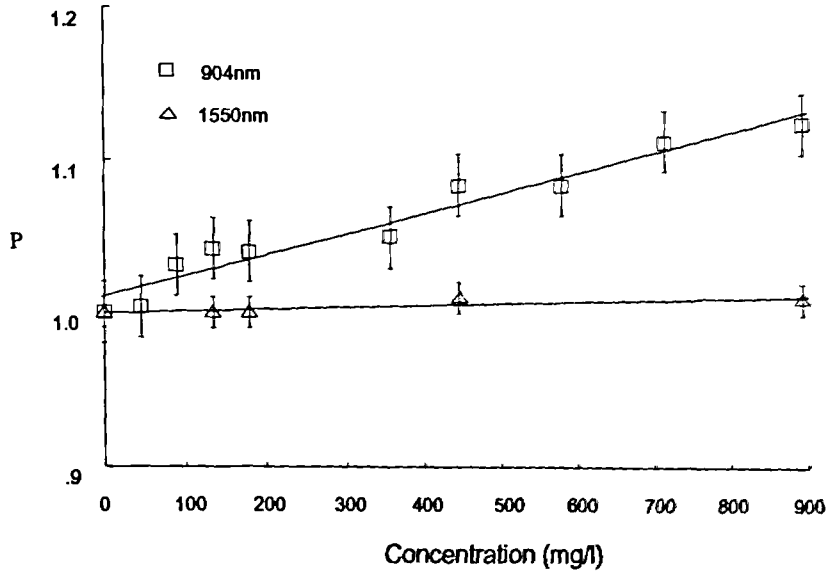

Fig. 5.8 Diode Laser Photoacoustic Measurement of Oil Emulsions

Diode laser experiments have also been conducted to measure the photoacoustic response to methanol concentration in water at 904 nm (5.16), and found a similar functional response to measurements made with the Raman fibre system, as described in Section 4.2. However, there remains a key difficulty in that the signal to noise ratios in photoacoustic measurements achieved with diode laser sources are not yet sufficient to meet the demands of measuring 40 ± 4 mg/l oil in water.

5.4.2. 2.0 μm Diode Lasers

InGaAsSb diode lasers grown by liquid phase epitaxy (5.6) were obtained from the A.F. Ioffe Physical Technical Institute, St. Petersburg and experiments performed to determine the suitability of such sources for the generation of photoacoustic waves in liquids. The emitted wavelength of these devices may be temperature tuned at a rate of 1 nm / K to cover approximately 200 nm with a single device. The devices were mounted at the focus of a parabolic reflector and the radiation brought to a focus with a 19 mm focal length lens.

Diode laser emission from the two end facets of the laser cavity, of approximate length 300 μm, was detected by profiling the laser beam in front of the reflector using a high speed InGaAsSb photodiode, also from the A.F. Ioffe Institute. At the focus of the lens the beam measured 1 mm by 0.75 mm (FWHM). A 1 mm pathlength quartz cuvette containing distilled water was positioned at the beam focus. Attached to the base of the cuvette, a 2.0 mm thick PZT element backed by a lead cylinder formed the acoustic detector. Amplification of 50 dB was used before the acoustic signal was monitored on an averaging oscilloscope. At room temperature the wavelength of the diode lasers was approximately 1.94 μm, very close to the peak of the strong water absorption feature centred on 1.92 μm. The peak driving current was 4 A and the pulse duration 350 ns (FWHM). In this configuration a photoacoustic signal of peak to peak voltage 1.0 ± 0.3 mV was observed. Quantitative analysis with this system could not be achieved because of the poor signal to noise ratio.

5.5. Discussion

The photoacoustic data obtained with the commercial diode lasers show the response to oil concentration in water under two quite different optical absorption conditions. At 904 nm, the background absorption of water is very low, approximately 0.07 cm^{-1} (5.17), whereas the absorption coefficient of the oil has been measured to be 14 cm^{-1}. In contrast at 1550 nm, the optical absorption coefficients of water and crude oil are similar. These differences in the optical conditions are borne out in the response to oil concentration. A theoretical curve (solid line) for the photoacoustic signal increase at 904 nm has been compared to a linear regression (dashed line) fitted to the data, in fig. 5.9. A similar graph shows the same curves for the case at 1550 nm (fig. 5.10). Linear variations in α, β, C_p, and υ have been assumed for the theoretical curves, with the exception that a constant optical absorption coefficient has been assumed for the 1550 nm case. This is regarded as being a reasonable assumption as the relatively high value of the absorption coefficient at 1550 nm (10 cm^{-1}) meant that there was almost total absorption of the optical beam within the confines of the cuvette for all samples and that therefore small changes in α had little bearing on the amplitude of the photoacoustic signal. For both wavelengths, there is general agreement between the theoretical and the measured data.

It is noticeable that at 904 nm the measured response is not as large as predicted by the theory. One possibility for this anomaly is that not all of the optical energy absorbed within the oil droplets is contributing to the generation of a photoacoustic signal. One likely explanation is that some of the absorbed energy is being released in radiative transitions in the form of fluorescence. It is likely that this would become even more of a consideration at shorter optical excitation wavelengths. The use of a diode laser emitting at 860 nm would be of considerable interest, since this coincides with the fourth harmonic of a C-H resonance in benzene, but it is quite possible that the fluorescence generated in oil by such an excitation wavelength could counteract any photoacoustic advantages. The results at 1550 nm indicate that the

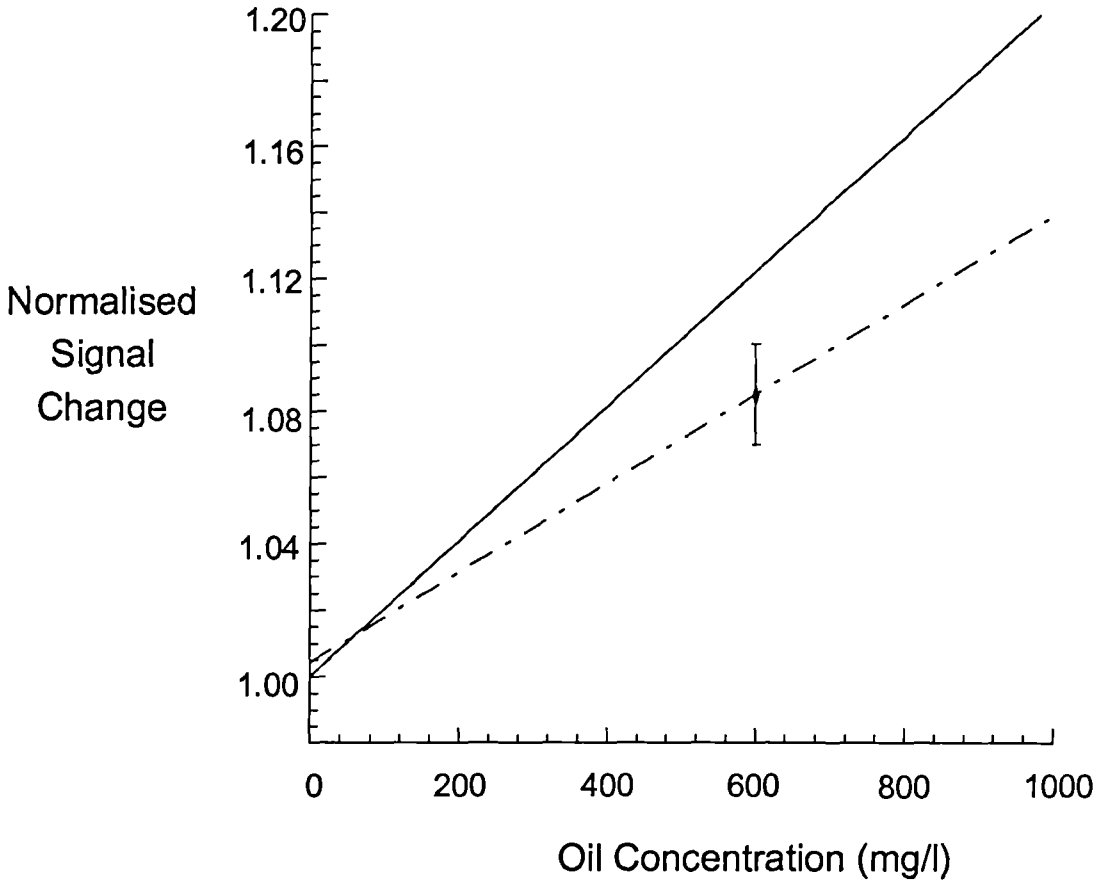

Fig. 5.9 Theoretical and Experimental Photoacoustic Response to Oil Concentration using a 904 nm Diode Laser

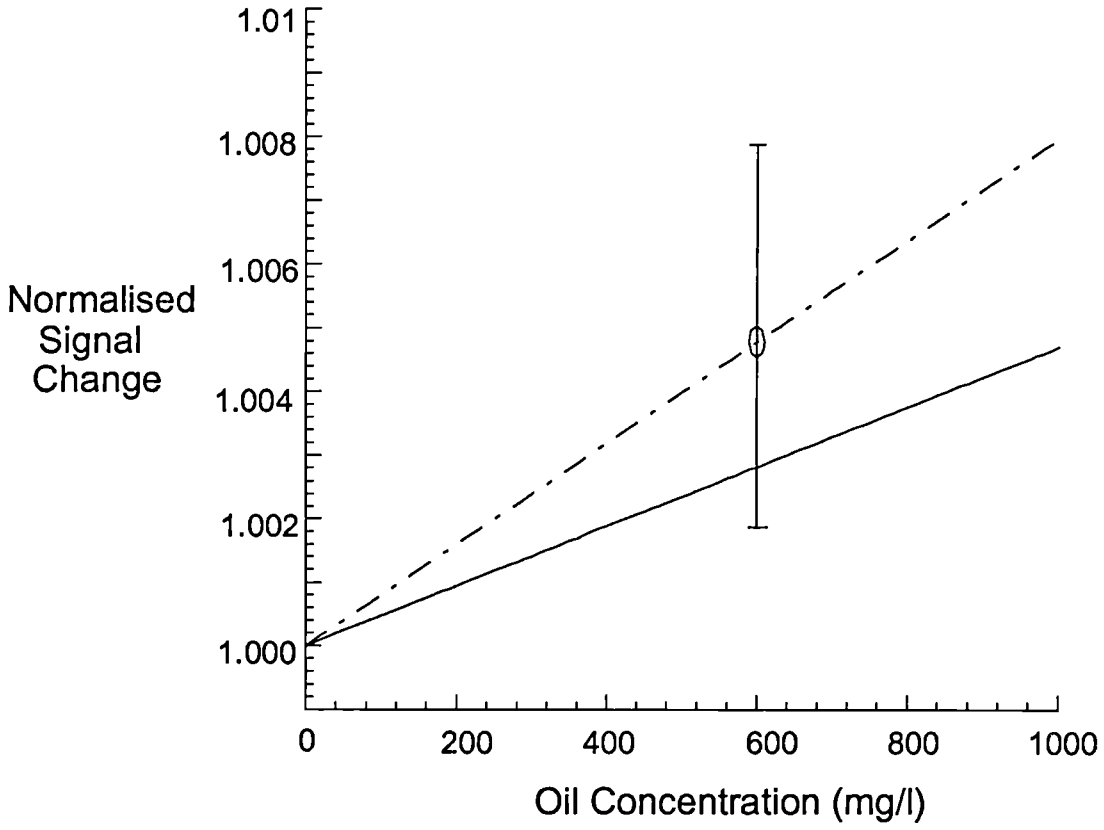

Fig. 5.10 Theoretical and Experimental Photoacoustic Response to Oil Concentration using a 1550 nm Diode Laser

small observed changes in the photoacoustic signal at that wavelength can be attributed primarily to changes in the physical parameters of the sample.

The emphasis of the research and development of new diode laser sources is shifting towards spectroscopic applications, matching the emission wavelength to key optical absorption features of analytes, such as methane, that are of interest in environmental monitoring. Developments in the other near infrared sources discussed in Section 5.2 will be of interest for photoacoustic and other forms of spectroscopy. The prospect of all solid state, widely tunable systems such as the diode pumped OPO is particularly exciting both for instrument development, and as a source with which fundamental studies of materials and of the photoacoustic process may be carried out.

5.6. References

(5.1) Ebrahimzadeh M., Robertson G., Dunn M.H., *Optics Lett.*, **16**(10), 767, 1991

(5.2) Robertson G., St. Andrews University, private communication

(5.3) Haub J.G., Johnson M.J., Orr B.J, Wallenstein R. *Appl. Phys. Lett.*, **58**(16), 1718 1991

(5.4) Kozlovsky, W.J., Nabors C.D., Eckardt R.C., Byer R.L., *Opt. Lett.*, **14**(1), 66, 1989

(5.5) Ebrahimzadeh M., Malcolm G.P.A., Ferguson A.I., *Opt. Lett.*, **17**(3), 183, 1992

(5.6) Baranov A.N., Danilova T.N., Dzhurtanov B.E., Imenkov A.N., Konnikov S.G., Litvak A.M., Usmanskii V.E., Yakovlev Yu.P., *Sov. Tech. Phys. Lett.*, **14**(9), 727, 1988

(5.7) Choi H.K., Eglash S.J., *Appl. Phys. Lett.*, **61**(10), 1154, 1992

(5.8) Walpole J.N., Calawa A.R., Harman T.C., Groves S.H., *Appl. Phys. Lett.*, **28**(9), 552, 1976

(5.9) Rossi J.A., Chinn S.R., Heckscher H., *Appl. Phys. Lett.*, **23**(1), 25, 1973

(5.10) Tabuchi H., Ishikawa H., *Electron. Lett.*, **26**(11), 742, 1990

(5.11) Reekie L., Mears R.J., Poole S.B., Payne D.N., *J. Lightwave Tech.*, **LT-4**(7), 956, 1986

(5.12) Hanna D.C., Percival R.M., Smart R.G., Tropper A.C., *Opt. Comm.*, **75**(3,4), 283, 1990

(5.13) Shi Y., Poulsen C.V., Sejka M., Ibsen M., Poulsen O., *Elec. Lett.*, **29**(16), 1426, 1993

(5.14) Zhan X., Kauppi E., Halonen L., *Rev. Sci. Instrum.*, **63**(12), 5546, 1992

(5.15) Ebrahimzadeh M., Henderson A.J., Dunn M.H., *IEEE J. Quant. Elec.*, **26**(7), 1241, 1990

(5.16) Dear A.R., "The Application of Laser Diodes in Pulsed Photoacoustic Spectroscopy", 4th Year Project, Dept. of Physics, Heriot-Watt University, 1992-93

(5.17) Palmer K.F., Williams D., *J. Opt. Soc. Am.*, **64**(8), 1107, 1974

CHAPTER 6

Photoacoustic Instrumentation

6.1. Overview

In this chapter, three aspects of photoacoustic instrumentation are considered, with particular emphasis on the application of monitoring oil in water in a pipeline. The utilisation of optical detection techniques is an attractive concept in many monitoring applications since it removes the necessity for electronics (susceptible to electromagnetic interference and a fire hazard) at the measurement point. Experiments using one optical technique, that of fibre interferometry, to detect photoacoustic waves are described.

In the second part of the chapter, the realisation of pre-prototype instrumentation for a demonstration of the measurement of oil in water in a pipeline using photoacoustic techniques is described. The principles involved and the construction of the detector are presented, along with preliminary results obtained on a pipeline demonstrator apparatus.

The overview of other instrumentation techniques to measure oil in water summarised in Chapter 1 is considered more completely. The principles of operation are discussed and through the discussion, comparisons with the photoacoustic technique are made. The advantages and disadvantages of a photoacoustic instrument for an oil in water measurement are detailed.

6.2. Optical Detection of Photoacoustic Waves

An instrument incorporating an all optical detection head has several attractive features. In particular, the removal of sensitive electronics away from the vicinity of a noisy and hazardous measurement region, as might be encountered on an oil production platform, could be of prime importance. In addition, optical techniques often have the advantage of being able to make non-contact, broadband and real-time measurements, and may give an absolute calibration of a parameter. The optical detection of acoustic waves has been achieved by many groups using several different principles, as outlined in Section 2.5.2. Experiments using optical fibre interferometry to detect photoacoustic waves are described here.

6.2.1. Optical Fibre Interferometers

A Michelson-based optical fibre interferometer has been used to make absolute measurements of the acoustic displacements at the surface of a liquid generated by the photoacoustic process within the liquid. A schematic of the experimental arrangement is shown in fig. 6.1. A Spectron Lasers Q-switched Nd:YAG laser operating at 1.064 μm was used to generate the photoacoustic waves. The pulse energy was 1.6 mJ, the duration 180 ns (FWHM) and the beam was brought to a 25 μm diameter focus in a quartz cuvette.

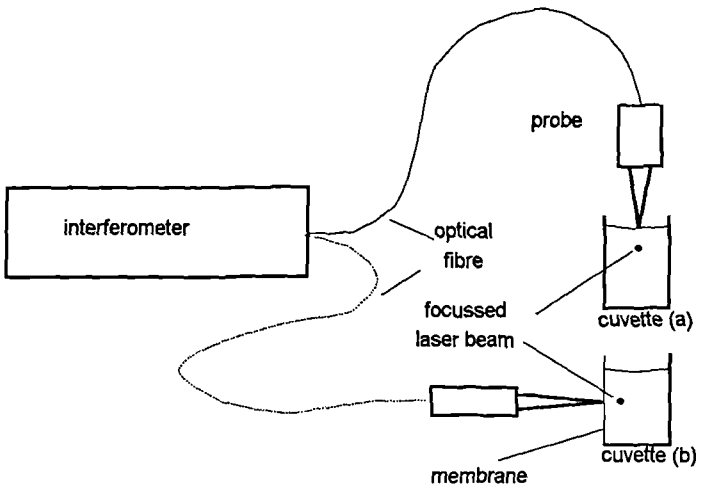

Fig. 6.1 Fibre Interferometer Experiments

Two configurations were used to detect the photoacoustic waves. Cuvette (a) had a pathlength of 5 mm, and the acoustic displacements at the surface of the liquid were detected. Cuvette (b) was of 2 mm pathlength. One side wall of the cuvette was cut away and replaced with a 25 μm thick highly reflecting membrane. Vibrations coupled from the liquid into the membrane were detected by the interferometer. More details of the experiments and of the interferometer itself may be found in reference (6.1).

6.2.2. Results

Acoustic displacements generated in water and in methanol were observed with both cuvette configurations. The reflectivity of both liquids in air is approximately 2%, resulting in a weak return signal when using cuvette (a) and a noise floor corresponding to a surface displacement of 0.1 nm over a 1 MHz bandwidth after 256 averages. In comparison, the high reflectivity (80%) of the membrane resulted in a noise floor of 0.01 nm when cuvette (b) was used. The displacement signal from a methanol sample in cuvette (b) is shown in fig. 6.2. A positive and negative going acoustic displacement was observed within 2 μs of the arrival of the pulse. Following this, the membrane relaxed to its original position, before a reflection from the other side wall of the cuvette arrived at the membrane, approximately 12 μs after the arrival of the first pulse. The peak displacement generated in methanol was 3.2 nm, and in water 0.23 nm.

6.2.3. Analysis

The peak acoustic pressure at position r, p(r) can be approximated to the acoustic displacement, d(r) by the relationship (6.2)

$$p(r) \approx \frac{\upsilon \rho d(r)}{\tau_d}. \qquad \{6.1\}$$

where ρ is the sample density, υ is the acoustic velocity and τ_d is the time for the displacement to reach its peak value. Thus the measured peak displacements in

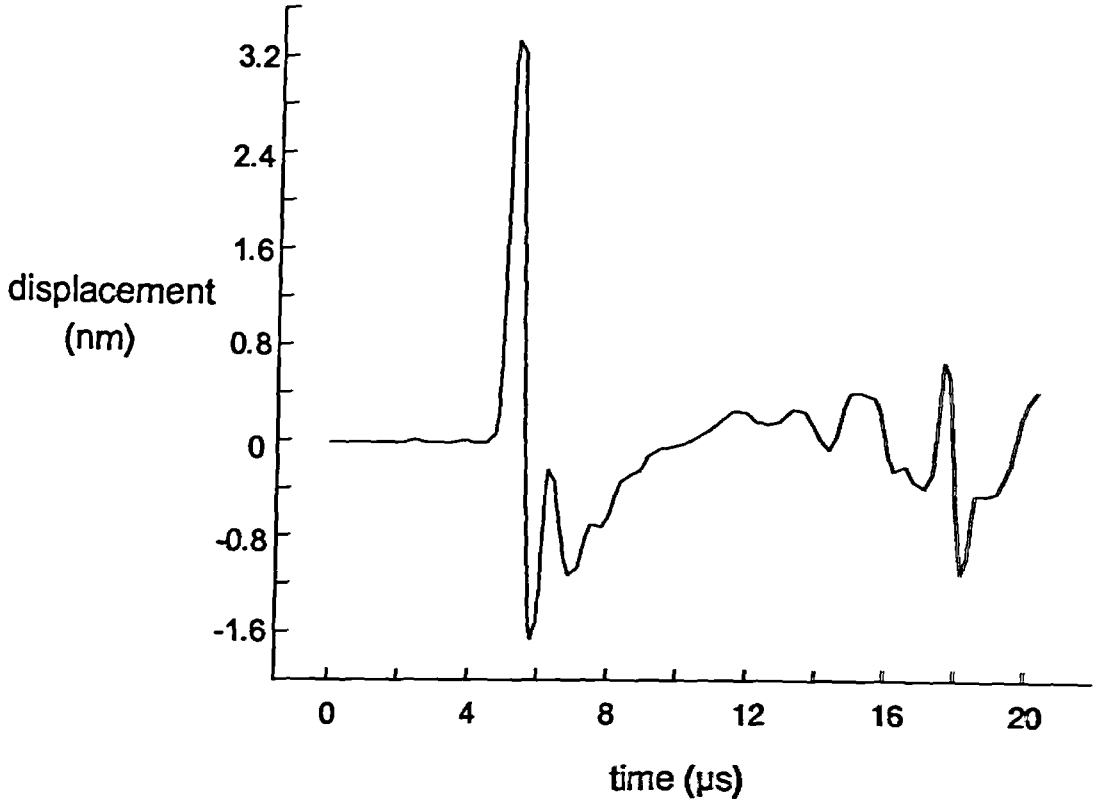

Fig. 6.2 Displacement Waveform Generated in Methanol

Measured by a Fibre Optic Interferometer

methanol and water correspond to excess peak pressures of 1.6 x 10^4 $N.m^{-2}$ and 1.9 x 10^3 $N.m^{-2}$ respectively. For a plane acoustic wave, the instantaneous pressure is proportional to the displacement velocity in the medium (6.3). A tenth order polynomial was fitted to the acoustic displacement waveform generated in methanol and differentiated to obtain the displacement velocity. This has been normalised to the peak pressure given above and is shown in fig. 6.3 (solid curve), along with the original displacement waveform (dashed curve) for the first 1 μs of the signal.

This derived pressure waveform may be compared to the actual pressure waveform measured by the broadband piezoelectric probe described in Chapter 4, and to the theoretical pressure waveforms of Lai & Young and Heritier (6.4, 6.5). According to Lai & Young, the time between the maximum compression and the maximum rarefaction is $2.35.\tau_e$. For the experimental conditions described above, τ_e ~ 181 ns so that the predicted time between the pressure maximum and minimum is 425 ns. The corresponding measurement of the time delay from the derived pressure waveform is 430 ns, in excellent agreement.

Since the optical interferometer provides a measurement calibrated to the wavelength of the laser used within the interferometer, this detection technique can be used to calibrate other elements of the photoacoustic system. The pressure generated in a weakly absorbing liquid by the photoacoustic effect can be related to the physical parameters in the sample through the formula

$$p = k.\frac{\alpha\beta v^{\frac{1}{2}}}{C_p}.E \qquad \{6.2\}$$

as discussed in Chapter 2, where k is a system constant which contains information about the geometrical arrangement of the measurement system and the optical pulse parameters. For the particular experimental conditions used to obtain the acoustic displacement data using the optical interferometer, values of k have been calculated from the water and methanol samples. Substituting the calculated pressure from the water result into equation {6.2} yields a value for k of 5.6 x 10^{10} $m^{-1/2}.s^{-3/2}$ and a similar value of 4.9 x 10^{10} $m^{-1/2}.s^{-3/2}$ from the methanol result. For the same

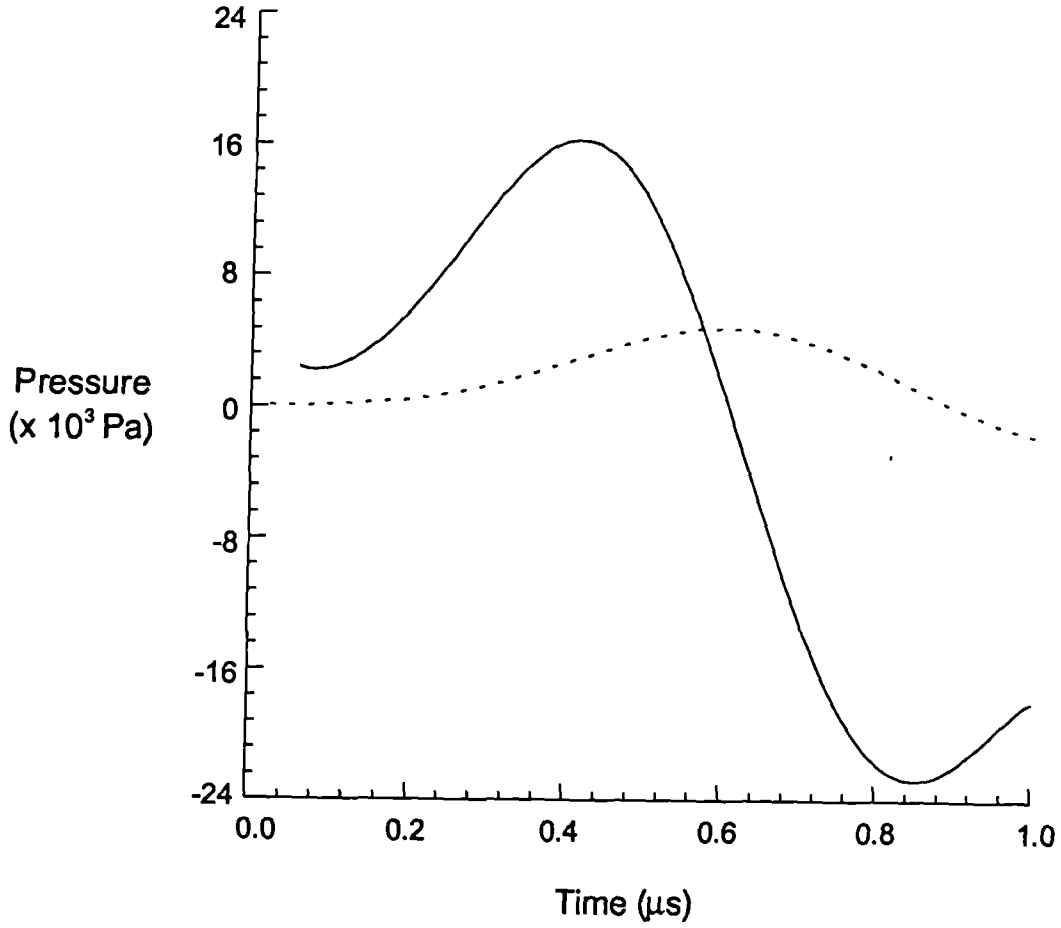

Fig. 6.3 Pressure Waveform (solid line) Derived from the Displacement Waveform (dashed line)

experimental arrangement the value of k should be essentially the same, and this is borne out by the good agreement of the two calculations above.

6.3. Pipeline Demonstration

The impetus behind much of the work presented in this thesis has come from the specific operational requirement of continuously monitoring the hydrocarbon content in the discharge water in a pipeline on an oil production platform. To prove the principle of an instrument to meet this requirement based on a photoacoustic measurement, a demonstration system has been constructed. This consisted of a short plastic pipeline through which a sample could be circulated, and an instrument that could be inserted into the pipeline to obtain the photoacoustic spectra from which an estimate of the oil concentration could be made. The primary mechanical targets for this pre-prototype instrumentation were that it should be installed in the pipeline through a single flange and that it should be encased in a housing no more than 1.5 inches in diameter.

6.3.1. Detector Design

Optics

One of the key features of the instrument was that it should incorporate fibre optic delivery of the near infrared radiation to the photoacoustic generation region, so that the rapid switching of high currents for the diode lasers was remote from the detector head and the sensitive electronics within. In addition, it was necessary to bring the radiation down to a small spot size, as either a focussed or collimated beam, in order to maximise the amplitude of the photoacoustic wave. Two custom units to meet these specifications were provided by Point Source, Winchester, SO21 1TH, U.K.. The first used a single, large core (1.5 mm diameter), 2 m long fibre to provide the light delivery. The second was designed to couple light emerging from the output slit of a monochromator to the photoacoustic interaction region and consisted of a

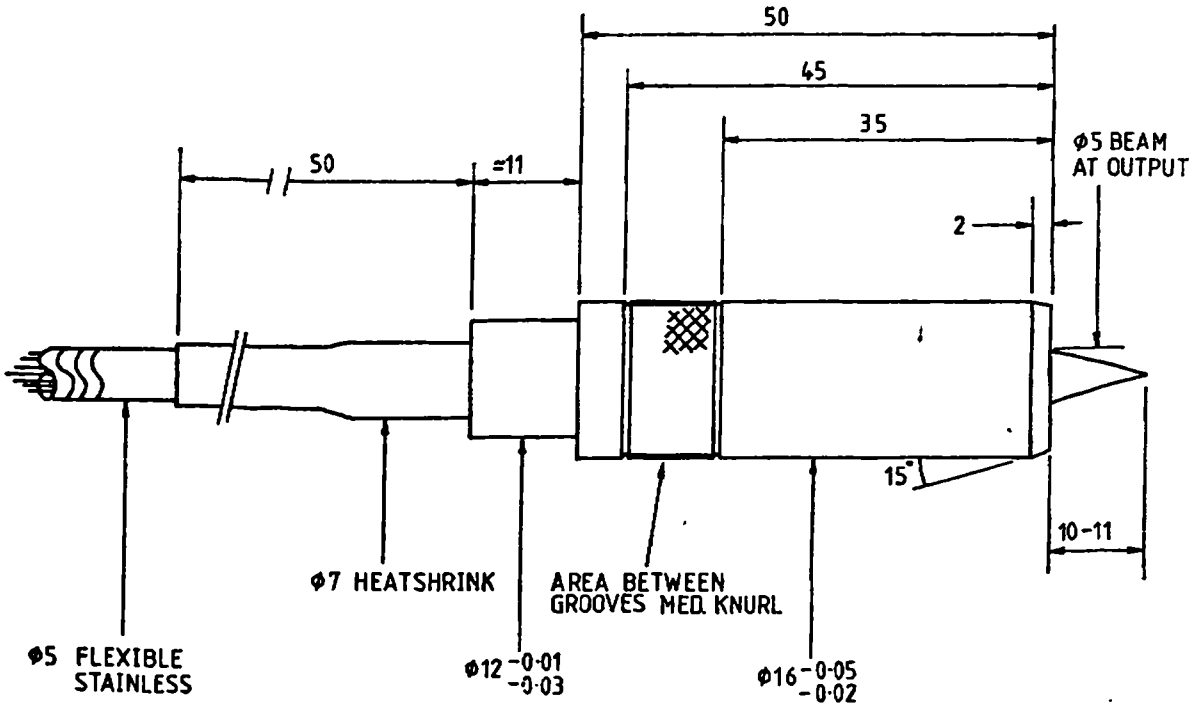

Fig. 6.4 Housing for Optical Elements

bundle of eight fibres (each with a 200 μm core diameter). The input stage was a linear array of the eight fibres. Seven of these fibres constituted the optical delivery link, and were formed into a 2 m long bundle with a circular cross-section at the output stage. The eighth fibre was left free to provide an option for energy monitoring.

An identical housing, 16 mm in diameter was attached to the output end of both fibre links. Within the housing, a lens system collected the light from the fibre(s) and brought it to a focus a few millimetres in front of the housing. A diagram of the housing is shown in fig. 6.4.

Acoustics

The acoustic detector was based upon a 1 mm thick, 5 mm diameter PZT 5A piezoelectric ceramic transducer mounted directly behind a thin (0.5 mm) polished flat surface over which the sample could flow. A backing element, attached to the rear face of the piezoelectric transducer with epoxy, provided acoustically impedance matched damping for the acoustic waves. The backing element was shaped so as to minimise the effect of acoustic reflections on the piezoelectric transducer. Electrical connections were made through the case and the backing element. A cap 20 mm in diameter, together with a silicon rubber mixture, sealed the acoustic detector unit from the liquid sample.

The optical and acoustic units were brought together in a three-part stainless steel housing, 38 mm in diameter, shown schematically in fig. 6.5. The near infrared beam was directed through a quartz window and brought to a focus approximately 3 mm above the polished flat surface, beneath which the piezoelectric element was positioned. Electronic circuitry on a printed circuit board (PCB) incorporating 50 dB amplification was mounted beneath the optics housing. Both these elements were clamped in position. An O-ring surrounding the optics unit and the electronics connection completed the sealing of that part of the unit that would be submerged. A single flange 80 mm in diameter was the means by which the instrument was attached

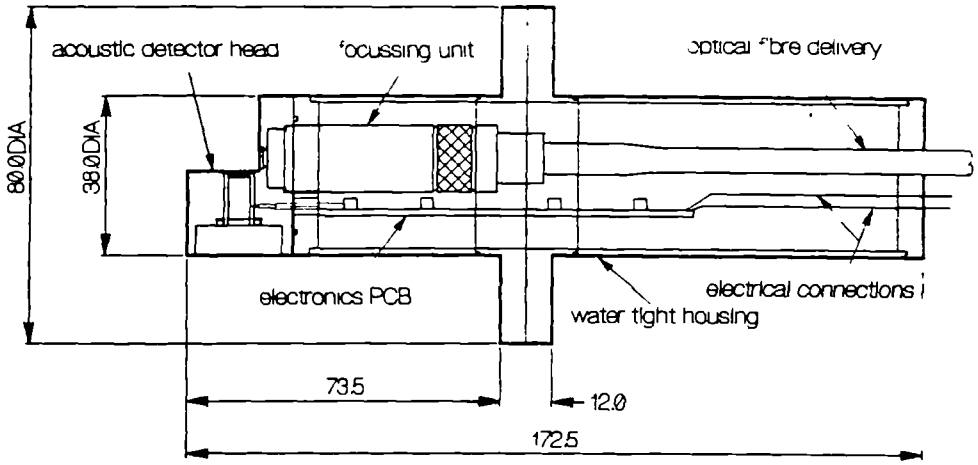

Fig. 6.5 Schematic Diagram of the Pre-Prototype Instrument

(a)

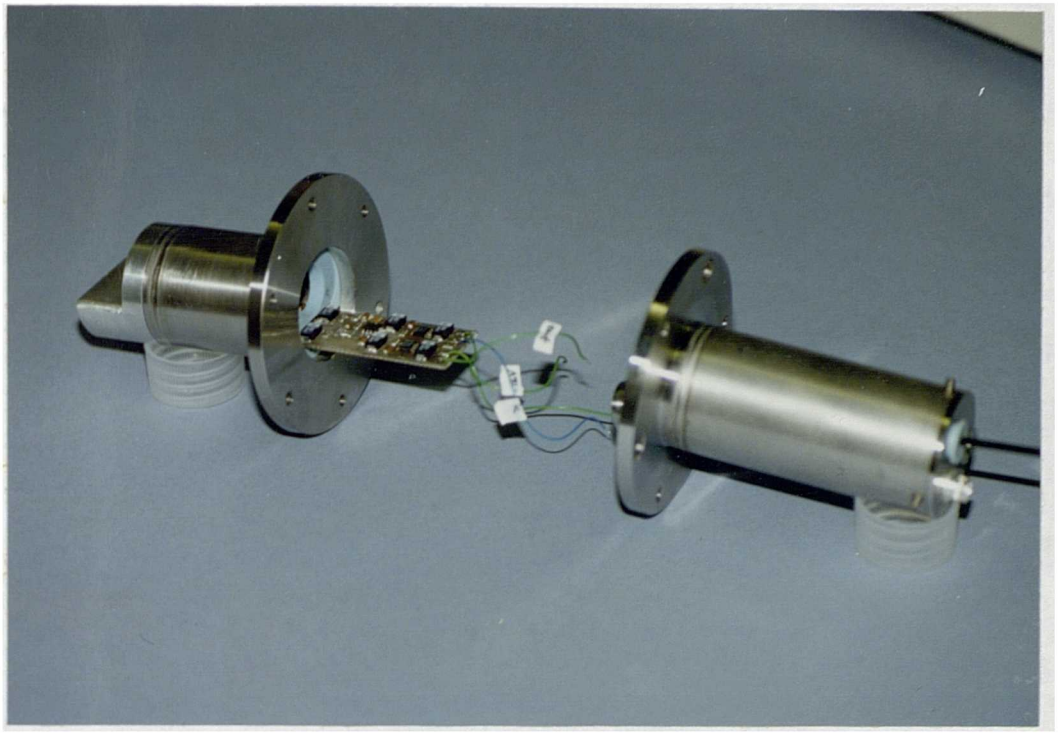

(b)

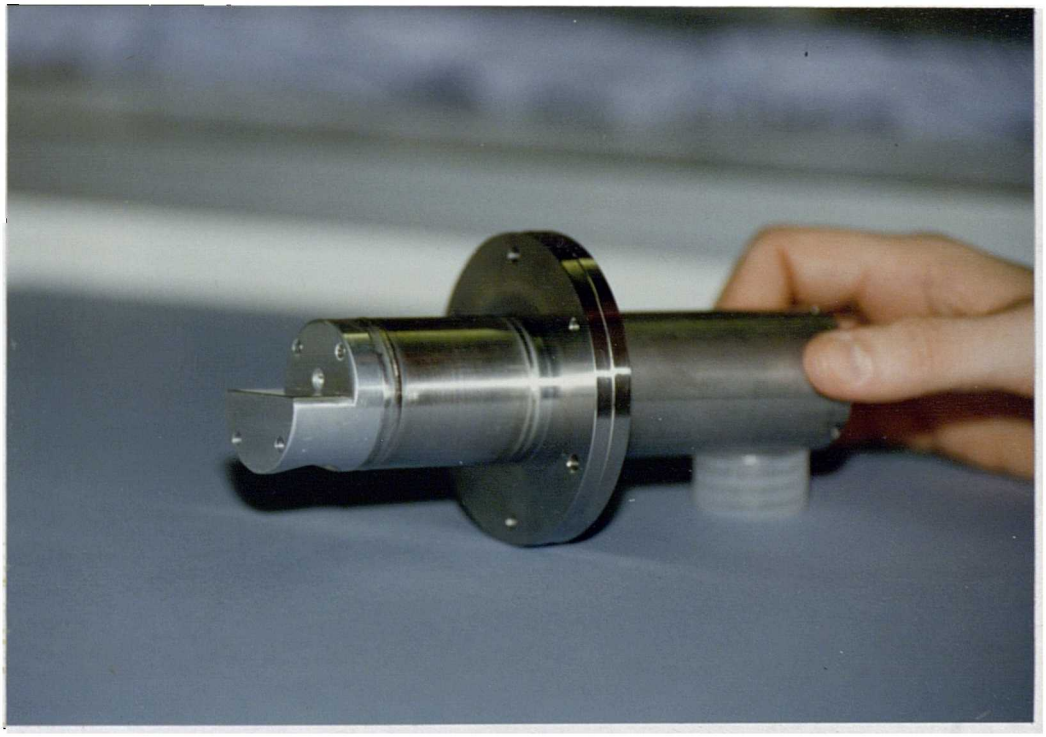

Fig. 6.6 Pre-Prototype Photoacoustic Oil in Water Monitor :

(a) showing interior detail

(b) assembled unit

to the pipeline. The optical fibre delivery and four electrical connections were made through the back plate of the housing.

Figure 6.6 a) & b) shows photographs of the instrument in close-up. Detail of the position of the electronics PCB and the vacancy for the optics unit above it may be seen in fig. 6.6 a) whilst in b), the position of the quartz window relative to the polished flat is apparent. Figure 6.7 shows the instrument mounted in the pipeline demonstrator and submerged in the sample process water. The fibre delivery (upper cable) and two electrical cables (lower) are clearly visible at the back of the instrument.

6.3.2. Experimental Results

Single Wavelength Measurement

Preliminary results were obtained from the pre-prototype instrument using Q-switched Nd:YAG laser radiation, launched into the 1.5 mm diameter fibre, as the optical source. A beam profile of the output from the optics unit showed that the focus was approximately 3 mm from the front face of the unit, and that in the region where photoacoustic generation would be most efficiently coupled to the piezoelectric transducer, the beam diameter was approximately 4 mm, considerably larger than the optimum for photoacoustic generation. Initially, the detector was dipped into a beaker of water and a well damped photoacoustic waveform of peak to peak amplitude 320 mV was observed. The noise level after 256 averages was 3 mV rms. The acoustic pulse duration was 4 μs, indicating a dominant frequency of approximately 250 kHz, somewhat less than the natural resonant frequency of the piezoelectric element as a result of the large optical spot size and the mounting around the element. The instrument was then installed into the pipeline, and a clean (tap) water sample was circulated. The photoacoustic signal detected was very similar to that detected in the beaker of water, but the noise level had increased (due to the water pump), so that the signal to noise ratio was 62:1 after 256 averages. The photoacoustic waveform is shown in fig. 6.8.

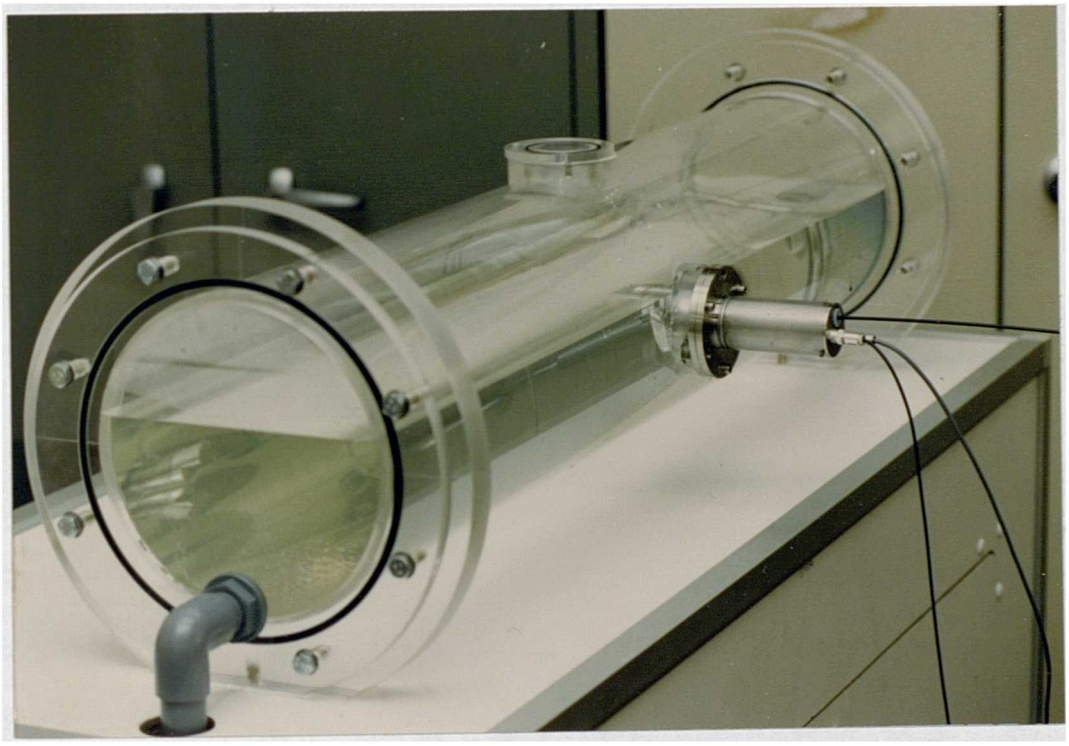

Fig. 6.7 Instrument Installed in a Pipeline

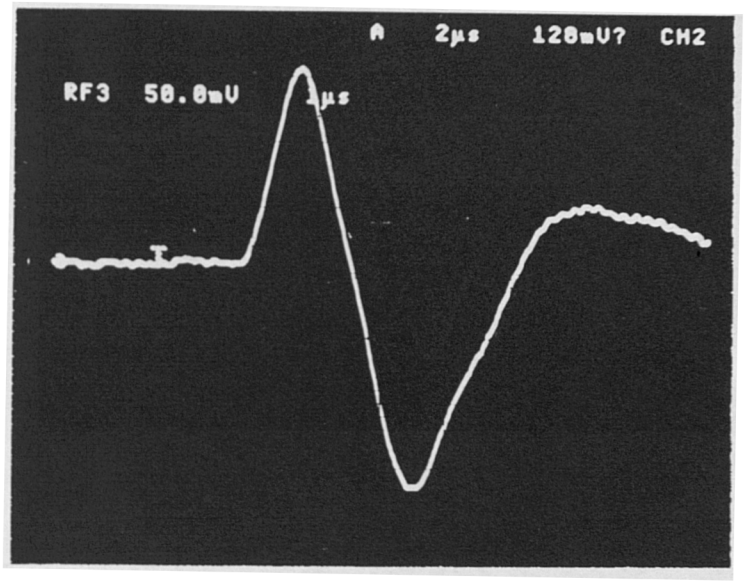

Fig. 6.8 Photoacoustic Waveform from Pre-Prototype Instrument

Near Infrared Spectra

The final experiment presented in this thesis was designed to demonstrate that a photoacoustic spectrum, similar in form to those acquired from a cuvette based detection system, could be obtained from the pre-prototype instrument. The Raman fibre source described in Chapter 3 was again used to provide tunable near infrared radiation in the range 1 to 2 μm. Following wavelength selection by the monochromator and energy monitoring as described in Chapter 3, the typical optical pulse energy available for photoacoustic generation was 1 μJ. This beam was launched into the 1.5 mm diameter delivery fibre, with an efficiency of approximately 50 %, with slight variations depending on the wavelength. A photoacoustic spectrum of distilled water was obtained by submerging the instrument head in a beaker containing the sample.

A total gain of 106 dB was used to amplify the piezoelectric transducer output, with an upper bandpass limit of 800 kHz. This signal together with that from the energy monitor were displayed on a Tektronix 2430A, from which the averages of 256 acquisitions were recorded and used to determine the normalised spectral response. The spectrum is shown in fig. 6.9.

Comparison of fig. 6.9 with the PA spectrum of distilled water obtained from a 1 mm cuvette (fig. 3.9) reveals that the two spectra show basically the same features. There is a general increase in the normalised photoacoustic signal with increasing wavelength, corresponding to the general increase in the optical absorption coefficient of water, and local maxima occurring at 1450 nm and 1900 nm. However the contrast between regions of low and high optical absorption is less in the spectrum from the instrument. This can be attributed to there being no physical containment of the sample. In this case, the effective interaction length of the detector geometry is determined by the dimension of the piezoelectric element in the direction of the optic axis, *i.e.* 5 mm, compared to that determined by the pathlength of the cuvette (1 mm). The response at wavelengths of lower optical absorption will be proportionally higher

because of this. In addition, since the centre of the piezoelectric element was mounted approximately 4.5 mm from the face holding the optical window, high absorbing wavelengths resulted in acoustic signals that coupled less efficiently to the piezoelectric element.

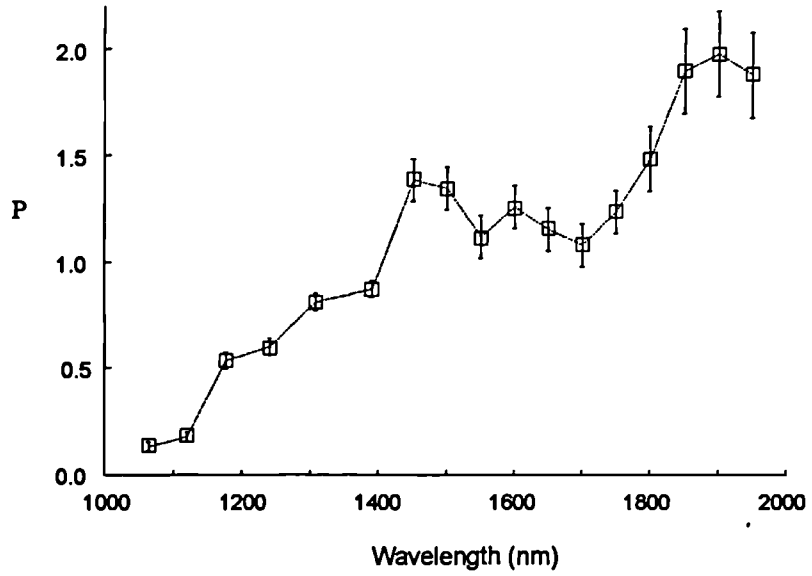

Fig. 6.9 Photoacoustic Spectrum of Distilled Water from the Pre-Prototype Instrument

6.4. Data Acquisition and Analysis

To a large extent the acquisition and analysis of the photoacoustic data obtained for the purposes of this thesis has been automated and controlled by a personal computer (PC). Much of the photoacoustic spectroscopy of pure compounds described in Chapter 3 was achieved using data acquisition and analysis techniques fully described elsewhere (6.6). As the project advanced towards the pre-prototype demonstrator, so these techniques were updated, to bring improvements in the speed of acquisition and the accuracy of the measurement. The most significant improvement was the replacement of the digitising oscilloscope with an eight bit A-D converter connected directly to the PC, to make the peak measurement of the

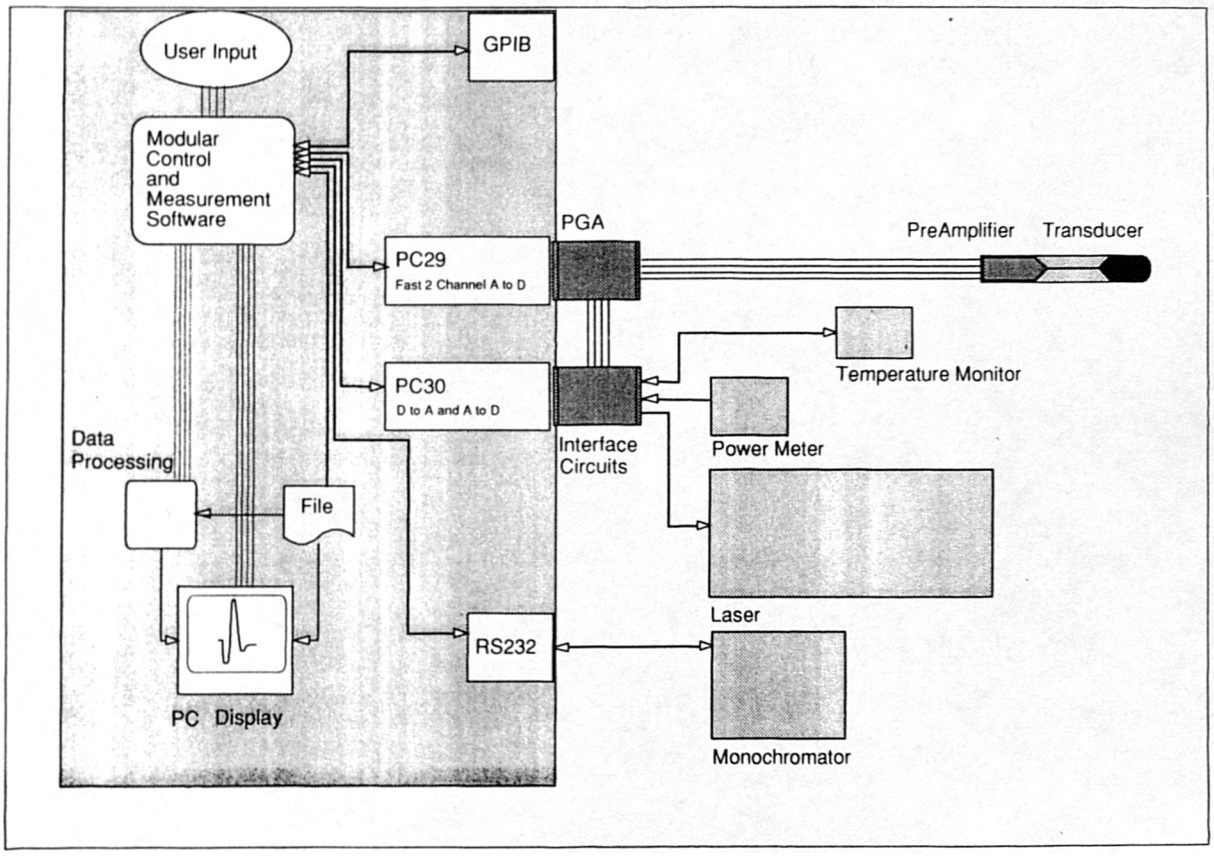

Fig. 6.10 Data Acquisition System

acoustic and energy signals. A block diagram of the most recent data acquisition system, developed at Napier University, Edinburgh, is shown in fig. 6.10. Continued developments in this aspect of the instrumentation are essential to the development of a field trial system.

6.5. Discussion

The use of a fibre optic interferometer to measure displacements in a liquid has demonstrated one manifestation of an all optical measurement of photoacoustic waveforms. Aside from the safety benefits of an all-optical measurement head, optical techniques in general have several other attractive features. Often they provide a calibrated measurement linked to the wavelength of laser radiation, a parameter that is usually known to a high degree of accuracy. This is especially useful when studying the fundamental processes of photoacoustic generation, such as the conversion efficiency of optical to acoustic energy. In addition, an optical measurement can be made without contacting the sample, and is inherently broadband.

If a single wavelength measurement were sufficient, the signal to noise ratio needed to achieve the accuracy and resolution required of the oil in water measurement would be of the order of 1000:1. The photoacoustic measurements reported in this thesis have not achieved such performance limits. When considering the use of diode lasers as photoacoustic sources in instruments, this problem is no less difficult. However certain advances in the photoacoustic generation and detection, the data acquisition and the analysis can be made in order to progress the measurement system towards the target specification.

There are two approaches to improving the signal to noise ratio in a measurement system : increase the signal and / or decrease the noise. There is scope for advances to be made in both ways in this project. The photoacoustic signal could be increased by employing more powerful optical sources. Diode laser arrays or

OPOs are potential candidates. Further advances could be made through the design and implementation of more sensitive acoustic detectors.

There are several approaches to decreasing the noise in a measurement. Firstly, there are continuing improvements in low noise electronics, such as new amplifiers and miniature hybrid circuits, the advantages of which could be brought to bear on this project. Secondly more averaging of the photoacoustic signal can be employed, to benefit from the $\sqrt{n}$ improvement in the signal to random noise ratio that should bring. An increase in the number of averages from 256 to 4096 would yield a theoretical improvement of four in the signal to noise ratio. A third approach is to tackle the problem by using high level statistical analysis to retrieve the maximum amount of information from the raw data. For the relatively simple samples analysed in the laboratory for the purposes of this thesis, univariate analysis has been sufficient to show a systematic response to crude oil concentration. Data obtained from a measurement in the field and subject to a wide range of operational conditions such as the presence of interfering analytes, will be more difficult to interpret accurately. Multi-variate analysis or neural networks will most likely be a necessary component in the data analysis.

Competing Technology

As mentioned in Chapter 1, there are several techniques currently in use, or being developed, to make the necessary oil in water measurement without the use of solvents. The operating principles most commonly used are optical scattering, ultraviolet (UV) absorption, UV fluorescence, direct infrared absorption and acoustics. The principles of operation and key features of each methodology are discussed below.

The largest group is those that operate by the scattering of optical radiation. Oil droplets suspended in the sample will scatter a light beam incident upon the sample. The attenuation of the direct beam together with a knowledge of the distribution of the scattered light can be correlated to the quantity of oil in the sample.

The system has a rapid response to sample variations, and a high sensitivity. However the presence of other particles in the sample can lead to an anomalous result if they themselves scatter the incident light. Similarly dissolved hydrocarbons remain undetected. Most instruments based on this principle therefore adopt a means of sample pre-treatment, by filtering and homogenisation. For the purposes of an in-pipeline measurement, this usually requires the provision of a bypass line.

Aromatic hydrocarbons strongly absorb UV radiation of wavelength 254 nm, and provided that the ratio of aromatic hydrocarbons to the total oil content remains a constant, a measurement of the absorption at this wavelength can provide an indication of the oil content. Although sensitive and having a rapid response, this technique is affected by the presence of solids in the sample and is specific to oil type.

After absorbing UV radiation, the aromatic hydrocarbons in an oil sample fluoresce strongly. This radiative emission can be related to the oil content and may be used to identify some of the oil constituents, providing a fingerprint identification of the oil. This is an extremely sensitive technique, but is again susceptible to the presence of solids as well as being specific to oil type. Since the absorption of the UV is so strong in the oils, this technique is more suited to the detection and source identification of oils on the surface of water, as would be encountered after an oil spill, and has found application in this manner (6.7).

A direct infrared absorption measurement compares the optical absorption coefficients at two wavelengths in the infrared (usually 3.4 μm and 3.6 μm), allowing a calculation of the oil content to be performed which incorporates a compensation for the presence of solids. Use of a filtered reference sample additionally allows compensation for any background absorption, but this has the disadvantage that dissolved oil components would be included in the background signal. Fibre optic

evanescent wave spectroscopy is a variant of the direct infrared absorption technique, and has recently been shown to be capable of detecting chlorinated hydrocarbons at levels of 100 μg/l in water (6.8).

Acoustic monitors operate by monitoring the reflections of a sound wave off oil particles suspended in the sample. A probe can be inserted directly into a pipeline, but acoustic reflections from other particles and gas bubbles in the sample stream may result in a spuriously high reading. Sample pre-treatment is therefore beneficial to the reliability of the measurement.

Photoacoustic Instrument

An oil in water monitor based on the photoacoustic technique can be installed through a single flange directly into a pipeline, avoiding the necessity for a bypass line. However, some form of sample pre-treatment may be necessary, for example if the effect of gas bubbles on the detected photoacoustic signal proves to be severe. The technique may also be sensitive to the oil type especially when using optical excitation in the shorter wavelength near infrared region such as is typical from diode laser sources, because of differences in the energy relaxation pathways. A photoacoustic monitor is capable of detecting dissolved and dispersed hydrocarbons and may be able to distinguish quantitatively between the two contributions to C-H content. A photoacoustic instrument is also insensitive to the presence of solids, and would be capable of providing a rapid response to changes in the oil concentration.

6.6. References

(6.1) Hand D.P., Hodgson P., Carolan T.A., Quan K.M., MacKenzie H.A., Jones J.D.C., *Opt. Comm.*, **104**(1-3), 1, 1993

(6.2) Tam A.C., *Rev. Mod. Phys.*, **58**(2), 381, 1986

(6.3) Seto W.W., "Schaum's Outline Series - Acoustics", McGraw-Hill, 1971

(6.4) Lai H.M., Young K., *J. Acoust. Soc. Am.*, **72**(6), 2000, 1982

(6.5) Heritier J-M., *Opt. Comm.*, **44**(4), 267, 1983

(6.6) Christison G.B., "The Determination of Blood Glucose Concentrations by Infrared Laser Photoacoustic Spectroscopy", Ph.D. Thesis, Dept. of Physics, Heriot-Watt University, 1992

(6.7) O'Neil R.A., Buja-Bijunas L., Rayner D.M., *Appl. Optics*, **19**(6), 863, 1980

(6.8) Krska R., Kellner R., Schiessl U., Tacke M., Katzir A., *Appl. Phys. Lett.*, **63**(14), 1868, 1993

CHAPTER 7

Conclusions and Future Work

7.1. Overview

The main conclusions to be drawn from the results and discussions presented in the preceding chapters, especially the experimental work described in Chapters 3 to 6 are highlighted in this chapter. On this basis, the advantages and disadvantages of the photoacoustic technique are re-iterated, with a particular emphasis on its applicability to the monitoring of oil in water in a pipeline. Proposals regarding the work that remains to be done, in order to bring the development of a prototype instrument to a stage where it would be suitable for field trialling are made. Further studies that would resolve some of the outstanding fundamental scientific issues behind the photoacoustic process in this type of trace analysis application are also discussed. The chapter, and this thesis, are concluded by putting forward several suggestions as to other potential applications for photoacoustic spectroscopy in the field of compositional analysis.

7.2. Conclusions

The photoacoustic effect has been shown to be an excellent basis for a physical measurement to distinguish between water and many organic liquids, including hydrocarbons. As a result of the key physical parameters of these liquids, in particular the thermal expansion coefficient and the specific heat capacity, the

conversion efficiency of optical to acoustic energy is over an order of magnitude greater for many hydrocarbons and alcohols than water. Thus the photoacoustic spectra of such liquids may be very different, even in regions in which the optical absorption coefficients are similar. Since the photoacoustic signal is also dependent upon the optical absorption, spectral selectivity is not greatly diminished when compared to conventional transmission spectroscopy. Indeed, spectral differences between samples may effectively be amplified by the unique dependence of the generated acoustic signal on the physical parameters.

The near infrared spectral region offers several advantages for trace analysis using photoacoustic spectroscopy. The optical absorption coefficients of water (and other liquids) in this region are low to intermediate (0.01 cm^{-1} to 10 cm^{-1}). This allows good penetration into a sample and a bulk measurement to be made, whilst signal saturation effects are generally avoided. There is good contrast in the optical absorption coefficients of water and oil, especially at the lower near infrared wavelengths (below 1.2 μm), resulting in a high responsivity to oil concentration. In addition, the availability of high power diode laser sources that emit in this region is of particular relevance to photoacoustic instrument development.

It has been shown that the performance of photoacoustic spectroscopy in certain conditions of optical scattering remains largely unaltered, with very little overall effect on the magnitude of a detected acoustic waveform, primarily because the photoacoustic effect results in a direct measurement of the energy absorbed when a sample is illuminated. For the scattering conditions likely to be encountered in a water discharge pipeline, there is an increase in the length of the mean photon path in the sample, and a consequent increase in the number of absorption events. Counteracting this effect is an increase in the size of the acoustic source, which reduces the energy density and as a consequence the initial temperature rise due to optical absorption. The overall result of these two opposing effects depends upon the magnitudes and the ratio of the optical absorption coefficient and the scattering coefficient, but in all cases experimentally tested, the presence of scattering particles

had a significant effect on transmission spectra, but no observable effect on photoacoustic spectra.

The amplification of spectral differences provided by the thermal parameters of many hydrocarbons persists at low concentrations, and leads to photoacoustic techniques being capable of detecting oil in water at concentrations less than the current key limit of 40 mg/l. However, the detection limits reported in this thesis using diode laser sources (400 mg/l) are not currently sufficient to meet the requirements demanded by the legislation. Significant improvements in the detection limit of between one and two orders of magnitude are necessary if diode laser sources are to be used in a successful instrument. Several methods by which this may be achieved are discussed in the following section. A summary of the detection limits achieved with the various optical sources described in this thesis is given in Table 7.1.

optical source	pulse energy (μJ)	wavelength (nm)	detection limit (mg/l)
Nd:YAG laser	2000	1064	4
Raman fibre system	0.2	1750	160
diode laser	2.3	904	400

Table 7.1 Summary of Detection Limits

The photoacoustic technique does have some significant advantages over the alternative techniques currently considered for an oil in water monitor. There is no need for a sample to be removed from the flow, meaning that the measurement can be on-line and continuous. Thus the instrument could be incorporated into process control as the feedback element. It is likely that such a unit would be low on consumables and maintenance, and be easy to install, since the geometry of the detector head requires single-flange insertion only.

As well as a good performance in scattering conditions, the photoacoustic technique is capable of detecting both dissolved and dispersed components. A distinction between the quantities of dissolved and dispersed components may also

be possible, through the utilisation of the differences in the form of their near infrared spectra that are particularly evident at low near infrared wavelengths.

Finally, schemes for the optical detection of acoustic waves present a longer term opportunity for the development of an all-optical measurement head, an attractive concept in a hazardous environment such as an operating oil platform.

7.3. Future Work

7.3.1. Oil Monitor

The most immediate shortcoming of the instrument development is currently the detection limit achievable with diode laser sources. Using a diode laser emitting at 904 nm, and with an optical pulse energy of 2.3 μJ, a detection limit of approximately 400 mg/l oil in water has been achieved. Several methods suggested below are available to improve this limit, although this list is certainly not exhaustive.

1) A more powerful diode laser source could be employed, such as a device with more emitting regions, or an array of diodes. Devices are currently available that provide more than an order of magnitude increase in the pulse energy compared to the devices used in the diode laser experiments reported in this thesis. However, since the emitting region is more distributed, this would require a higher degree of optical optimisation to utilise the energy increase efficiently.

2) An increase in the number of data averages from 1280 to 4096 should lead to a signal to noise improvement of approximately 2.

3) Although low noise amplifiers were used in the electronics, immediate advances could be made, perhaps improving the signal to noise ratio by a factor of five.

4) Improving the sensitivity of the acoustic detector unit is a further field of activity that could bring significant results. The current geometrical arrangement means that approximately 15 % of the generated acoustic energy impinges on the

transducer surface. Of this energy, in the region of 80 % is reflected, resulting in only 3 % of the originally generated acoustic energy coupling into the transducer. New detector units to intercept more efficiently the generated acoustic energy could be constructed, for example from cylindrical piezoelectric elements, multiple elements or shaped elements, leading to a six-fold increase in the detected signal. Reducing the acoustic reflection coefficient is dependent upon finding a better impedance match between the liquid and the piezoelectric transducer.

5) Novel schemes of data collection and interpretation may also lead to significant improvements in the detection limit. Analysis in the frequency domain of changes due to oil concentration, for example, is one avenue yet to be explored. The proper use of sophisticated software techniques such as multi-variate analysis and neural networks would ensure that the maximum amount of information could be gleaned from the raw spectral data.

Although the undertaking of studies to improve the signal to noise ratio of the oil in water measurement is seen as the priority, several other experiments are suggested as future programmes of work. As has been emphasised earlier in the thesis, several optical wavelengths will be necessary to make a field measurement of oil in water. Results using three diode laser sources have been presented in this thesis and this could readily be extended to five or six. Of most relevance are high peak power diode laser devices emitting at short NIR wavelengths, where the contrast between the optical absorption coefficients of oil and water are greatest.

In parallel with this, a study of the relaxation pathways for the absorbed energy should be undertaken. This should in particular be conducted with diode laser excitation of crude oil samples, in which fluorescence is expected to be a significant energy relaxation mechanism.

A further suggestion is to undertake studies to determine the effects of more of the field variables on photoacoustic generation and detection. Two of the key aspects are predicted to be the presence of gas bubbles leading to greater acoustic scattering,

and the presence of interfering analytes and their effect on the detection limits particularly when using diode laser sources. Others include the water salinity, oil type and further temperature dependency studies.

7.3.2. Other Applications

Photoacoustic spectroscopy (PAS) is well suited to applications of trace analysis in which there is a large disparity in the optical absorption coefficient, the thermal expansion coefficient, the specific heat capacity and / or the speed of sound of the analyte and the background medium. Thus there are many applications, other than oil in water monitoring, in which the use of PAS could bring significant benefits. Perhaps the most apparent other application in the light of this thesis is the corollary of oil in water monitoring; *i.e.* monitoring water in emulsion in oil. Using typical values of the key physical parameters listed above for crude oil, and assuming a linear variation of all these parameters as the water concentration is decreased, a theoretical plot (based on equation {2.21}, for m = 0.5) of the photoacoustic signal magnitude versus oil concentration is shown in fig. 7.1, for an optical source wavelength of 904 nm.

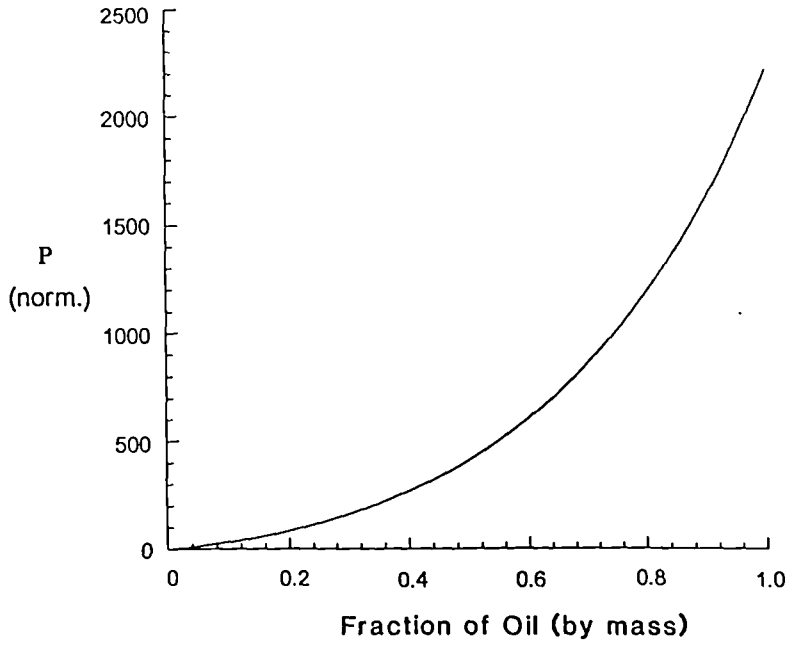

Fig. 7.1 Theoretical Plot of the Photoacoustic Response of Water and Oil Mixes

This shows the same type of curve as predicted and measured for methanol concentrations in water. The response displays a near quadratic dependence on oil concentration. Thus the gradient of the curve is at its greatest for high concentrations of oil and therefore the sensitivity of the photoacoustic technique is predicted to be greater for water in oil measurements than oil in water measurements.

Other applications in the water quality industry could also benefit from an instrument based on a photoacoustic measurement. Chlorophyll has an optical absorption coefficient peak at approximately 670 nm that could be the physical basis of an algae monitor using diode laser sources. Quality control applications, for example in the food and drinks industries, may also be suited to a photoacoustic instrument. The near infrared spectral region is already used extensively in conventional transmission and reflectance spectroscopy in these industries. The performance of photoacoustic spectroscopy under scattering conditions may give this technique a significant advantage. Monitoring processes in the alcoholic beverages industry is one application that could be of particular interest, because of the large photoacoustic response from alcohols compared to water.

Despite the long history of photoacoustics, very few commercial instruments based on the technique are currently commercially available. There is now an expanding wavelength coverage from more powerful, more compact and more reliable laser sources. With the strong scientific arguments in favour of photoacoustic monitoring, together with the need for new monitoring techniques, photoacoustic instrumentation could be well placed to provide complementary scientific measurements in many applications.

Statement of Originality

Throughout my studies for this thesis, I have drawn on the work of others, as is the nature of scientific endeavour. Thus, as well as presenting my own work in this thesis, I have included brief, fully referenced descriptions of the work of others where this is appropriate and important to the overall understanding of my work. I include this statement of originality to further make it clear which aspects of this thesis are my own work, and which are the work of others.

All the experimental photoacoustic (and transmission) results are my own work. I was responsible for designing and commissioning many of the optical aspects of the tunable Raman fibre photoacoustic experimental system. I designed, constructed and performed photoacoustic experiments on several other arrangements, notably using diode lasers, the optical interferometer and the OPO at St. Andrews University. I also played a significant role in the development of acoustic detectors. However, I was not responsible for the development of either the interferometer or the OPO, nor in the development of the PC based data collection systems.

I was responsible for the preparation and characterisation of oil emulsions, the time and frequency domain studies of photoacoustic signals generated in oil emulsions, and for fitting theoretical curves to photoacoustic data, especially to calculate the limits of detection. The theory of photoacoustic generation in liquids outlined in Chapter 2, and the theoretical plots of a photoacoustic waveform and its frequency content are not my work.

The comparison of the photoacoustic technique and competing technologies for an oil in water measurement is a blend of my own work and that of the Institute of Offshore Engineering, at Heriot-Watt University. The design of the instrument prototype described in the thesis was a joint effort between myself, Hugh MacKenzie and Ke Ming Quan, of the Physics Department. My particular responsibilities were the optics, electronics, and the overall housing. I was also responsible for the construction and testing of the unit.

PUBLICATIONS and CONFERENCE PRESENTATIONS

Hodgson P., MacKenzie H.A., Christison G.B., "The Detection of Hydrocarbons and Alcohols in Water by Photoacoustic Spectroscopy", EUROPT(R)ODE 1, Graz, April 1992

Christison G.B., MacKenzie H.A., Hodgson P., "The Laser Photoacoustic Determination of Glucose in Blood", EUROPT(R)ODE 1, Graz, April 1992

Hodgson P. MacKenzie H.A., Christison G.B., Quan K.M., "Laser Photoacoustic Detection of Organic Analytes in Aqueous Media", in NIR '92, eds. Hildrum, Isaksson, Naes, Tanberg, Ellis Horwood, 407, 1992

Hodgson P. Christison G.B., MacKenzie H.A., Quan K.M., "Laser Photoacoustic Detection of Hydrocarbon Pollutants in Water", Applied Optics and Opto-Electronics Conference, Leeds, September 1992

MacKenzie H.A., Christison G.B., Hodgson P., Blanc D., "A Laser Photoacoustic Sensor for Analyte Detection in Aqueous Systems", *Sensors and Actuators B*, **11**, 213, 1993

Hodgson P., MacKenzie H.A., Christison G.B., Quan K.M., "The Detection of Crude Oil Pollution in Water using Laser Photoacoustic Spectroscopy", CLEO '93, Baltimore USA, May 1993

Hodgson P. MacKenzie H.A., Quan K.M., "Near Infrared Liquid Phase Photoacoustic Spectroscopy and its Application to Pollution Monitoring", XXVIII CSI, York, July 1993

Hand D.P., Hodgson P., Carolan T.A., Quan K.M., MacKenzie H.A., Jones J.D.C., "Detection of Photoacoustic Waves in Liquids by Fibre Optic Interferometry", Sensors & their Applications VI, Manchester, September 1993

Hand D.P, Hodgson P., Carolan T.A., Quan K.M., MacKenzie H.A., Jones J.D.C., "Detection of Photoacoustic Waves in Liquids by Fibre Optic Interferometry", *Opt. Comm.*, **104**(1-3), 1, 1993

Quan K.M., Christison G.B., MacKenzie H.A., Hodgson P., "Glucose Determination by a Pulsed Photoacoustic Technique: an Experimental Study using a Gelatin-Based Tissue Phantom", *Physics in Med. & Biol.*, **38**, 1911, 1993

Quan K.M., MacKenzie H.A., Hodgson P., Christison G.B., "Photoacoustic Generation in Liquids with Low Optical Absorption", *Ultrasonics*, **32**(3), 181, 1994

Hodgson P., Quan K.M., MacKenzie H.A., Freeborn S.S, Johnston E., Greig F., Binnie T.D., "Applications of Pulsed Photoacoustic Sensors", EUROPT(R)ODE 2, Florence, April 1994